VIBRATIONAL SUM FREQUENCY STUDY ON BIOLOGICAL INTERFACES

A Dissertation

by

SOON MI LIM

Submitted to the Office of Graduate Studies of
Texas A&M University
in partial fulfillment of the requirements for the degree of

DOCTOR OF PHILOSOPHY

May 2006

Major Subject: Chemistry

VIBRATIONAL SUM FREQUENCY STUDY ON BIOLOGICAL INTERFACES

A Dissertation

by

SOON MI LIM

Submitted to the Office of Graduate Studies of
Texas A&M University
in partial fulfillment of the requirements for the degree of

DOCTOR OF PHILOSOPHY

Approved by:

Chair of Committee,	Paul S. Cremer
Committee Members,	D. Wayne Goodman
	David H. Russell
	Michael A. Bevan
Head of Department,	Emile A. Schweikert

May 2006

Major Subject: Chemistry

ABSTRACT

Vibrational Sum Frequency Study on Biological Interfaces.

(May 2006)

Soon Mi Lim,

B.S., Inha University; M.S., Inha University, South Korea

Chair of Advisory Committee: Dr. Paul S. Cremer

Vibrational sum frequency spectroscopy (VSFS) is a nonlinear optical process. The sum frequency signal is proportional to the square of second order nonlinear susceptibility, which is proportional to the average of polarizabilities of molecules, which is related to molecular orientation. Since the polarizabilities of molecules in bulk phase will be canceled out, a sum frequency signal can only be generated from interfaces where the inversion symmetry is broken. Because of its interfacial specificity, VSFS has been applied to study many interfacial phenomena. In this dissertation we investigated various biological interfaces with VSFS. Fibrinogen adsorption was studied at the protein/solid interface in combination with atomic force microscopy (AFM), immunoassay, and VSFS. Astonishing changes in the interfacial water orientation accompanied by the pH changes provided fibrinogen's adsorption mechanism up to the amino acid level. Enzymatic fragmentation of fibrinogen revealed that the adsorption property of fibrinogen was mainly from the alpha C fragments of the protein.

Mimicking of the fibrinogen binding site with polypeptides was successfully performed and showed very similar properties of fibrinogen adsorption.

Protein stability is sensitive to the salts in solutions. The ability of ions to stabilize protein was ordered by Hofmeister in 1888 and the order is $SO_4^{2-} \cong HPO_4^{2-} > F^- > Cl^- > Br^- > NO_3^- > I^- (\cong ClO_4^-) > SCN^-$. Even though the phenomenon was observed in various biological systems, the origin of those ionic effects is still not well understood. We studied ion effects on alkyl chain ordering and interfacial water structure for octadecylamine, dimethyldidodecylammonium bromide, and dilauroylphosphotidyl choline monolayers. Because of its ability to probe a hydrophobic moiety and interfacial water at the same time, VSFS provided further information to understand the Hofmeister series. We found that the Hofmeister effect is a combinatorial effect of screening effects, ion binding, and dispersion forces.

ACKNOWLEDGMENTS

I would like to thank to my advisor, Dr. Paul S. Cremer, for his support during my Ph.D. course scientifically and financially. Without his cheer, generosity and patience, I might not have been able to go through my Ph.D. course.

I also would like to thank to my committee members, Dr. D. Wayne Goodman, Dr. David S. Russell, and Dr. Michael A. Bevan for their time and comments on my dissertation and my defense.

I appreciate all the help from past and present Cremer group members. They taught me how to use instruments and the importance of co-working. Most of all, they have been precious friends through my graduate life. I enjoyed all the time spent with them discussing scientific issues as well as gossip. I would like to give credit to Gibum Kim for pioneering work on the fibrinogen project, Seungyong Jung for building up mechanisms for the fibrinogen adsorption, and Marc Gurau for his accomplishments on air/water studies.

Special thanks to my family members who always prayed for me and believed in me. Mom, Dad, Sulhee and Mark, and Byoungil, I will not forget your prayers and support. There are no words to express my thanks to my husband, Gie-Seung Lee. He was always supportive and prefers to think about me rather than himself all the time. He is the main source of my peace and my power. He brought me self esteem with love. I appreciate all the joy from my two kids, Dohyun and Hayoung. Dohyun was in my tummy during my study of fibrinogen and was born right after my preliminary exam. Now he is very active and funny. He makes me laugh so hard that I cry. Hayoung was

with me when I lifted the 10 gallon waste bottle from the Langmuir trough experiments for the Hofmeister study. She was born right before I wrote the dissertation and she taught me how to split time between family and work. As a lovely three month old girl, every time she giggles and coos at me she raises me to the highest happiness a human being ever can get. She melted all my burdens and tiredness from work and gave me new energy to start another day. If I did not have my kids, I might have been able to publish a couple of more papers, but they are more precious than a Nobel Prize. To my family, I love you all.

Last but not least I thank God for everything he offered me. I believe that everything He allowed to happen to me was for good. Thank you Lord and I praise you.

TABLE OF CONTENTS

Page

CHAPTER Page

LIST OF FIGURES

FIGURE Page

FIGURE Page

LIST OF TABLES

CHAPTER I

INTRODUCTION

Interactions of bio molecules with surfaces are of importance for biocompatibility and improvement of the effect of biomaterials[1], but are very hard to understand because there are many forces affecting on interfacial interactions: van der Waals forces, electrostatic forces, solvation forces (hydrophobic and hydrophilic forces), and steric forces.[2, 3] There are various interfaces in an organism, such as protein-membrane, polysaccharides-membrane, cell-cell, and protein-protein interfaces.[3] There have been multiple approaches to study those biological interfaces with Brewster angle microscopy (BAM), neutron reflectivity, Infrared spectroscopy, and atomic force microscopy (AFM). Because of the interfacial specificity and ability to give vibrational and orientation information of a molecule at the interface, sum frequency spectroscopy (SFS) has become a powerful tool to study interfaces.

Sum frequency generation is a nonlinear optical process that gives vibrational information of molecules at interfaces. A fixed green beam excites molecules electronically and tunable IR excites molecules vibrationally at the same time. When an IR frequency is resonant to a vibrational level of molecule, a frequency-summed signal is enhanced. The intensity of sum frequency signal is proportional to square of second-

---

This dissertation follows the style of the *Journal of the American Chemical Society*.

order nonlinear susceptibility as well as the intensities of visible and IR beams. Nonlinear susceptibility is a combination of a resonant term and a non-resonant term and the resonant term is proportional to the number of molecules and ensemble average of polarizabilities of molecules, which is related with molecular orientations. Since the polarizabilities of molecules in bulk phase will be canceled out, sum frequency signal only can be generated from interface where the inversion symmetry is broken. Experimental details of VSFS including its specific selection rule will be explained in the chapter II.

The first example of VSFS study on biological interfaces in this dissertation is the study on protein/solid interface, which is the mimic of protein interactions with medical implants. Over the last few decades medical implants have been developed vigorously and include joint and dental implants as well as vessel implants. Understanding protein adsorption on these implanted surfaces is critical for biocompatibility and efficiency. Some adsorptions help growth of bone and formation of stable interfaces between the implant and the body, but other adsorptions such as protein adsorption on contact lenses causes infection and disease. In addition, efficient adsorption is required for biological activity of biosensors. Chapter III describes VSFS study of fibrinogen adsorption to silica surface.[4] Fibrinogen adsorption has been studied by numerous researchers for decades because of its important role in blood coagulation, which is a serious issue in medical implants. Blood clots consist of fibrins that form insoluble fibrous networks. Fibrin is converted from fibrinogen by thrombin. Fibrinogen is composed of two αC domains connected to D domains that are connected

to a central E domain and its molecular weight is 340 kD.[5] Two αC domains are known to interact with the central E domain differently at various pH. We investigated the role of α-C domains in fibrinogen absorption with sum frequency spectroscopy (Chapter IV).

The following two chapters deal with the Hofmeister effect, which is originally proposed based on the effect of salts on protein stability.[6] Protein stability is affected by many factors; among them are hydrophobic interactions, ionic strength, and hydrogen bonding interactions. In 1888 Hofmeister found different concentrations of ions were required to salt out "hen egg white" protein and he made a series of ions according to their salting-out strengths[6]:

$SO_4^{2-} \cong HPO_4^{2-} > F^- > Cl^- > Br^- > I^- > NO_3^- > ClO_4^- > SCN^-$.

This series, called Hofmeister series, has been used regularly for protein precipitation. Ions before Cl^- are known as kosmotropes, which are known to be "water structure makers" and stabilize proteins. Ions after Cl^- are chaotropes or "water structure breakers", and destabilize proteins. The Hofmeister ions not only affect protein stability but also enzyme activities, crystallization of biological macromolecules, DNA-protein interactions[7], polystyrene latex particles[8] and even pH measurements[9, 10]. The origin of this ion effect is still controversial, but classically it has been understood as an indirect water structure change caused by ions.[11] Collins and Washabaugh suggested that the solvation shells of kosmotropes are tightly bound to the ion with strong hydrogen bonding resulting in salting out effects. There have been many papers supporting this explanation and recently Hribar and co-workers performed molecular calculation and presented consistent results with Collins.[12] Another hypodissertation proposed the origin

of the Hofmeister effect as direct interactions between the ions and non-polar groups by increasing the solution free energies and modifying the phase equilibrium.[13] Neutron diffraction studies[14] and fluorescence studies[15] supported the direct interaction hypodissertation. A recent study by the Bakker group showed ions did not affect water-water hydrogen bonding and they claimed that the Hofmeister effect is not related with water-structuring ability of ions but only related to ion interactions.[16] We applied vibrational sum frequency spectroscopy (VSFS) and tried to find a deeper explanation of the Hofmeister effect. We studied ion effects on alkyl chain orientation of amphiphile molecules as well as on interfacial water structure between the monolayers and solutions (Chapter V).

The last chapter of this dissertation is the summary of the dissertation (Chapter VI).

CHAPTER II

EXPERIMENTAL AND INSTRUMENTAL BACKGROUND

VIBRATIONAL SUM FREQUENCY SPECTROSCOPY (VSFS)

Sum frequency generation (SFG) is a nonlinear optical process that gives vibrational information of molecules at interfaces.[17] A fixed visible beam and tunable IR beam are used for VSFS. When the frequency of IR is resonant with a vibrational frequency of a molecule, frequency summed signal is enhanced. SFG signal intensity is proportional to the square of the second order nonlinear susceptibility as well as the intensities of the IR and visible beams.[18, 19]

$$I_{SFG} \propto |P|^2 \propto \left|\chi^{(2)}\right|^2 I_{IR}(\omega_{IR}) I_{vis}(\omega_{VIS}) \qquad (1)$$

Where P is the polarization, $\chi^{(2)}$ is the second-order nonlinear susceptibility, $I_{IR}(\omega_{IR})$ is the intensity of the IR radiation, $I_{vis}(\omega_{VIS})$ is the intensity of visible light. The second-order nonlinear susceptibility can be expressed as a sum of the resonant term, $\chi_R^{(2)}$, and the non-resonant term, $\chi_{NR}^{(2)}$.

$$\chi^{(2)} = \left|\chi_R^{(2)} + \chi_{NR}^{(2)}\right|^2 \qquad (2)$$

The resonant term is proportional to the number of molecules at the interface, *N*, and the ensemble average of the molecular polarizability, β, which depends on molecular orientation.

$$\chi_R^{(2)} = N < \beta^{(2)} > \qquad (3)$$

Sum frequency signal cannot be generated where there is inversion symmetry because the average polarizability will cancel out. Therefore the SFG signal only comes from an interface where the inversion symmetry is broken. Also the resonant susceptibility can be related with resonant vibrations:

$$\chi_R^{(2)} \propto \sum_n \frac{A_n}{\omega_{IR} - \omega_n + i\Gamma_n} \qquad (4)$$

where A_n , ω_{IR}, ω_n, Γ_n are the oscillator strength, IR frequency, resonant frequency, and damping constant of the nth vibrational mode.

Various polarization combinations of the incident and outgoing fields can be used in sum frequency spectroscopy to obtain information about the orientation of interfacial molecules. The four available combinations are SSP, SPS, PSS, and PPP with the order of sum frequency, visible, and infrared.[20] The SSP combination is used for IR transition moment components perpendicular to the interfacial plane, SPS and PSS probe modes that have IR transition moment components in the plane of the interface, and PPP probes all components of the allowed transitions.

The interfacial specificity of sum frequency spectroscopy successively applied to investigations of various interfaces and provides valuable information, which was not accessible with other conventional techniques. Mostly VSFS has been used to study interfacial water and alkyl moieties of molecules. Interfacial water gives sum frequency signal in the range of 3000 cm^{-1} ~ 3800 cm^{-1}. There are three major water peaks at 3200 cm^{-1}, 3400 cm^{-1}, and 3700 cm^{-1}. The first one is called the ice-like peak because pure ice shows only a 3200 cm^{-1} peak. It is from fully hydrogen-bonded water molecules, which

have tetrahedral coordination. Understanding of the 3400 cm^{-1} peak is still controversial but is understood as being from less ordered water molecules. The water peak at 3700 cm^{-1} is usually sharp and assigned to a free OH stretch, which does not have hydrogen bonding. The greater the hydrogen bonding, the wider and more red-shifted the water peaks. Interfacial water structure has been studied by VSFS at the air/liquid interface[17, 18, 21], the liquid/liquid interface[22-24], and the solid/liquid interface for the adsorptions of bovine serum albumin BSA[25], polyelectrolytes[26], and lipid bilayers[27].

The hydrophobic residues of a molecule give CH peaks between 2800 cm^{-1} and 3100 cm^{-1}. The peaks from CH_2 moieties give signal at 2850 cm^{-1} and 2920 cm^{-1}; the CH_2 symmetric stretch and the CH_2 asymmetric stretch, respectively. CH_3 peaks are at 2875 cm^{-1} and 2965 cm^{-1}. These are the CH_3 symmetric stretch and CH_3 asymmetric stretch, respectively. Sum frequency studies on CH residues have been reported at the air/water interface and solid/water interface for proteins and lipid molecules.[28-31]

The laser system used in dissertation was a passive-active mode-locked Nd:YAG laser (PY61c, Continuum, Santa Clara, CA) equipped with a negative feedback loop in the oscillator cavity to provide enhanced shot-to-shot stability. The laser was operated at a 20 Hz repetition and the pulse duration was 21 ps. Tunable IR and 532 nm radiations were obtained from an optical parametric generator/amplifier (OPG/OPA) stage (Laser Vision, Bellevue, WA), which was composed of two parts. First 1064 nm radiation from the Nd:YAG laser was split and half of the beam was sent to the first stage of OPG/OPA, which is an angle-tunable potassium titanyl phosphate (KTP). The rest of the 1064 nm beam was converted to 532 nm through a potassium titanyl phosphate (KTP). Some of

532 nm beam was sent to the sample stage and meet near-IR radiation, while the rest of 532 nm beam was mixed with the other half of 1064 nm at the first stage of OPG/OPA to generate near-IR radiation between 1.35 ~ 1.85 μm. The second stage of OPG/OPA is an angle-tunable potassium titanyl arsenate (KTA) stage, where near-IR and fundamental radiations are mixed and converted to 2000 ~ 4000 cm^{-1} tunable IR beam with the full width at the half maximum of 7 cm^{-1}. At the sample stage tunable IR and 532 nm radiations were focused together and radiated to generate sum frequency signal (Figure 1). Signal generated from the interface was collected by a photomultiplier tube (R647, Hamamatsu, Japan) and sent to a gated integrator (SR250, Stanford Research Systems, Sunnyvale, CA) and the intensity of signal was recorded on a computer with a homemade LabView (National Instruments Corporation, Austin, TX) program. All data in this dissertation was taken with polarization combination of $S_{SFG}S_{VIS}P_{IR}$. A signal from z-cut crystalline quartz was used for background correction.

ATOMIC FORCE MICROSCOPY (AFM)

Atomic force microscope is a nondestructive probe to image a surface and to measure the force between the probing tip and the surface being imaged. It was invented by Binnig, Quate and Gerber in 1986 based on scanning tunneling microscope (STM).[32] The tip used for an AFM instrument is attached at the end of a cantilever. The cantilever deflects when it encounters a height change on the surface. Mechanical motion of the cantilever to x and y direction is created by applying voltage on a piezoelectric transducer.[33] The motion of the cantilever can be detected by the reflection of a laser

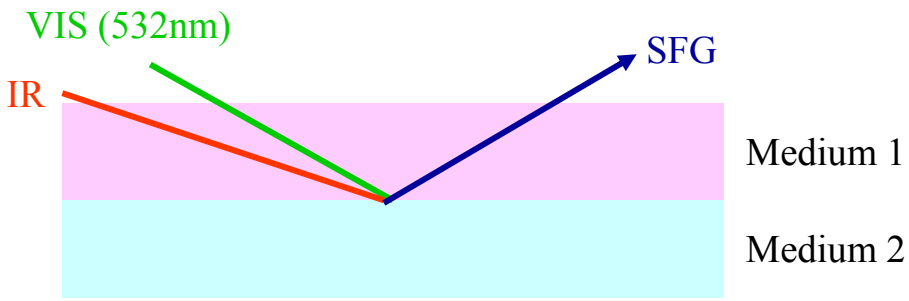

Figure 1. Vibrational sum frequency spectroscopy (VSFS). The signal is generated at the interface of medium 1 and medium 2.

light, which is radiated on the backside of the cantilever, onto an array of photodiodes. The changes in cantilever deflection are recorded as changes in the intensity of laser light. Force is measured by utilizing the relationship between the motion of a cantilever and the applied force. Unlike STM, AFM does not offer conductance of the sample, hence it is highly applicable for biological samples. Recently AFM has been applied to imaging and force studies of nucleic acids, biological membranes, cell surfaces, and proteins.[34-36]

TOTAL INTERNAL REFLECTION FLUORESCENCE MICROSCOPY (TIRFM)

When the light propagates through the interface of two different media with different reflective indices, such as liquid (~1.33) and glass (1.5), some of the light passes through the interface and the other will reflect. Total internal reflection occurs when the incident angle is greater than the critical angle, where all the light reflects. The critical angle, θ_c, can be expressed by

$$\theta_C = \sin^{-1}(\frac{n_2}{n_1}) \qquad (5)$$

where n_2 and n_1 are the refractive indices of the liquid and the glass, respectively.[37] However, some of the incident beam propagates a short distance (a few hundred nanometers) into the liquid and generates an evanescent wave parallel to the surface in the plane of incidence (Figure 2). The intensity of the evanescent wave, *I(z)* decays exponentially with perpendicular distance *z* from the interface:

$$I(z) = I_0 e^{-z/d} \qquad (6)$$

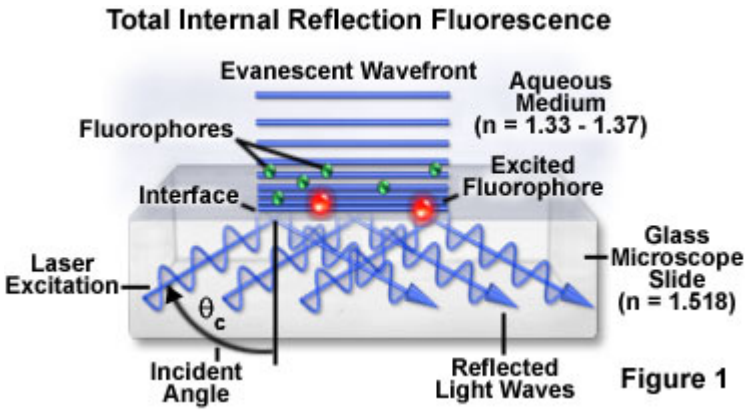

Figure 2. Schematic diagram of total internal reflection fluorescence (TIRFM).[38]

where,

$$d = \frac{\lambda_0}{4\pi}[n_1^2 \sin^2 \theta - n_2^2]^{-1/2} \qquad (7)$$

for angles of incidence $\theta > \theta_c$ and light wavelength in vacuum λ_0. Depth d is independent of the polarization of the incident light and decreases with increasing θ. Depth d is on the order of λ_0 or smaller, except for $\theta = \theta_c$ (where $d \rightarrow \infty$). If there is a fluorophore molecule within the evanescent wave it can absorb photons and be excited. Since the intensity of evanescent wave exponentially decays to the distance from the interface, only the molecules presenting near the interface can be excited in the TIRFM. In this way, it is possible to get fluorescence with a very low background of excitation light. TIRFM has been intensely applied to study biological phenomena at surfaces and interfaces such as antibody-antigen bindings.[39, 40]

QUARTZ CRYSTAL MICROBALANCE (QCM)

The quartz crystal microbalance with dissipation factor (QCM-d) was applied to study adsorption behavior of proteins and fragments. When a piezoelectric material is subject to a mechanical strain, an electrical field is being created within the material, and vice versa: When an electrical field is applied over such a material, it will be strained. The direction and magnitude of the piezoelectric straining is directly dependent on the direction of the applied electric field relative the crystal axis. Most QCM systems use AT-cut quartz crystals because it ensures that an applied electrical field will induce a mechanical shear strain in the crystal. The crystal is excited by resonance frequency and

adsorbed material decreases the frequency. The relationship between adsorption mass and frequency shift is given by the Sauerbrey equation[41]:

$$\Delta m = -\frac{C \cdot \Delta f}{n} \qquad (8)$$

where, Δm is the mass change, C = 17.7 ng Hz^{-1} cm^{-2} for a 5MHz quartz crystal, Δf is the frequency shift, and n = 1, 3, 5, 7 is the overtone number. The QCM technique was originally applied in vacuum and gas environments, but recently it became available for the samples in liquid phases, which results exclusive usage of AFM into biological applications.[42] It also has been proven to be sensitive and practical tool for real-time measurements of macromolecule adsorptions. Most common applications in biochemistry are protein-adsorption kinetics, antibody-antigen interaction, and lipid vesicle adsorption and fusion to supported lipid bilayer. Unfortunately frequency shift is not proportional to the mass change in case of soft materials, such as proteins, because films dissipate significant amount of energy to quartz oscillation. More accurate value of frequency shift due to adsorption can be obtained by considering dissipation energy, which also gives the information of how rigid or soft the film is.[43] Dissipation energy can be measured by switching off the driving power to the piezoelectric crystal oscillator and monitoring the decay curve. By recording the voltage during the decay and by fitting the curve with equation as shown below, both resonance frequency and dissipation factor can be achieved simultaneously.

$$D = \frac{1}{\pi f \tau} \qquad (9)$$

where τ is the decay time constant and *f* is the frequency. The decay constant, *D*, is bigger for thick and soft films and smaller for thin and rigid films.

SURFACE POTENTIAL MEASUREMENT

Surface potential can be measured by a Kelvin prove, which was proposed by Lord Kelvin in 1898.[44] Modern Kelvin probes provide non-contact and non-destructive technique. When two conducting materials with different work functions are brought together, a potential is generated due to electrons in the material with the lower work function flow to the one with the higher work function.[45] If these materials are made into a parallel plate capacitor, the voltage developed over this capacitor can be measured by applying an external potential to the capacitor until the surface charges disappear (Figure 3). The potential at this point equals the potential between two conducting materials. The capacitance of a potential measurement depends on the surface area of the plates (electrodes), the length of the gap between the plates and the nature of the medium between them. The capacitance of the parallel-plate capacitor can be expressed as:

$$C = \frac{\varepsilon \varepsilon_0 A}{D} \qquad (10)$$

Where, *C* is the capacitance of a capacitor [*F*], ε is the relative electric permittivity of the material between the electrodes, ε_0 is the electric permittivity of vacuum (8.85×10^{-12} [F/m]), A is the surface are of the plate, *D* is the distance between two plates. If the probe plate is grounded, the voltage U (|U1-U2|) between electrodes of the capacitor is

equal to the potential difference between two plates. The charge on the tested surface can be calculated as:

$$Q = U \cdot \frac{\varepsilon \varepsilon_0 A}{D} [F] \qquad (11)$$

When there is any change on the distance of the plates, the measurements has to be corrected by removing some of the electric charge from the probe. To obtain this correction, vibrating capacitor method was developed, which was originally introduced by William Zisman in 1932. This technique automatically tracks shifts in the contact potential due to changes in the work function of the sample. The probe vibrates in the direction perpendicular to the tested surface and the current flowing to and from the probe changes proportionally to the amplitude and frequency of the vibration. This technique allows accurate measurements of mean capacity, which can be used to perform scanning measurements at a constant height.

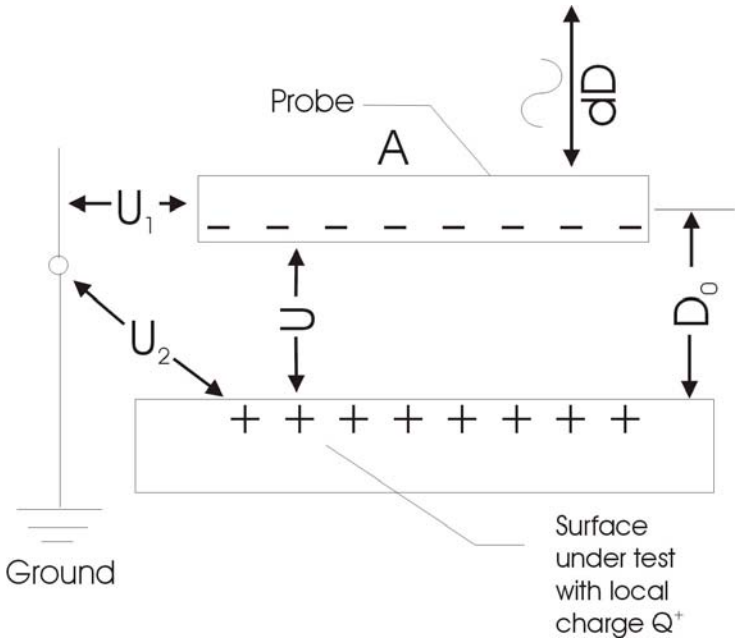

Figure 3. Vibrating capacitive probe.

CHAPTER III

VIBRATIONAL SUM FREQUENCY STUDY ON INTERACTIONS OF FIBRINOGEN PROTEIN WITH FUSED SILICA*

INTRODUCTION

The formation of biofilms on man-made surfaces affects fields ranging from food processing to biosensor design.[46, 47] One particularly important topic is the adsorption of blood and related biofluids onto nascently implanted materials such as artificial hips.[48] Leo Vroman and Ann Adams first demonstrated in the late 1960s that protein adsorption from blood plasma involves a complex series of adsorption and displacement steps.[49] This phenomenon, now known as the Vroman effect,[49-52] has subsequently been shown to involve the initial adsorption from the fluid phase of abundant but weakly surface-active proteins. These early adsorbers are subsequently displaced by more strongly binding species that are present in solution at lower concentration. Despite speculation regarding possible mechanisms for this phenomenon,[5] no definitive experimental evidence has been available to explain it. This is unfortunate because a mechanistic understanding of the Vroman effect could aid in the search for biocompatible materials.

---

* Reproduced with permission from "The Vroman Effect: A Molecular Level Description of Fibrinogen Displacement" by Seung-Yong Jung, Soon-Mi Lim, Fernando Albertorio, Gibum Kim, Marc C. Gurau, Richard D. Yang, Matthew A. Holden, and Paul S. Cremer, *J.Am.Chem.Soc*. **2003**, *125*, 12782-12786. Copyright 2003 American Chemical Society.

Indeed, proteins are usually the first species to arrive at a nascently formed biological/artificial interface and the nature and concentration of these adsorbates strongly influence subsequent cellular recruitment, platelet adhesion, and thrombosis.[53, 54]

One of the classic Vroman effects involves the displacement of human plasma fibrinogen (FRN) from a silica substrate.[55-57] Over the past few decades, it has been shown that fibrinogen displacement by other plasma proteins such as kininogen and clotting factor XII depends on numerous factors including temperature, the extent of dilution of the plasma, and the specific surface chemistry.[50, 58] FRN consists of two peripheral D domains and one central E domain linked together by triple-stranded α-helical coiled coils (Figure 4).[5] Additionally, there are two αC domains that interact with the central E domain in a pH specific manner.[59] Namely, near neutral pH, the αC domains are strongly bound to E, but upon lowering the pH below 3.5 they become reversibly detached.[5, 54, 60] FRN is net negatively charged at pH 7.4 with the highest concentration of negatively charge residues residing on the E and D domains. On the other hand, the αC domains, which are rich in Arg and Lys residues, are actually positively charged. The hydropathic index for FRN indicates that the E and D domains are substantially more hydrophobic than the αC domains.

The work presented here employs a combination of techniques including atomic force microscopy, vibrational sum frequency spectroscopy (VSFS), immunochemical assays, and kinetic experiments to help elucidate the FRN displacement mechanism.

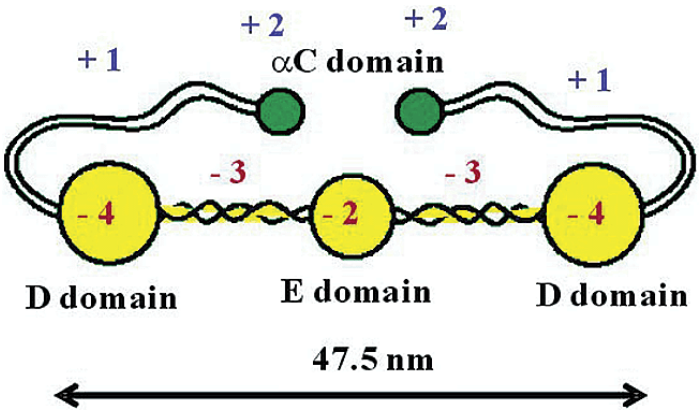

Figure 4. Molecular structure of human plasma fibrinogen (FRN). The D and E domains are formed from two sets of three polypeptide chains (Aα, Bβ, and γ) connected by 29-disulfide bonds. The N-termini of these chains form the E domain while the C-termini of the Bβ and γ chains make up the two D domains. FRN is 90 × 475 × 60 Å with a molecular weight of 340 kD.[15]

The results demonstrate that the protein's αC domains play the critical role. When the protein is adsorbed to a hydrophilic surface via these moieties, its displacement rate in the presence of human plasma is approximately ~170 times faster than when these domains are not in direct surface contact. Even more significantly, spectroscopic studies show evidence for highly aligned Arg and Lys residues interacting with the negatively charged substrate only when the αC domains make direct surface contact. The interfacial ordering of these residues appears to be the hallmark of a weak and labile electrostatic attraction between the substrate and the adsorbed macromolecule.

MATERIALS AND METHODS

Materials

Human plasma fibrinogen (>95% purity) was purchased from Sigma and its purity was verified in our laboratory using size exclusion chromatography with an Akta purifier (Amersham Bioscience). The results showed the protein to be at least 98% pure. Stock solutions of FRN were made by dissolving the macromolecule in a $NaHCO_3$/ Na_2CO_3 buffer (pH 9.0, 50 mM) at a concentration of 3.0 mg/mL. These solutions were aliquoted and stored at -80 °C. Just before use, the protein solutions were thawed and diluted in appropriate phosphate buffers. Human plasma was purchased from CBR Laboratories (Woburn, MA) and diluted to a 5% solution in water (NANOpure Ultrapure Water System, Barnstead, Dubuque, IA) before use. The water employed had a minimum resistivity of 18 MΩ·cm. Anti-fibrinogen Aα chain (Aα 529-539) antibody was purchased from Accurate Chemical & Scientific Corp. (Westbury, NY) and labeled

by Alexa Fluor-594 dye from Molecular Probes (Eugene, OR). IR grade fused silica cleaned in a dichromate-sulfuric acid cleaning solution and annealed at 1050 °C for 12 h disks, which were used in all experiments, were purchased from Quartz Plus Inc. (Brookline, NH).

Atomic Force Microscopy (AFM)

AFM images were taken with a Nanoscope IIIa Multimode SPM (Digital Instruments, Santa Barbara, CA) equipped with a type "J" scanner. The silica substrates were pretreated with an H_2 - O_2 flame for 5 min. The pretreated substrates were then in a kiln. Finally, the disks were O_2 plasma treated immediately before use. To perform an experiment, a piece of silica was mounted onto a stainless steel disk for placement into a liquid cell. Protein solution at 0.5 μg/mL was introduced into the cell, which was equipped with an O-ring seal and allowed for exchange of the bulk solution. This concentration was chosen because higher concentrations made it difficult to keep track of the individual FRN molecules. The same concentration was therefore also used for all other experiments except VSFS. In that case, 5.0 μg/mL was employed to obtain sufficient signal. All AFM images were obtained with 100 nm long oxide-sharpened triangular probes (silicon nitride, spring constant: 0.58 N/m) in fluid tapping mode at a scan rate of 1-2.5 Hz. The drive frequency was 8-9 kHz and the drive amplitude was 0.25-0.7 V. The set point was chosen at 85-90% of the free amplitude. The only treatment applied to the images was flattening.

Vibrational Sum Frequency Spectroscopy (VSFS)

Theories and experimental details about VSFS are mentioned in earlier chapter (Chapter II). A flow cell equipped with two IR-grade quartz windows was use for this experiment. Flow was generated by gravity and pH of the solution was measure at the outlet. Data were taken after 30 minute from the protein solution was introduced. The flow cell was rinsed with the same pH buffer to remove excess protein in the bulk. Polarization combination for this work was ssp for sum frequency, visible, and IR respectively.

Total Internal Reflection Florescence Microscopy (TIRFM)

All protein solutions were prepared in phosphate buffered saline (PBS) (0.05 M NaH_2PO_4; 0.15 M NaCl) at pH 8.0. Alexa Fluor-594 dye was used to label the fibrinogen for TIRFM. To minimize the effect of the dye on the adsorption properties, the labeling degree was kept to 0.7 dyes/protein. Alexa-594 FRN was employed at a concentration of 0.5 μg/mL. Samples consisted of a silica substrate surrounded by simple poly(dimethylsiloxane) walls to prevent solutions from spilling off the surface. A cover slip could be placed over the top to prevent evaporation. To begin an experiment, Alexa-594 FRN was allowed to adsorb onto the substrate from a protein solution for 20 min. The bulk solution was then rinsed away with PBS at pH 8.0. This process and subsequent displacement experiments were monitored via total internal reflection fluorescence microscopy using a Nikon E800 fluorescence microscope equipped with a Micromax 1024 CCD camera (Princeton Instruments). All images were acquired under a 10× objective. TIRFM was performed by reflecting a 1 mW 594 nm Helium-Neon

laser beam (Uniphase Manteca, CA) off the sample/solution interface using a dove prism setup, which was optically coupled to the backside of the planar silica substrate through immersion oil. Displacement studies were performed by replacing the buffer with diluted human plasma, which was incubated over the surface for the duration of the experiment.

RESULTS

Protein Displacement Kinetics

To investigate fibrinogen displacement kinetics, silica samples were coated with fluorescently labeled FRN by introducing a 0.5 μg/mL protein solution in PBS at pH 8.0 over the substrate. The solution was allowed to incubate for 20 min and then replaced with pure buffer. Next, 5% human plasma was incubated over the surface and the displacement rate of the labeled FRN was monitored as a function of time using TIRFM. As can be seen from the data, the fibrinogen was displaced from the interface as a function of time in an exponentially decaying manner (Figure 5, ●).[61] Roughly 80% was removed after 90 min. On the other hand, hardly any protein was displaced from the surface if only buffer was introduced instead of the 5% plasma solution (Figure 5, ▼). Finally, the displacement rate was probed under conditions that should allow the αC domains to be detached from the E domains and then subsequently reattached.[60] This was accomplished by replacing the pH 8.0 buffer with a similar PBS solution at pH 3.2 and then rinsing again with pH 8.0 buffer before attempting to displace the surface adsorbed FRN with 5% human plasma (Figure 5, ○). The results from this final kinetics

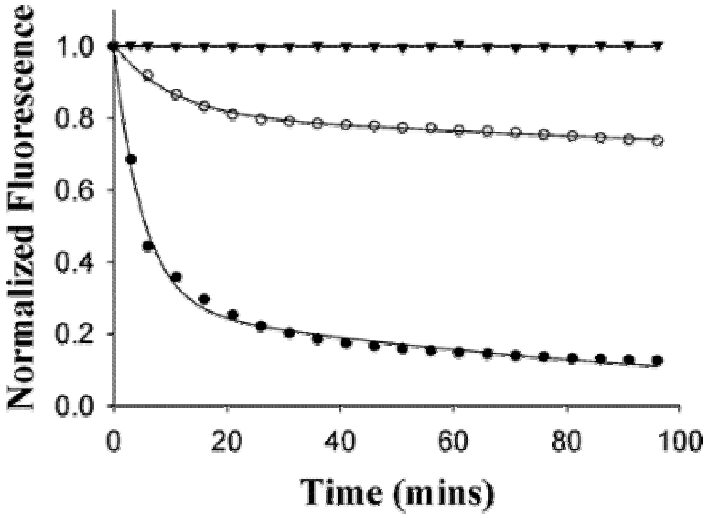

Figure 5. Displacement of Alexa 594-labeled fibrinogen from a silica surface by a 5% human plasma solution. The closed circles (●) indicate experiments with 5% human plasma after only exposing the sample to PBS at pH 8.0. The open circles (○) show displacement kinetics with 5% human plasma after pH cycling through 3.2 and back to 8.0. The inverted triangles (▼) represent a control experiment where only buffer was introduced over the FRN coated surface.

experiment showed a severe atte2nuation in the amount of protein that could be displaced from the surface. The data sets taken with 5% plasma could be fit to double exponential decay curves,

$$y = a_1 e^{-t/\tau_1} + a_2 e^{-t/\tau_2} \qquad (12)$$

where t is time, y is the fluorescence intensity, a_1 and a_2 are coefficients between 0 and 1 such that $a_1 + a_2 = 1$, and τ_1 and τ_2 are the time constants. All data sets were repeated 5 times. Fitting the data and averaging gave the time constants and surface fractions of the fast and slow exchange components: as indicated, 72% of the protein from the standard pH 8.0 sample can be displaced with a time constant, τ_1, of just over 5 min. Furthermore, the pH cycled sample shows nearly the identical τ_1 value, but the surface concentration of this fraction was reduced to just 20%. There is a reasonable fraction of protein that is more difficult to remove, even on the sample that was not exposed to acidic conditions (28%). Substrate defects, trace surface impurities, differences in the orientation of the protein at the interface, as well as other factors may all potentially contribute to this slow component, τ_2. Significantly, τ_2 is substantially affected by pH cycling. Indeed, the 909 min time constant seems to reflect a restructuring of the adsorbed protein and the majority of FRN molecules (80%) now fell under the slow classification. To elucidate the origin of the pH cycling effect, atomic force microscopy, immunochemistry, and vibrational sum frequency experiments were performed.

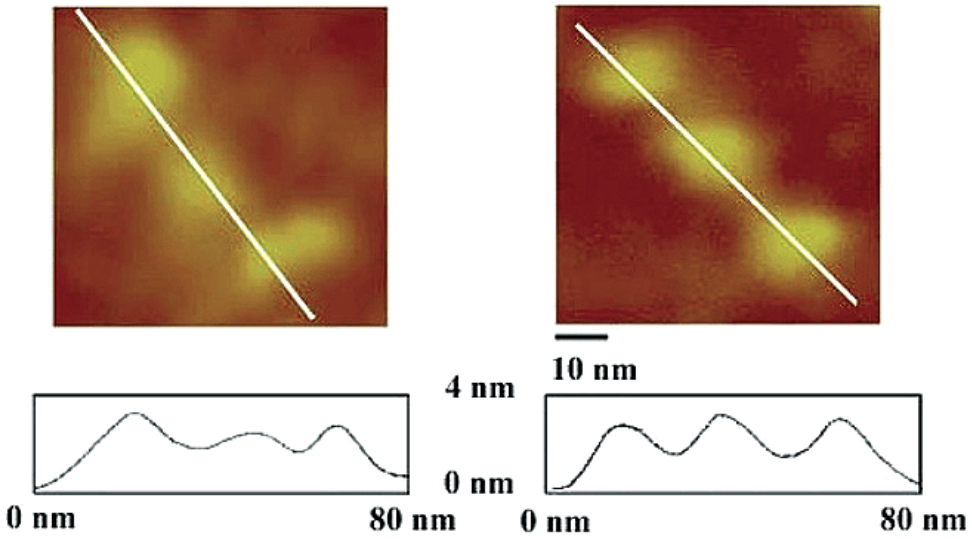

Figure 6. AFM images of a single FRN molecule adsorbed at the silica/buffer interface (a) at pH 8.0 and (b) at pH 8.0 after cycling to pH 3.2. The line profiles for height *vs* position (from the white lines) are shown below each image.

Atomic Force Microscopy and Immunochemistry

FRN was imaged by atomic force microscopy at the silica/buffer interface. As above, a 0.5 μg/mL protein solution in PBS at pH 8.0 was flowed over a planar silica substrate, incubated for 20 min, and replaced with pure buffer before an image was obtained. Under these conditions, approximately 2.5% of the substrate was found to be covered with protein. A close-up picture of a typical fibrinogen molecule is shown in Figure 6-a. The average length of the adsorbed molecules was 59.8 ± 3.4 nm. This number is approximately 30% larger than the value obtained from electron microscope[62] mostly because of convolution with the finite-sized AFM tip and perhaps also because of a small amount of surface spreading by the protein. The three main domains of FRN (one central E domain and two D domains) were clearly identifiable. The height of the D domains averaged 2.7 ± 0.2 nm, whereas the E domain was 2.3 ± 0.4 nm. These numbers are in good agreement with previous data fromhydrophilic mica surfaces.[63] At this point, the pH of the solution was lowered to pH 3.2. Images of adsorbed FRN under these conditions showed little change from the initial conditions at 8.0; however, substantial changes were noted when the pH was cycled back to 8.0 (Figure 6-b). As can be seen, the central E domain was raised significantly, whereas the D domains showed only minor changes. Specifically, the heights of the D domains were still the same (2.6 ± 0.3 nm) within experimental error, whereas the E domains increased to 3.4 ± 0.4 nm. The single molecule experiment was repeated dozens of times and the ~1 nm height increase of the E domain with little change in the D domains occurred roughly 80% of the time.

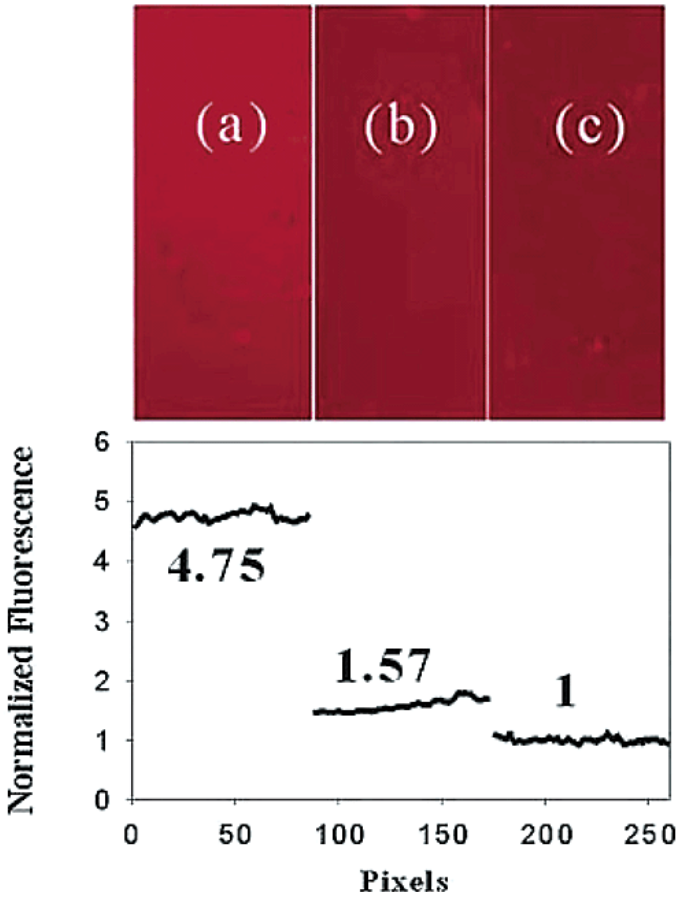

Figure 7. Fluorescence images of Alexa 594-labeled anti-fibrinogen (anti- αC domain) antibody applied to (a) an FRN coated surface after pH cycling, (b) an FRN coated surface at pH 8.0 without pH cycling and (c) an uncoated silica surface. To help inhibit nonspecific adsorption of the anti-fibrinogen antibody, 0.1 mg/mL of generic rabbit IgG was incubated over the surface before the specific binding experiments were commenced.

The other 20% of the time, little or no changes were observed in either the D or E domains. The presence of the minority component is in good agreement with the kinetic experiments, which also showed the presence of two populations.

The AFM studies suggested that for the majority of the FRN, the αC domains migrated from the silica interface to the top of the E domain after pH cycling. To verify this conclusion, immunochemical assays were performed. FRN was deposited onto the surface of three silica samples under the same conditions used above. In the first, the pH was cycled to 3.2 and back to 8.0. A 100 μg/mL solution of dye labeled IgG raised against the αC domains (peptide sequence Aα 529-539) of FRN was introduced above the substrate for 20 min and washed away. The results showed a significant amount of binding of the IgG at the interface as indicated by the high fluorescence signal (Figure 7-a). The binding experiment was repeated with the second sample without pH cycling (Figure 7-b). In this case, the binding was substantially reduced. Finally, a control experiment was performed by adding the IgG over a substrate surface that was not coated with protein (Figure 7-c). Subtracting the nonspecific background found in this third experiment from the data in the first two and taking the ratio of these revealed that 6.6 times as much IgG was specifically adsorbed after pH cycling than before cycling.[64] In other words, the accessibility of the αC domains to the IgG was substantially increased upon cycling. In fact, the αC domains are almost certainly at least somewhat beneath the rest of the protein upon initial FRN adsorption, since they are inaccessible to the IgG. They should also be directly bound to the E domain.[60] Once the pH was lowered to 3.2, however, these moieties became unbound from the E domain, which

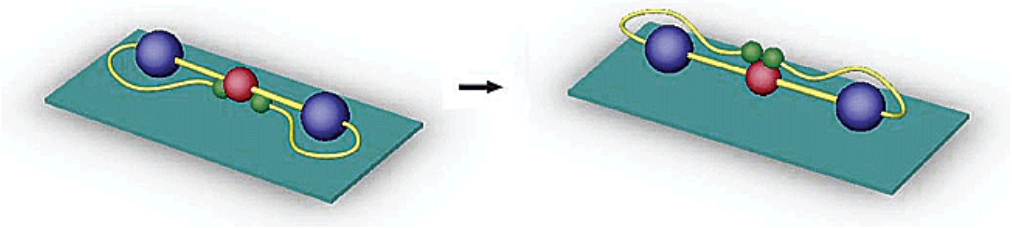

Figure 8. Proposed mechanism for interfacial FRN rearrangement upon pH cycling.

allowed the rest of the protein to come into direct contact with the silica surface. When the pH was subsequently raised to 8.0, these species were forced to rebind to the E domain from the top side of the molecule as the bottom was no longer accessible (Figure 8).

Vibrational Sum Frequency Spectroscopy

VSFS is a surface specific vibrational spectroscopy that can be employed to probe interfacial protein alignment and water structure even in the presence of an overwhelming contribution from bulk aqueous solution.[28, 65-68] Experiments were carried out by first introducing protein free pH 8.0 PBS into a flow cell. An SFS spectrum of the silica/water interface in the OH stretch region of the vibrational spectrum (2800-3600 cm^{-1}) is shown in Figure 9-a. The two peaks visible near 3200 and 3400 cm^{-1} correspond to water molecules with tetrahedrally coordinated structure and water with less ordered bonding, respectively.[18, 20, 69] The interfacial water is ordered by the charged hydrophilic silica surface. At this point, 5.0 μg/mL FRN was flowed into the cell, allowed to incubate for 20 min, and washed out with pure buffer. The surface coverage of fibrinogen was approximately 32% as judged by additional AFM measurements. The VSFS spectrum showed specifically, the 3200 cm^{-1} feature increased in intensity and shifted upward in frequency to near 3280 cm^{-1}. Such a result is very atypical for OH stretch peaks from water at a hydrophilic interface upon the adsorption of a net negatively charged protein.[25] In fact, the charged macromolecules and their counterions should cause a suppression of the water features under these circumstances due to charge

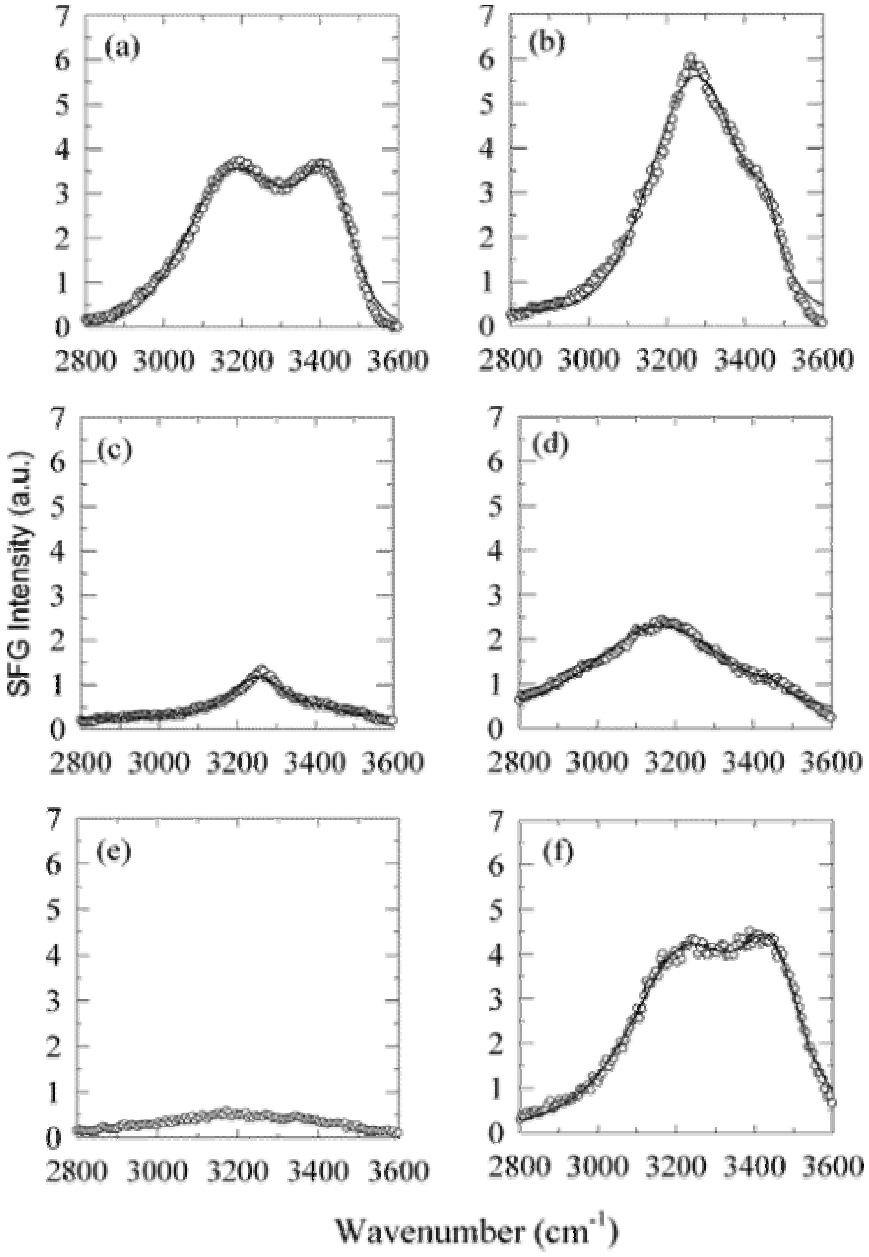

Figure 9. Sum frequency spectra of (a) a bare silica/water interface at pH 8.0, (b) an FRN coated surface at pH 8.0, (c) an FRN coated surface at pH 5.5, (d) an FRN coated surface at pH 3.2, (e) an FRN coated surface at pH 5.5 after cycling to pH 3.2, and (f) an FRN coated surface at pH 8.0 after cycling to pH 3.2.

screening. This is strong evidence that an additional feature is convoluted with the water peaks.

The additional peak could be revealed by lowering the system's pH to the isoelectric point near pH 5.5,[59] which almost completely eliminated the signal from organized water molecules (Figure 9-c). In this case, a small sharp feature near 3280 cm^{-1} was revealed, which can be assigned to the NH stretch of aligned primary amine moieties on lysine residues and the related NH stretches on Arg.[70] Confirmation that this was not an OH stretch peak was obtained by repeating all the experiments in $H_2{}^{18}O$ and noting that the 3280 cm^{-1} feature hardly moved while the OH peaks red shifted by ~12 cm^{-1}, as expected. The spectra at pH 5.5 and 8.0 were shown to be completely reversible by pH cycling between them; however, when the pH was subsequently cycled through 3.2 (Figure 9-d), both the pH 5.5 and 8.0 spectra were changed irreversibly (Figure 9, parts e and f) and the NH stretch peak disappeared.

The presence of an NH stretch upon initial protein adsorption is direct molecular level evidence that lysine and arginine residues become highly oriented at the negatively charged silica interface. Indeed, such orientation is also in excellent agreement with the idea that adsorption via the αC domains is largely electrostatic in nature. It should be noted that when the VSFS experiments were repeated at lower concentration of FRN, that the NH stretch signal became substantially weaker. Because most of the fibrinogen molecules still remained distinct from each other at 32% surface coverage, there is little reason to suspect that the NH stretch peak is the result of protein-protein interactions. Indeed, no major changes in the peak intensity were observed when very high

concentrations (50 μg/mL) of FRN were employed. Under these last conditions, all protein molecules are in contact with their neighbors at the interface. Finally, it should be mentioned that no CH stretch peaks were observed in these spectra, which probably indicated that a high degree of alignment was not achieved for residues other than Arg and Lys. In fact, CH alignment from proteins[28] and polymers[26] at the silica/buffer interface has typically been found only at high pH (e.g., 9-12) where the electric field emanating from the surface was quite large. Even then, CH stretch observation was limited to cases where the macromolecules possessed a net positive charge.

DISCUSSION

The facile displacement of FRN from a silica interface is remarkable given the protein's large size. This property is clearly related to the αC domain's ability to prevent other portions of the protein from making stronger contacts than those afforded by simple electrostatic binding between Arg/Lys residues and deprotonated surface silanols. In the somewhat analogous problem of analyte retention on chromatography columns,[71-73] the literature indicates that very long retention times on silica can be related to isolated surface silanol groups which afford strong hydrogen bonds. On the other hand, interactions with deprotonated silanols seem to be associated only with shorter retention times. In the case of proteins, strongly adsorbing species almost certainly interact with the substrate through hydrogen bonding, van der Waals, and related hydrophobic interactions.[3] The key point for fibrinogen is that these types of interfacial contact can be

substantially attenuated near physiological pH by the intervention of the positively charged αC domains.

The final issue to be addressed here is the role αC domains play in FRN's function in vivo. It is well established that the cleavage of small peptides from the C-terminus of fibrinogen's α and β polypeptides by thrombin forms the active protein, fibrin.[74] Fibrin readily cross-links to form a blood clot in a process known as thrombosis. It is believed that the αC domains can perform a supporting role in maintaining a cross-linked fiber's integrity by interacting with other αC domains on neighboring molecules.[60, 75] Because several of the steps in the blood clotting cascade can be accelerated by the presence of a phospholipid membrane, it is reasonable to consider whether the αC domains may also play a role in keeping fibrinogen soluble in the bloodstream until it is needed. Indeed, many cell membranes are negatively charged and might be expected to interact with the positively charged portion of FRN. Such labile interactions might help prevent fibrinogen from strongly adsorbing to cell surfaces before conversion to fibrin has commenced. It would be curious if the Vroman effect for this molecule were a consequence of such a role for the αC domains. Further experiments will be needed to test this hypodissertation.

SUMMARY

The molecular level details of the displacement of surface adsorbed fibrinogen from silica substrates were studied by atomic force microscopy, immunochemical assays, fluorescence microscopy, and vibrational sum frequency spectroscopy. The results

showed that human plasma fibrinogen (FRN) could be readily displaced from the interface by other plasma proteins near neutral pH because the positively charged αC domains on FRN sit between the rest of the macromolecule and the underlying surface. The αC domains make weak electrostatic contact with the substrate, which is manifest by a high degree of alignment of lysine and arginine residues. Upon cycling through acidic pH, however, the αC domains are irreversibly removed from this position and the rest of the macromolecule is free to engage in stronger hydrogen bonding, van der Waals, and hydrophobic interactions with the surface. This results in a 170-fold decrease in the rate at which FRN can be displaced from the interface by other proteins in human plasma.

CHAPTER IV

VIBRATIONAL SUM FREQUENCY STUDY ON INTERACTIONS OF FIBRINOGEN'S α-C DOMAINS WITH FUSED SILICA

INTRODUCTION

The adsorption of proteins at the solid/liquid interface involves the diffusion of the biopolymer from the bulk solution to the interface, surface denaturation, and rearrangement of the adsorbed layer.[3] It is important to understand these phenomena for immunology,[76] pharmaceutical development,[77] artificial implant construction[77, 78] and chemical/biological sensor design[79, 80]. One of the most important proteins in regard to biocompatibility is human plasma fibrinogen (FRN), an abundant species in the blood stream with a concentration of approximately 3 mg/ml.[81] The X-ray crystal structure of fibrinogen is currently known to a resolution of 5.5 Å.[82] Fibrinogen is a fibrous macromolecule with dimensions of 90 Å × 450 Å x 60 Å and a molecular weight of 340 kD. It consists of two globular D domains and one central E domain linked together by two triple-stranded α-helical coiled coils and has an isoelectric point of ~5.5. Fibrinogen plays a major role in blood clotting by linking platelets together via its polymerization.[83] Several adsorption studies have been performed with fibrinogen on various solid substrates, such as polymers,[84, 85] self assembled monolayers,[86-88] and polyelectrolytes.[89] It has been shown that the adsorption of FRN onto cells and artificial surfaces may lead to problems ranging from heart disease and inflammation to rejection of an artificial

implant.[90] One interesting characteristic of fibrinogen is its unusual behavior on implantable substrates. In coexistence with other plasma proteins in solution, such as kininogen, FRN is known to adsorb early in the adsorption process. Later, however, it is displaced by smaller and less abundant proteins in a process known as the Vroman effect.[49, 50, 52, 58] Fibrinogen adsorbs less well and is more easily displaced from hydrophilic substrates than from hydrophobic substrates.[91] Attempts have been made to follow conformational changes during the time course of adsorption and displacement.[90, 92, 93] For example, ATR-FTIR experiments have been performed, but no definitive information was obtained about the conformation of the protein at the interface.[92, 94] On the other hand, vibrational sum frequency spectroscopy (VSFS) has been proven to be a powerful tool to give information for protein adsorption because of its selectivity for the molecules at the interface.[28, 95] Quartz crystal microbalance (QCM) also has been applied to acquire mass change and conformation change of proteins upon adsorption.[96-98]

We employed a variety of surface specific techniques to probe the conformational changes of adsorbed FRN as a function of pH.[4] A combination of vibrational sum frequency spectroscopy (VSFS), atomic force microscopy (AFM), and immunochemical assays revealed that fibrinogen undergoes a dramatic change in conformation at the silica/aqueous interface upon cycling the pH from 8.0 to 3.2 and then back to 8.0. Specifically, it was found that the αC domains of this protein were initially adsorbed on the surface, protecting the rest of the molecule from intimate surface contact. However, when the bulk pH was cycled to 3.2, the αC domains became detached from the central E domain allowing the rest of the protein to make direct

substrate contact. Raising the pH back to 8.0 forced rebinding to occur between the αC domains and the E domain on the side of the macromolecule facing away from the substrate. This change was directly related to the rate at which 72% of fibrinogen could be displaced from the interface by other proteins in human plasma in about 5 minutes.

In this chapter we will discuss further study on fibrinogen adsorption through protein fragmentation and mimic of fibrinogen adsorption site based on experimental results from VSFS, quartz crystal microscopy (QCM) and fluorescence microscopy. We wished to cleave the fibrinogen molecule into its αC domains and fragment X to compare their respective behavior at the silica/water interface. Specifically, we wanted to identify the strong and sharp peak at 3280 cm^{-1} observed by VSFS and to clarify whether adsorption of fibrinogen is attributed to the αC domains or if other portions of the molecule were also involved. Furthermore, we would like to specify the spectral feature of fibrinogen adsorption at amino acid level. To mimic the adsorption site of αC domains, we designed two peptides; one with alanine and lysine residues and the other with alanine and arginine. Studies with these peptides revealed that the lysine and arginine residues of αC domains were alone responsible for the observed presence of the unique spectral feature of fibrinogen adsorption in the VSFS spectra.

MATERIALS AND METHODS

Materials

Ultrapure water from a NANOpure Ultrapure Water System (Barnstead, Dubuque, IA) with a minimum resistivity of 18 MΩ·cm was used to prepare samples and clean all apparatus during these experiments. Buffers at pH 3.2, 5.5 and 8.0 were made by dissolving appropriate amounts of sodium phosphate into solutions. The pH was adjusted to within 0.1 pH units of the desired value by adding HCl or NaOH. Sufficient NaCl was added to all buffers to raise the total ionic strength to 0.030 M. Human plasma fibrinogen and all the salts and chemicals were purchased from Sigma-Aldrich (St. Louis, MO) if not mentioned specifically. 95% enriched $H_2{}^{18}O$ was used purchased from Medical Isotopes (Pelham, NH) and D_2O (99.9%) was purchased from Cambridge Isotope Laboratories, Inc. (Andover, MA). D_2O solution was prepared by sodium phosphate (monobasic), sodium chloride, and sodium hydroxide-d were used to get the same ionic strength as the PBS H_2O solution and pD of 8.4, which is relevant to pH 8.0.

Lysine peptide and arginine peptide were designed to have helical structures and lysine or arginine residues to be aligned on one side of the helices. The peptide sequence for Lysine peptide was TSKAAAKAAKAAAKAAKAAAKAS, and the same sequence was used for Arginine peptide only by replacing lysine with arginine. Both of the peptides were purchased from SynPep (SynPep co., Dublin, CA) and used as we received. Molecular mass was measured with MALDI and helical structure was confirmed with circular dichroism for each peptide sample.

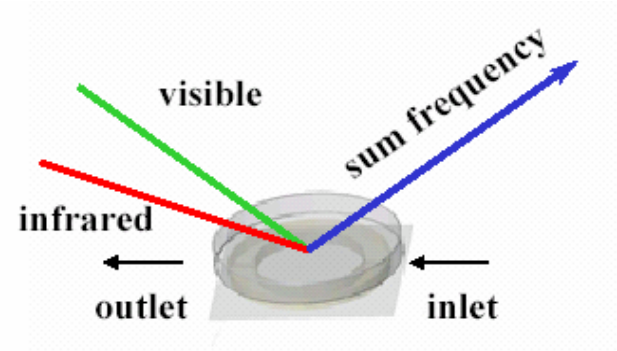

Figure 10. Diagram of the flow cell setup used for adsorption studies of fibrinogen and αC domains at the silica/water interface. The laser beams used in the VSFS experiments are color coded: red for the tunable infrared radiation, green for the 532 nm beam, and blue for the sum frequency beam.

Vibrational Sum Frequency Spectroscopy (VSFS)

Theoretical and experimental details were mentioned in the previous chapters (Chapters II and III). VSFS spectra were taken with two types of flow cells; one with two quartz windows on a Teflon body with sample volume of 2 mL and the other with a quartz plate on a poly(dimethylsiloxane) (PDMS) body with the volume of 200 μL, which was assembled by sandwiching a glass cover slip and a quartz disc on either side of a 2 mm thick PDMS slab containing an 11 mm diameter hole (Figure 10). PDMS body and glass plates or quartz plates were cleaned with plasma cleaning before bonded together. Small volume of flow cell was used for $H_2{}^{18}O$ experiments and peptide experiments to reduce the dead volume. All the quartz plates are cleaned with chromic acid for 4 hours and rinsed with copious distilled water and rinsed with DI water, and baked in the oven for 5 hours at 350 °C. Glass plates were cleaned with 7X detergent and rinsed with distilled water and DI water, and annealed at 450 °C for 5 hours. Each flow cell was equilibrated with pH 8.0 PBS buffer solution before the protein solution was introduced. After 20 minutes of incubation time, extra protein was rinsed with the same buffer solution. Very little difference was noted between these two sets of spectra. Therefore, only spectra after rinsing are presented here. Ellipsometry measurements also confirmed that little change in the protein layer thickness occurred upon rinsing.[81]

A data acquisition program written in LabView 5.0 (National Instruments, Austin, TX) was used to acquire spectra for each experiment. The fitting of each VSFS spectrum was performed with a Voigt profile by a program written in MatLab version 5.3 with the optimization toolbox version 2.0 (MathWorks Inc., Natick, MA). After

collection, the data were transferred to SigmaPlot 2001 (SPSS Inc., Chicago, IL) for further treatment.

Quartz Crystal Microbalance (QCM)

Frequency shift (Δf) and dissipation constant change (ΔD) due to adsorption and desorption were measured with QCM-D (Q-Sense Inc., Newport Beach, CA) with the resolution in Δf and ΔD of 1 Hz and 1×10-6 respectively. The relation between frequency shift and mass change can be written as the Sauerbrey relation below.[41]

$$\Delta f = -n\frac{1}{C}\Delta m \qquad (13)$$

where Δm is mass change, n is resonance number, and C is the mass sensitivity. For a 5 MHz quartz, C is 17.7 ng cm^{-1} Hz^{-1} at its fundamental mode (n=1). Dissipation change of an adsorbate on a surface is due to its conformation change and/or to the interaction between adsorbates. A 5 MHz crystal coated with SiO_2 was used for this study and plasma-cleaned before being used. The quartz plate was equilibrated with DI water and pH 8.0 buffer solution before protein solutions were introduced. The results shown in this paper are presented after pH 8.0 equilibrium.

Total Internal Reflection Fluorescence Microscopy (TIRFM)

Desorption experiments with αC domains were performed by labeling these molecules with Alexa Fluor-594 dye from Molecular Probes (Eugene, OR). The labeling degree was kept to 0.5 dyes/αC. Time dependent monitoring was done by total internal reflection fluorescence microscopy (TIRFM) using a Nikon E800 fluorescence

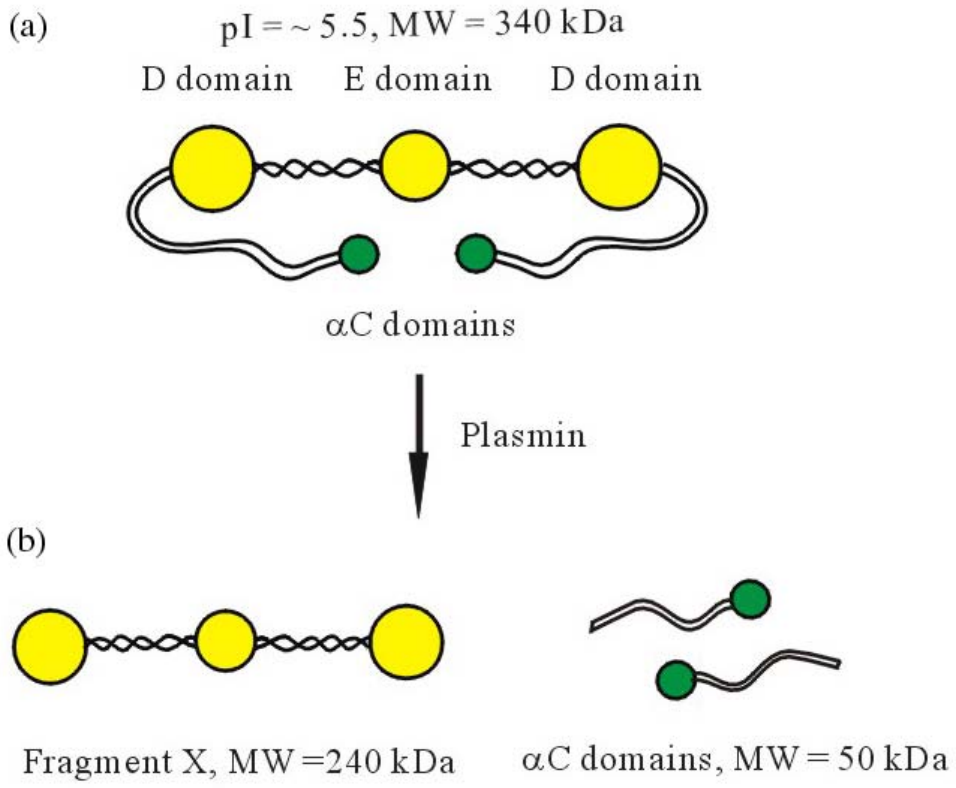

Figure 11. Schematic diagram of the structure of (a) an intact fibrinogen molecule and (b) its fragment X and αC domain components produced by cleavage with plasmin.

microscope equipped with a Micromax 1024B CCD camera (Princeton Instruments). All images were acquired under a 10X objective. TIRFM was performed by reflecting a 1 mW 594 nm Helium-Neon laser beam (Uniphase Manteca, CA) off the sample/solution interface using a dove prism setup, which was optically coupled to the backside of the planar silica substrate through immersion oil.

Enzymatic Cleavage of Fibrinogen

The concentrations of FRN solutions were determined by absorption measurements at 280 nm in an UV/visible spectrometer with the adsorption coefficient of 1.51. To prepare αC domains (~50 kD) and the fragment X species, fibrinogen (20 mg/ml) in a 10 mM, pH 7.2 phosphate buffered saline (PBS) solution was digested with plasmin (0.02 caseinolytic unit/ml, United States Biological, Swampscott, MA) at 25 °C for 6 hours.[60] (Figure 11) After cleavage, 1 mM of 4-(2-aminoethyl) benzenesulfonylfluoride, HCl (AEBSF, Calbiochem, San Diego, CA) was added as a protease inhibitor to stop the reaction. The fragments were purified and separated using an AKTA FPLC (Amersham Biosciences, Piscataway, NJ) with a Superdex 200 HR 10/30 size exclusion column. Molecualr weights of fragments were determined by matrix-assisted laser desorption/ionization (MALDI) mass spectroscopy. The isoelectric point of α-C fragment was measured as 6.5 by Imaging Isoelectric Focusing (Convergent Bioscience, Toronto, Canada).

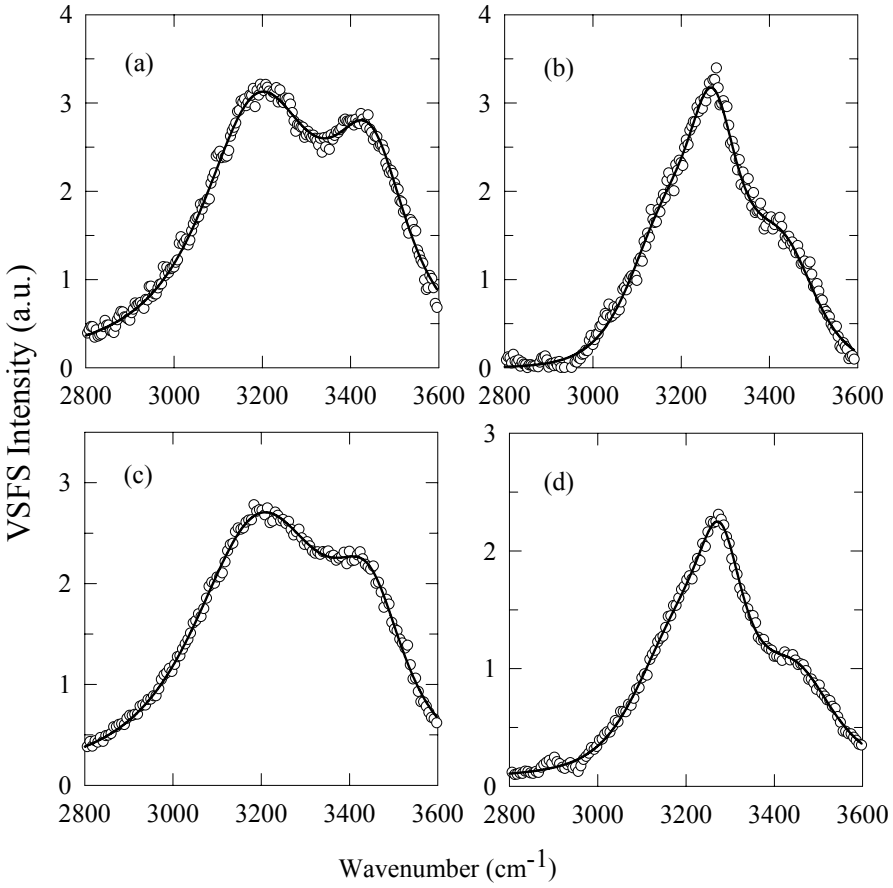

Figure 12. Sum frequency spectra of (a) bare quartz/water interface at pH8.0 PBS buffer solution, and adsorptions of (b) fibrinogen (c) fragment X and (d) alpha C domains on quartz surfaces in pH 8.0 PBS buffer solutions.

RESULTS AND DISCUSSION

Fragment X and αC Domains Adsorbed at pH 8.0 in H_2O

Human plasma fibrinogen was cleaved into fragment X and αC domains as described in the experimental section. Adsorption experiments were attempted with fragment X at pH 8.0 from a protein solution in PBS (Figure 12-c). The VSFS spectrum looks almost identical to that for the bare silica/water interface. The peaks from the bare silica/water system have been assigned in previous studies.[18, 20, 69, 99] There are two major peaks in the spectra and the first near 3200 cm^{-1} is associated with the OH stretch of interfacial water tetrahedrally coordinated to neighboring molecules. The feature near 3450 cm^{-1} is from water molecules that lack full complement of hydrogen bonds, and is, hence, somewhat disordered respect to the first species.[100] However, adsorption experiments with the αC domains under the same conditions led to large spectral changes (Figure 12-d). The major peaks from bare silica/water spectrum are attenuated and a new feature at 3280 cm^{-1} is dominating. The whole spectrum could be well fit with a three-peak model. The same peak observed from the intact fibrinogen molecules again appears at the same wavenumber. (Figure 12-b) In fact, the spectrum looks almost identical to the one from adsorbed fibrinogen under the same condition. This result is in agreement with the idea that fibrinogen adsorption occurs via the αC domains and that this portion of the molecule is responsible for the highly aligned peak seen around 3280 cm^{-1}. We will discuss more about contribution of αC domains on the fibrinogen adsorption at the discussion section of TIRFM. Even though the VSFS experiments with fibrinogen fragments gave discerning information that the spectral feature of fibrinogen

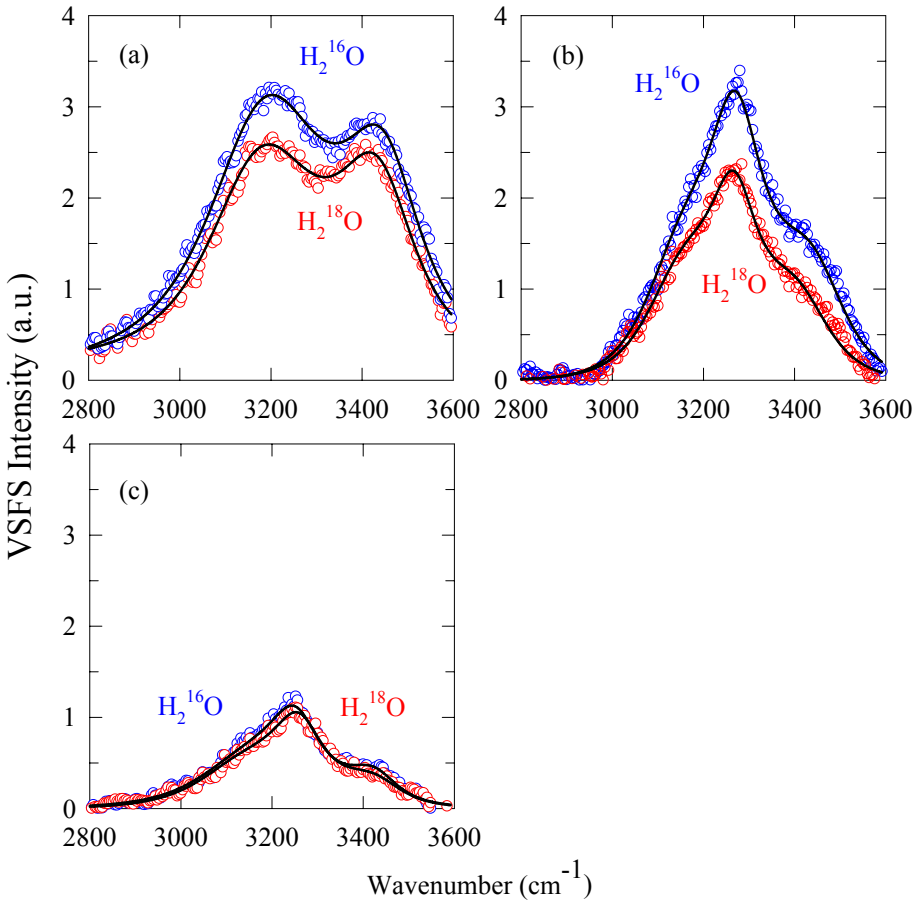

Figure 13. Sum frequency spectra of (a) a bare silica/water interface at pH 8.0 in PBS buffer, (b) an FRN coated silica/water interface at pH 8.0, and (c) an FRN coated silica/water interface at pH 5.5. In these spectra $H_2{}^{16}O$ data are plotted with blue circles and $H_2{}^{18}O$ with red circles.

adsorption was mainly from αC domains of the protein, the identity of the peak was still not clear.

Fibrinogen Adsorption in ^{18}O Labeled Water

There are two possibilities for the 3280 cm^{-1} peak, which are OH or NH stretches. We performed fibrinogen adsorption experiments in $H_2{}^{18}O$ solutions to determine the identity of the peak. VSFS spectra of the silica/water interface in the presence of $H_2{}^{16}O$ and $H_2{}^{18}O$ are shown in Figure 13-a. It is expected that both the frequency and intensity of the OH stretch features should be red-shifted through isotopic labeling. Isotope labeling experiments were performed with 95% isotopically pure $H_2{}^{18}O$ and less than 0.2 mol% sodium hydroxide ($Na^{16}OH$), which was added to prepare the appropriate PBS buffers. The peak shift caused by isotopic substitution is expected to be on the order of ~10 cm^{-1} by simple reduced mass arguments. Experimentally, red-shifts of 7 and 11 cm^{-1} have been measured for the 3252 and 3405 cm^{-1} peaks of water via Raman and FTIR spectroscopy.[101, 102] The fitting the VSFS spectra revealed that the oscillator frequency for the lower peak shifted from 3185 to 3172 cm^{-1}, while the higher frequency stretch moved from roughly 3444 to 3434 cm^{-1} (Figure 13-a). What is easier to observe by eye, however, is the reduction in intensity of the peaks, which has also been observed in the corresponding infrared experiments.[103, 104] This occurs because the magnitude of the dynamic dipole is smaller for the ^{18}OH stretch than it is for the ^{16}OH stretch.

Figure 13-b shows VSFS spectra of the silica/water interface in the presence of an adsorbed fibrinogen layer at pH 8.0 in PBS with $H_2{}^{16}O$ and $H_2{}^{18}O$. The fibrinogen was deposited from a protein solution and the excess was washed away with the same

buffer solution after 20 minutes of incubation. Again, the intensity from the ^{18}OH spectrum is weaker than that from ^{16}OH. The data were curve fit and showed an approximately 12 cm^{-1} shift for the water peaks, but a significantly smaller shift for the third feature from 3279 to 3273 cm^{-1}. Since this peak overlapped strongly with the OH peaks and was difficult to resolve, the origin of this partial shift was not clear. To discern this, the data were repeated at pH 5.5 where the intensity of the water peaks could be greatly diminished (Figure 13-c). The OH attenuation occurred because the ζ-potential of the fibrinogen coated silica surface was close to zero.[59] Under these conditions, no difference was seen in the VSFS intensity between the $H_2{}^{16}O$ and $H_2{}^{18}O$ labeled systems. Peak fitting in this case revealed that there was no measurable peak shift within experimental error. Such isotopic labeling data represent strong evidence that the feature in question is not from an OH stretch, but rather from an NH stretch. In fact, the frequency of this peak is an excellent match for the corresponding lysine and arginine residues.[105, 106]

Peptides Adsorbed at pH 8.0 in H_2O

Since we identified the 3280 cm^{-1} peak as an NH stretch, it would be clearer if we could reproduce the same peak from a synthesized molecule. The positive charge on the lysine and arginine moieties was supposed to provide driving force to adsorb the peptide on a negatively charged surface. Thus we designed peptides that have lysine or arginine residues on a helical side. The schematic of lysine adsorption on a quartz surface at pH 8.0 is presented on figure 14. Upon peptide adsorption, the water peaks were diminished by cancellation of the charge at the interface and the peak from the NH

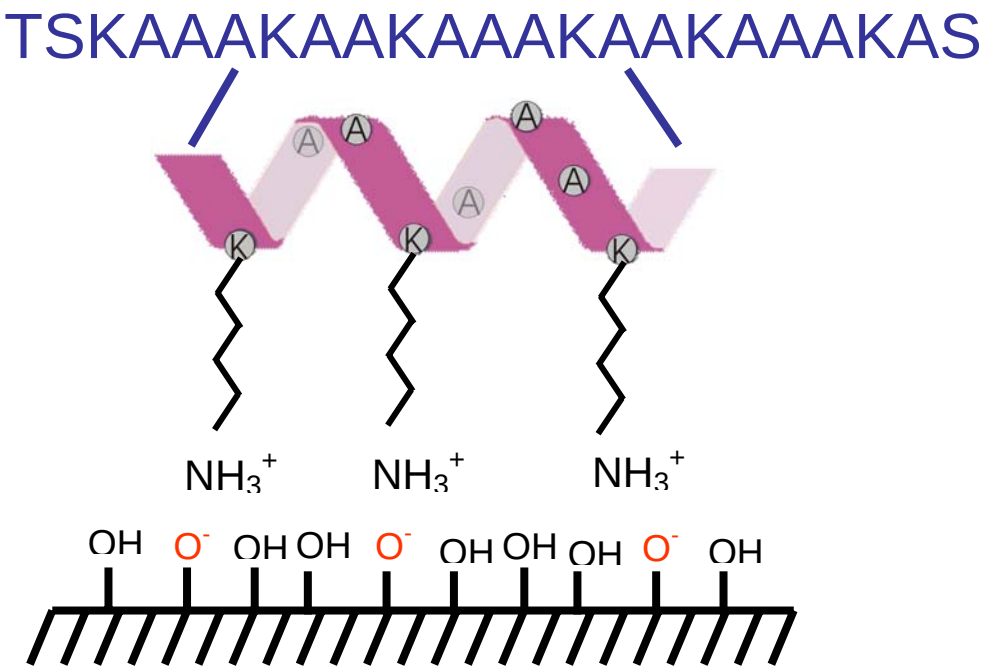

Figure 14. Schematic figure of lysine peptide binding to the quartz surface. Lysine residues of the peptide aligned on one side of the helical peptide. For the arginine peptide, the sequence was the same as that of lysine peptide except that the lysine was replaced with arginine.

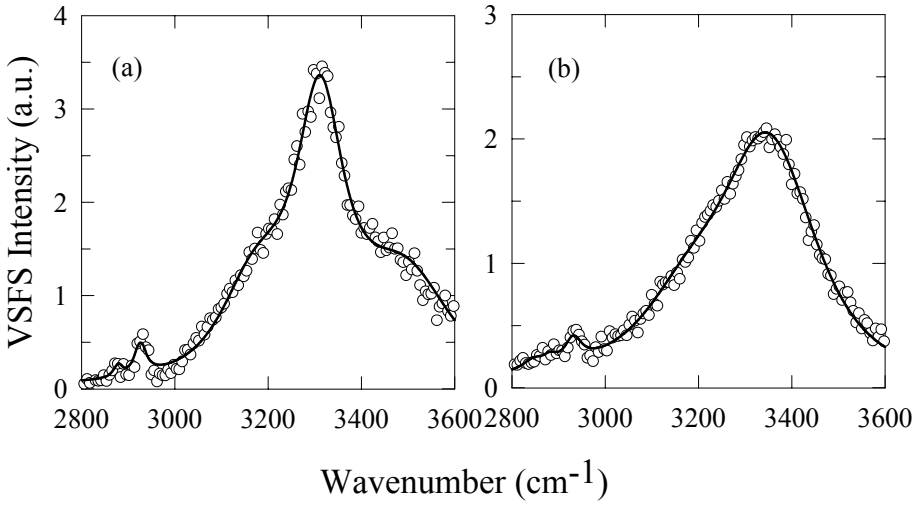

Figure 15. Sum frequency spectra of (a) lysine peptide and (b) arginine peptide on quartz surfaces.

stretch was magnified by alignment of the same functional groups on one side of the peptide since the VSFS intensity is proportional to the square of the averaged polarizabilities of active molecules at the interface. VSFS spectra of lysine peptide and arginine peptide adsorbed on the surface (Figure 15-a and -b) at pH 8.0 showed similar NH peak as from fibrinogen and α-C fragments even though the peak positions were slightly different from that of fibrinogen. The NH peak from the lysine peptide is at 3310 cm^{-1} and the peak from the arginine peptide is at 3330 cm^{-1}. The lysine and arginine residues in fibrinogen is assumed to be experiencing high degree of hydrogen bonding, which causes red shift of the NH peak compared to the peak from the peptides. The NH peak of arginine-peptide was not as sharp as that of lysine-peptide, which is reasonable because the amine groups of arginine are in resonant structure and the positive charge is shared by three amine groups.

H/D Isotope Exchange on Lysine Peptide

We successfully mimicked the NH peak of fibrinogen from synthesized peptides, but it does not provide conclusive information on which NH stretch we are observing. Namely, the protein molecule contains both a backbone NH as well as the side chains of the lysine and arginine. The backbone NH can give rise to a single amide A band around 3300 cm^{-1}, while the latter leads to two peaks for the lysine amine, an asymmetric as well as a symmetric stretch (with the symmetric being in the same frequency range as the amide), and a single amine peak for the arginine.[107] In the present case only signal from the symmetric stretch is seen as this mode is probably aligned normal to the interface, while the asymmetric stretch is in plane. It is far more likely that

the signal comes from the side chains rather than from the backbone. These moieties are positively charged and should be directionally oriented toward negatively charged quartz surface. This argument is bolstered by analogous data from polydiallyldimethyl-ammonium chloride orientation at the silica/buffer interface, which shows that only the methyl groups attached to the charged quaternary nitrogen are oriented at the interface, rather than the CH_2 groups from the backbone of the polymer.[26] To figure out which NH is responsible for the VSFS peak, we pursued H/D isotope exchange experiment on lysine peptide. We adsorbed lysine peptide on a quartz surface at pH 8.0 and introduced D_2O into the flow cell, and monitored the intensity change of NH peak at 3310 cm^{-1} with VSFS. The sample volume was 200 μL and we flowed 2 mL of D_2O solution in 30 seconds. As shown in figure 16-a, the NH peak intensity dropped right after D_2O was introduced and the peak disappeared within the flow time, which means the exchange rate for the NH peak was much faster than our experimental limit. It is already known that the H/D exchange rate for side chain amine group is less than a second.[108] The exchange rate for backbone hydrogens is varied from seconds to weeks depending on the environments that peptide or proteins are experiencing. Especially when the amide hydrogens are in intramolecular bonding as well as hydrogen bonds, H/D exchange requires weeks to months to exchange.[108, 109] Since the amide hydrogens of the lysine peptide are connected to other amide hydrogen with hydrogen bonds forming helical structure, isotope exchange rate for the backbone is expected to be much slower. That means the fast H/D exchange observed from our experiments only could happen from

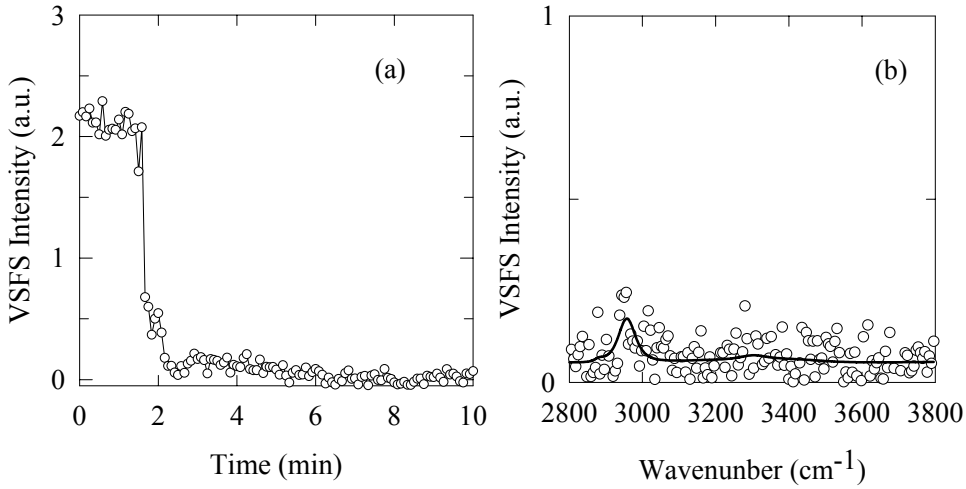

Figure 16. H/D isotope exchange for lysine peptide. (a) Time dependent sum frequency signal of NH peak. D_2O was introduced at 1.7 minute. (b) Sum frequency spectra of lysine peptide after isotope exchange.

the amine groups of lysine or arginine residues on the peptide, not from the backbone. Here we assumed that the lysine peptide conserves its helical structure upon adsorption and it is already known that the helical structure of fibrinogen well maintained on a hydrophilic surface with Grazing Angle FTIR (GA-FTIR).[110] An SFG study also showed that a helical peptide stayed on its helical conformation at solid/liquid interface.[111] The VSFS spectrum of lysine peptide after the D_2O exchange was shown in figure 16-b. All the water peaks and the NH peak had disappeared and only a trace of CH region was left on the spectrum.

Quartz Crystal Microbalance

Quartz crystal microbalance was used to measure mass change and conformation change upon adsorption and desorption of the protein and peptides. Figure 17 showed QCM results for the fibrinogen (a), αC fragments (b), the lysine peptide (c), and the arginine peptide (d). Adsorption mass for each sample after rinsing with pH 8.0 was 1.13 μg cm^{-2}, 156 ng cm^{-2}, 127 ng cm^{-2} and 143 ng cm^{-2} for the fibrinogen, αC fragments, the lysine peptide, and the arginine peptide respectively. For the lysine peptide and the arginine peptide, the adsorption mass decreased to about 40% of the original mass after rinsing with pH 3.2, where the quartz surface is almost neutral. The results showed that the driving force for peptide adsorption on the quartz surfaces at pH 8.0 was mainly electrostatic interaction between negatively charge surface and positively charged lysine and arginine residues. In contrast, fibrinogen remaining on the surface after pH change was 73% and almost all αC fragments (93%) stayed on surface even when there is

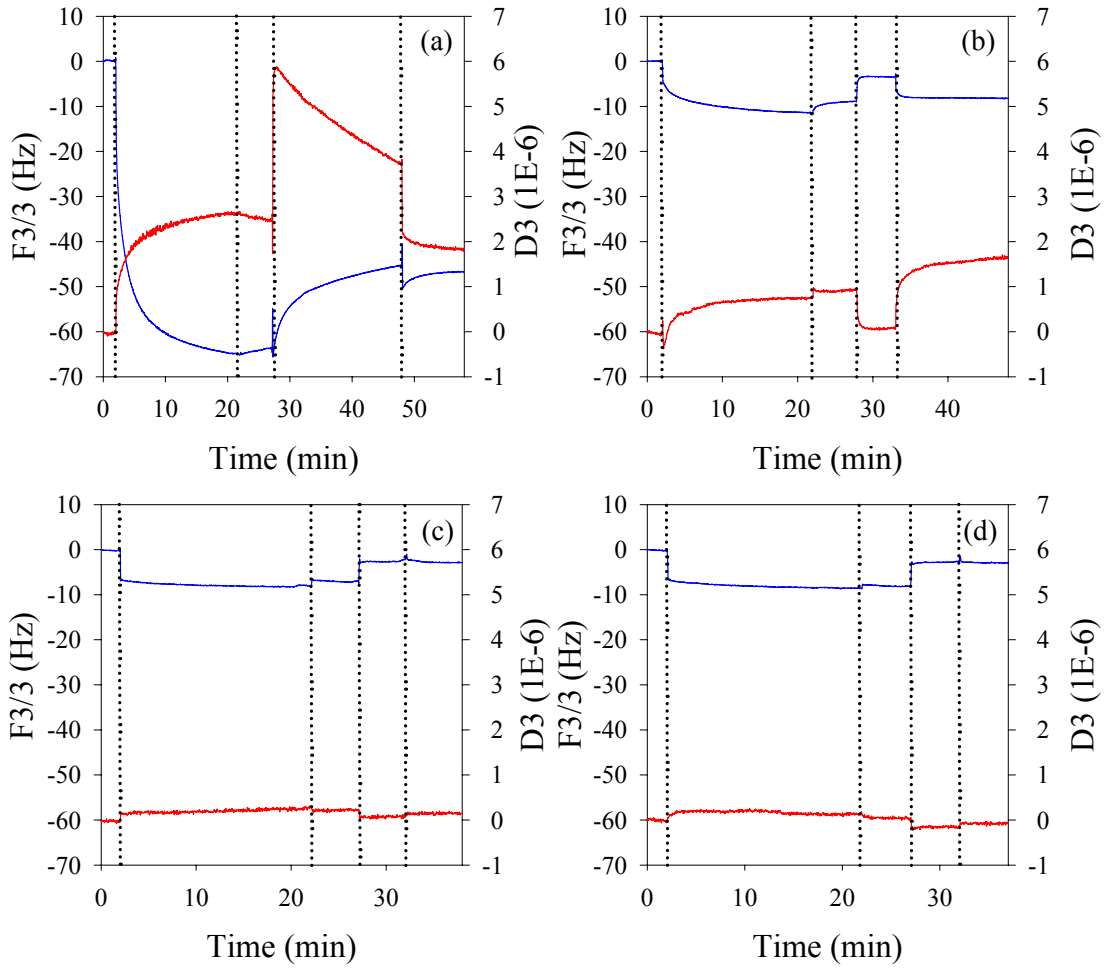

Figure 17. Frequency shift (blue) and dissipation constant change (red) by adsorption and rinsing for (a) the fibrinogen (b) alpha C fragments (c) the lysine peptide (d) the arginine peptide. Initial condition is PBS buffer solution of pH 8.0. The first line is for flowing adsorption material, the second is for pH 8.0, the third line is for pH3.2 rinsing and the last line is for pH 8.0 rinsing.

almost no charge on the surface, which means adsorption process of those species is driven by more than electrostatic force and could be combination of hydrogen bonding and electrostatic interaction. Surprisingly, the number of serine and threonine residues takes about 25% of the total number of amino acid sequence in each αC fragment and there are plenty of sections where there are 3-5 of serine and threonine residues in a row next to the lysine or arginine residues.[112] VSFS experiments already showed that the fibrinogen adsorption is mediated by αC domains via positively charged lysine and arginine residues and we propose the hydrogen bonding of serine and threonine is doing supporting role for the adsorption. It was also possible to monitor conformational change of fibrinogen and fragments adsorptions from changes for dissipation constants measured by QCM. Peptides showed very little change in dissipation constant upon pH change, but fibrinogen and αC fragments showed distinctive difference due to pH change. The results showed that fibrinogen and αC experienced significant conformation change while peptides did not.

Time Dependent αC Domain Displacement

We already showed that the spectroscopic feature of fibrinogen adsorption was very similar with that of αC domains. Furthermore, we tried to figure out whether the Vroman effect would be similar for those two species. The αC domains were fluorescently labeled with Alex 594 as described in the experimental section. Displacement experiments were monitored with TIRFM by using a sample that was optically coupled to a dove prism. To conduct the experiments, 10 μg/ml of fluorescently labeled αC domains were first coated on the silica surface from PBS

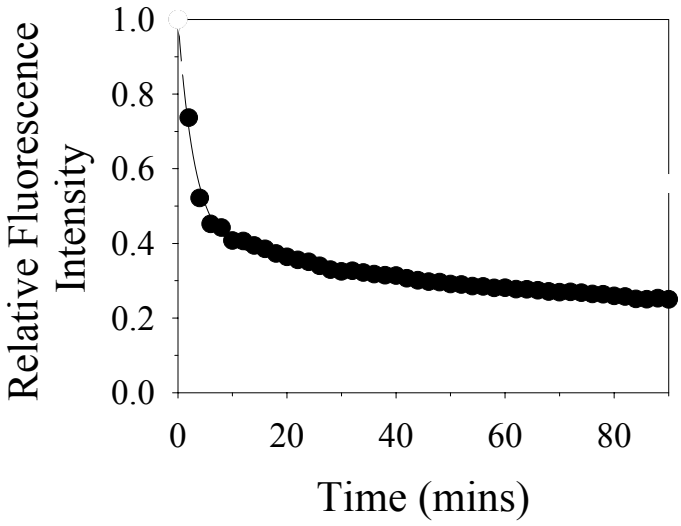

Figure 18. Displacement of Alexa 594 labeled αC domains from a silica surface. The closed circles (•) indicate displacement experiments with 5% human plasma at pH 8.0.

solutions for 20 minutes. Next, 5% human plasma was introduced to the interfaced at time t = 0 min. As can be seen from the data (Figure 18), the αC domains were displaced from the interface in an exponentially decaying fashion. The data fit well to a double exponential where the first time constant, $\tau = 3 \pm 2$ min, corresponded to about 60% of the adsorbate population. The rest of the adsorbate population (~40%) could be assigned to a slower time constant, $\tau = 175 \pm 63$ min. This same double exponential behavior was noted in our previous experiments with intact fibrinogen molecules under the identical displacement conditions.[4] In fact, the two time constants for displacement were identical within experimental error; however, the fast time constant represented a slightly larger fraction of the surface adsorbed material, 72%, in the case of the whole protein.

The fact that the displacement behavior for intact fibrinogen matches so closely with that of the αC domains is evidence that the two time constants arise from similar interactions in each case. For whole fibrinogen molecules, it would have been conceivable that the faster time constant would have been more closely associated with contact by only the αC moieties, while the slower time constant arose from portions of fragment X. However, since αC displacement alone can give rise to the same time constants, it is more likely that this portion of the protein interacted with the surface was primarily responsible for both constants even in the case of the whole protein. Indeed, heterogeneous silica surface chemistry may give rise to the two types of interactions of the αC domains with the interface. Areas where lone silanols are present might be responsible for the more tenaciously bound population.[73, 113] It is also possible that

slightly different configurations for the αC domain adsorption could give rise to the kinetics observed. Based upon the evidence from the chromatography literature,[113] however, the former is probably the more likely explanation.

A curious result from the above data was the slight difference in the populations for the displacement kinetics at pH 8.0 by human plasma for αC domains from intact fibrinogen. At first glance one might have expected the fraction of αC domains that were quickly displaced to be higher than the FRN. This would be based on the idea that any additional interactions of the fragment X portion of the molecule with the underlying substrate would lead to slower displacement. However, if the αC domains can protect the overwhelming majority of FRN molecules from further interactions with the substrate, then this need not be the case. In fact, the αC domains probably have the potential for increased interaction with the silica when they are not associated with the rest of the macromolecule. For intact FRN at pH 8.0 the C-termini of the αC domains interact strongly with central E domain,[60] and, therefore, probably avoid direct surface contact. In the case of the fragment, however, this moiety is free to interact with the underlying silica surface and may contribute to a modest reduction in the population, which can undergo rapid displacement. Indeed, the C-terminus of the αC domain is the only part of this species, which is globular (Figure 11), and it actually contains a single disulfide linkage. [112]

The behavior of αC domains, which play an important role in the Vroman effect for fibrinogen, was investigated by VSFS and other techniques. Earlier study showed that fibrinogen adsorption gave a sharp and narrow peak at 3280 cm^{-1}. On this chapter

we performed enzymetic cleavage on fibrinogen and demonstrated that only αC domains were responsible for the spectral feature. Furthermore, we proved by using ^{18}O labeled water, that the 3280 cm^{-1} feature observed in the VSFS spectra was not from an OH stretch, but rather from an NH stretch. This is consistent with the VSFS results from synthesized peptides, which showed similar NH peaks due to adsorption of lysine and arginine residues aligned on the surfaces. Also QCM results suggested that the main driving force for αC domains adsorption onto the hydrophilic substrate was more than electrostatic interactions but combination of hydrogen bonding and other interactions. Finally, it was shown that variable interactions between the αC domains and the substrate alone could account for the complex displacement kinetics of the protein by human plasma seen at pH 8.0.

SUMMARY

Understanding protein adsorption is important for the development of biosensors and biomaterials and vibrational sum frequency spectroscopy (VSFS) has been applied to study adsorption behavior of proteins at biological interfaces. Our previous study showed VSFS spectra of fibrinogen adsorption on a quartz surface presented a new peak at 3280 cm^{-1}. In this section, we successfully assigned the peak to NH stretch by ^{18}O isotope experiments and also showed that only αC domains are responsible for the spectral feature of adsorbed fibrinogen, which suggested that the fibrinogen adsorption proceed via αC domains contacting on the surface. Total internal reflection fluorescence microscopy (TIRFM) also showed similar kinetics between αC domains and the protein

itself. VSFS with synthesized peptides showed that the NH peak was from the side chains of lysine and arginine residues and it was supported by H/D exchange experiments. Mass change and conformation change of the protein and the peptides were monitored by quartz crystal microbalance-D (QCM-D) by measuring frequency shift and change of dissipation constant. Based on the QCM results and amino acid sequence of αC domains, hydrogen bonding in addition to electrostatic interaction was suggested as a driving force for the fibrinogen adsorption on silica surface.

CHAPTER V

VIBRATIONAL SUM FREQUENCY STUDY ON ION EFFECT ON ALKYL CHAIN OF LIPID MONOLAYER*

INTRODUCTION

Protein conformation is sustained by the subtle balance between intra- and inter-molecular forces such as electrostatic forces, hydrogen bonding forces, and hydrophobic forces.[74] Protein denaturation happens when the balance among those forces are broken by heating, pH change, adding detergents or water-soluble organic substances into the solution. Salt effect on protein conformation is prominent because it could function as both stabilizing and destabilizing effect depending on the ion species. The effect has been studied for more than a century and the order of ions' ability to stabilize hen egg white protein is known to be the Hofmeister series.[6] Anions in the order of stabilization is $SO_4^{2-} \cong HPO_4^{2-} > F^- > Cl^- > Br^- > NO_3^- > I^- (\cong ClO_4^-) > SCN^-$. The ions on the left side of chloride are known to stabilize proteins and ions on the other side of chloride are to destabilize. Protein-stabilizing ions are called kosmotropes, which are also known as "water-structure makers" and destabilizing ions are chaotropes or "water-structure breakers".[11] Several characteristics of the Hofmeister effects were summarized by

---

* Part of this chapter reproduced with permission from "On the Mechanism of the Hofmeister Effect" by Marc C. Gurau, Soon-Mi Lim, Edward T. Castellana, Fernando Albertorio, Sho Kataoka, and Paul S. Cremer, *J.Am.Chem.Soc*. **2004**, *126*, 10522-10523. Copyright 2004 American Chemical Society.

Collins and Washabaugh. The effect is dominated by anions in the concentration range of 0.01 ~ 1.0 M, where electrostatic contribution is screened. The Hofmeister series has attracted scientists for more than a century because it has been found not only in protein solubility, but also in many other biological phenomena such as enzyme activity, DNA-protein interactions, and ion-vesicle interactions.[7, 114] Collins and Washabaugh tried to explain the effect by ion ability to alter hydrogen-bonding properties of water and suggested three water layers around ions.[11] The first layer is highly dependent on hydrogen bonding ability of ions, the second layer depends on competition between the hydrogen bonding effect and bulk property, and the third layer is bulk-like. The first interfacial water layer was proposed to be tightly bound to the kosmotropes but loosely for the chaotropes. Hribar and co-workers performed molecular calculation and showed consistent results with Collins.[12] The water-structuring concept has been admitted as a proper explanation for decades but recently there are many debates over its fidelity. Among them were vibrational relaxation studies of water by Bakker *et al.*[16, 115] They showed that bulk water was not affected by ions, but the solvation shells of ions showed differences because of ions, which is very useful to understand the Hofmeister effect as interfacial phenomenon, even though there were not enough studies focused on the interfaces related to the Hofmeister series.[116]

Others suggested explaining the Hofmeister effect with screening effect, ion-binding, and dispersion contribution. Different degrees of screening effect from various ions also important to understand the Hofmeister effect, especially for charged systems.[117] The screening study of proteins showed that the effect is higher for

denaturing salts in the concentration range of 0-1M, even though the screening effect is considered important for lower concentrations (<10mM) of salt solutions.

Another explanation is the ion-binding theory.[118-120] There could be three types of binding; direct, indirect, and bridging. Direct binding should include losing hydration shell from ions, indirect one would be more properly called adsorption and ions in this case will keep their hydration shell or partially lose, and anion-bridging was reported in *t*-butanol study in salt solutions.[14] Nonetheless, there was no direct evidence to show how water behaves related with those various types of binding.

Dispersion force has been suggested as an important factor in Hofmeister effect especially in biological conditions where ionic strength is high enough to screen electrostatic interactions. Ninham and co-workers published theoretical and experimental results to prove the importance of dispersion force in various biological environments.[121, 122] Dispersion force is a part of van der Waals force, which is a combination of induction, orientation, and dispersion.[2] For polarizable molecules, those three factors are all important, even though the dispersion is still the most important factor, but between non-polarizable molecules, the van der Waals is purely dominated by the dispersion force. Unique behavior of the Hofmeister ions is showing a different effect caused by the ions with the same charge and it cannot be explained by DLVO (Derjaguin-Landau-Verwey-Overbeek) theory, which is combination of Poisson-Boltzmann description for the electrostatic forces and Lifshitz theory for the van der Waals forces.[123] Whereas, the Hofmeister effect in biological environment could be

explained by difference in dispersions forces, which is originated from induction of polarization, since the ions have different polarizabilities.[124]

The Hofmeister effect can be understood as a full figure only when there were enough explanations given for hydrophobic residues as well as water structure. There were many attempts to explain the Hofmeister effect for conformational change of biological molecules such as proteins, DNA, and cell membranes, as well as water structures around these molecules, but there was not enough study to show the ionic effect on hydrophobic residues, which is in many cases main structural component. Sum frequency generation (SFG) is nonlinear optical process that gives vibrational information of molecules at interface.[4] SFG signal intensity is proportional to the square of nonlinear polarizability, which depends on nonlinear susceptibility that is a sum of non-resonant and resonant part. Resonant susceptibility is proportional to the average number of molecules and the orientation average of them.[18, 19] Therefore SFG signal from the bulk, which has inversion symmetry, will be canceled and only molecules at interface give sum frequency signal. The advantage of VSFS is that both the interfacial water structure as well as the ordering of the monolayer can be followed directly. Ionic effect on chain ordering at the interface of charged surface and solution was reported for CTAB. [125] The efficiency of surfactant was the highest for fluoride and the lowest for bromide, but there was no strong evidence for anionic effects on the structure of the monolayers. They also tested the result of counter ion concentration effect, but no effect was observed from the added counter ions.

Anion effects on interfacial water structure were reported by Allen and co-workers and their results showed that iodide ion induced more water alignment than fluoride at the air/water interface.[126] However, they only covered halide ions and the ion distribution at the interface was only driven by hydrophobic property of air and no correlation to the Hofmeister effect was discussed.

Herein we investigated the Hofmeister effect in octadecylamine (ODA), dimethyldidodecylammonium bromide (DDAB), and 1,2-Dilauroyl-*sn*-Glycero-3-Phosphocholine (DLPC) monolayers spread on salt solutions by using vibrational sum frequency spectroscopy (VSFS). [65, 99, 116, 127-130] Better understanding for the Hofmeister effect is drawn from the present work by comparing ion effects on alkyl chain conformation on the monolayers and interfacial water for various combinations of charge and hydrogen bonding abilities on monolayers. ODA was chosen for a positively charged and hydrogen-bonding surface, DDAB was for a positively charged surface without hydrogen bonding ability, and DLPC was for neutral and hydrogen bonding surface. The result showed dramatically different ion effects on alkyl chain ordering and interfacial water depending on characteristics of the monolayers and provides profound information to understand the Hofmeister effect.

MATERIALS AND METHODS

Materials

1,2-Dilauroyl-*sn*-glycero-3-phosphocholine (DLPC) was purchased from Avanti Polar Lipids (Alabaster, AL) as dissolved in chloroform and diluted to 1 mg/mL with

chloroform. Solid sample of octadecylamine (ODA) was purchased from Sigma-Aldrich (St. Louis, MO) and dimethyldidodecylammonium bromide (DDAB) was purchased from Acros Organics (Fisher Scientific International Inc., Hampton, NH). To avoid complication of interference between CH and OH detection regions, chain-deuterated DDAB (d_{50}-DDAB) was used for interfacial water study. Deuterated DDAB was generously gifted and used as we obtained. Molecular weight of d_{50}-DDAB was confirmed by MALDI mass spectroscopy and deuteration was checked with NMR. Solutions of ODA and DDAB were prepared by dissolving each amphiphile in chloroform, which was purchased from Merck (Merck and Co. Inc., Whitehouse Station, NJ), to get concentration of 1mg/mL respectively. All the salts used in this work were purchased from Sigma-Aldrich and used as we received. Purities of the salts were >99% except for sodium thiocyanate and sodium perchlorate, which were >98% of purities. Salt solutions were made by dissolving adequate amount of salts into deionized (>18.2MΩ) water, which was obtained from NANOpure Ultrapure Water System (Barnstead, Dubuque, IA). Since the ionic strength of sulfate is three times higher than other salts, sulfate solution with the equivalent ionic strength was also compared. Deuterium oxide (D, 99.9%) was purchased from Cambridge Isotope Lab. Inc. (Andover, MA).

Monoalyer Formation

A Langmuir trough (601M, Nima Technology Ltd., United Kingdom) was filled with 50 mL of a salt solution and monolayers of ODA, DDAB, and DLPC were generated by placing adequate amount of lipid solutions on subphases. Data was taken

after 15minutes from spreading a lipid solution to get the chloroform totally evaporated. Surface pressure was hold to 15 mN/m during the data acquisition.

Surface Potential Measurements

Surface potentials were measured by a KSV5000 Langmuir Trough (KSV Instruments Ltd, Finland) with a Kelvin prove based on vibrating capacitor method. The oscillator vibrates the upper electrode of the capacitor with a frequency of 80~120 Hz. The lower electrode of the capacitor is under the surface of the subphase. Changing of the capacitance caused by a potential difference between the electrodes induces an AC current, which is detected by a phase detector as well as the signal from the oscillator. The phase detector generates a DC current that charges the following feedback capacitor until no currents occur, where the compensating voltage equals the surface potential. The detection range of the potential meter was ± 10 V with error range of 5 mV. For each measurement the trough was filled with 3.5 L of a solution and the reference electrode was inserted into the solution right under the potential probe. Surface pressure and surface potential were zeroed before monolayer was applied, and surface potential was measured at surface pressure of 15mN/m.

RESULTS

VSFS was applied to investigate the ion effects on interfacial water structures for three different amphiphile monolayers on salt solutions. Each amphiphile is representative for combinations of two characteristics: charge and hydrogen bonding ability. ODA was chosen for a positively charged and hydrogen-bonding surface,

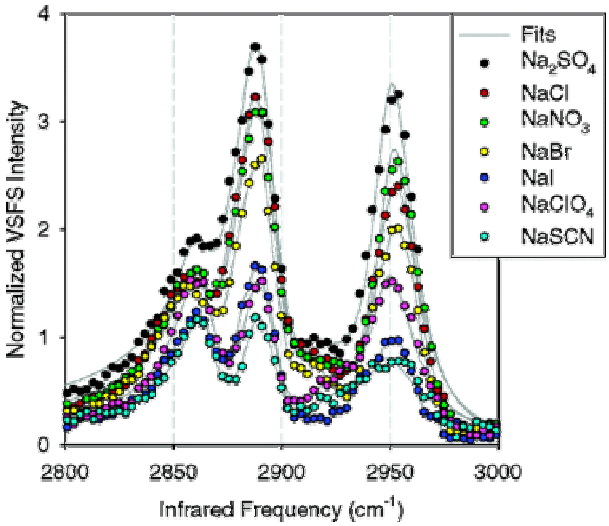

Figure 19. Sum frequency spectra of ODA monolayer on 10mM sodium salt solution. The lines are the Lorentzian fit to the data.

DDAB was for a positively charged surface without hydrogen bonding ability, and DLPC was for neutral and hydrogen bonding surface. Since the ionic strength of sulfate is three times higher than other salts, sulfate solution with the equivalent ionic strength was also compared. The results showed that the degree of alkyl chain ordering and water intensity for sulfate solutions at equivalent ionic strength was slightly different from equivalent concentrations but the orders between the ions were not affected.

The Hofmeister Effect on Octadecylamine (ODA) Monolayer

Alkyl Chain Ordering

VSFS data were collected from ODA monolayers spread on D_2O subphases containing various sodium salts. The vibrational spectra collected in the CH stretch range showed dramatic differences in the degree of ordering in the alkyl chains as a function of the specific anion in the subphase (Figure 19).

As can be seen from Table 1, the ratio of oscillator strengths from the methyl symmetric stretch, ν_s (CH_3) at 2891 cm^{-1}, to the methylene symmetric stretch, ν_s (CH_2) near 2863 cm^{-1}, changed quite substantially. It is already well established that the higher this ratio, the more ordered the monolayer is under a given set of conditions.[31, 130-132] The ratios for the anions follow a series from the most ordered to least ordered monolayer as:

$$SO_4^{2-} > Cl^- > NO_3^- > Br^- > I^- > ClO_4^- > SCN^-$$

Table 1. CH symmetric stretch ratios (A_{CH3ss}/A_{CH2ss}) for ODA, DDAB, and DLPC monolayers on subphases containing 10 mM salt (ODA and DDAB) and 100 mM salt (DLPC).

Salts	ODA	DDAB	DLPC
No salt	4.4	1.6	1.2
Na_2SO_4	6.0	1.4	1.2
NaCl	4.7	1.7	1.4
$NaNO_3$	4.1	2.1	0.99
NaBr	3.3	2.6	0.96
$NaClO_4$	1.1	3.1	0.54
NaSCN	0.8	3.5	0.63

This is recognizable as the Hofmeister series. The basis for this ordering is related to an individual anion's ability to penetrate into the alkyl chain portion of the monolayer,[133-135] thereby disrupting the hydrocarbon packing. Sulfate, chloride, and nitrate ions show relatively little tendency to do this, while iodide, perchlorate, and thiocyanate go in more facilely. Bromide appears to display intermediate behavior. CH peak ratios for ODA monolayer were plotted against various ion properties and the best relationship was found with surface potential and ion volume. (Figure 20)

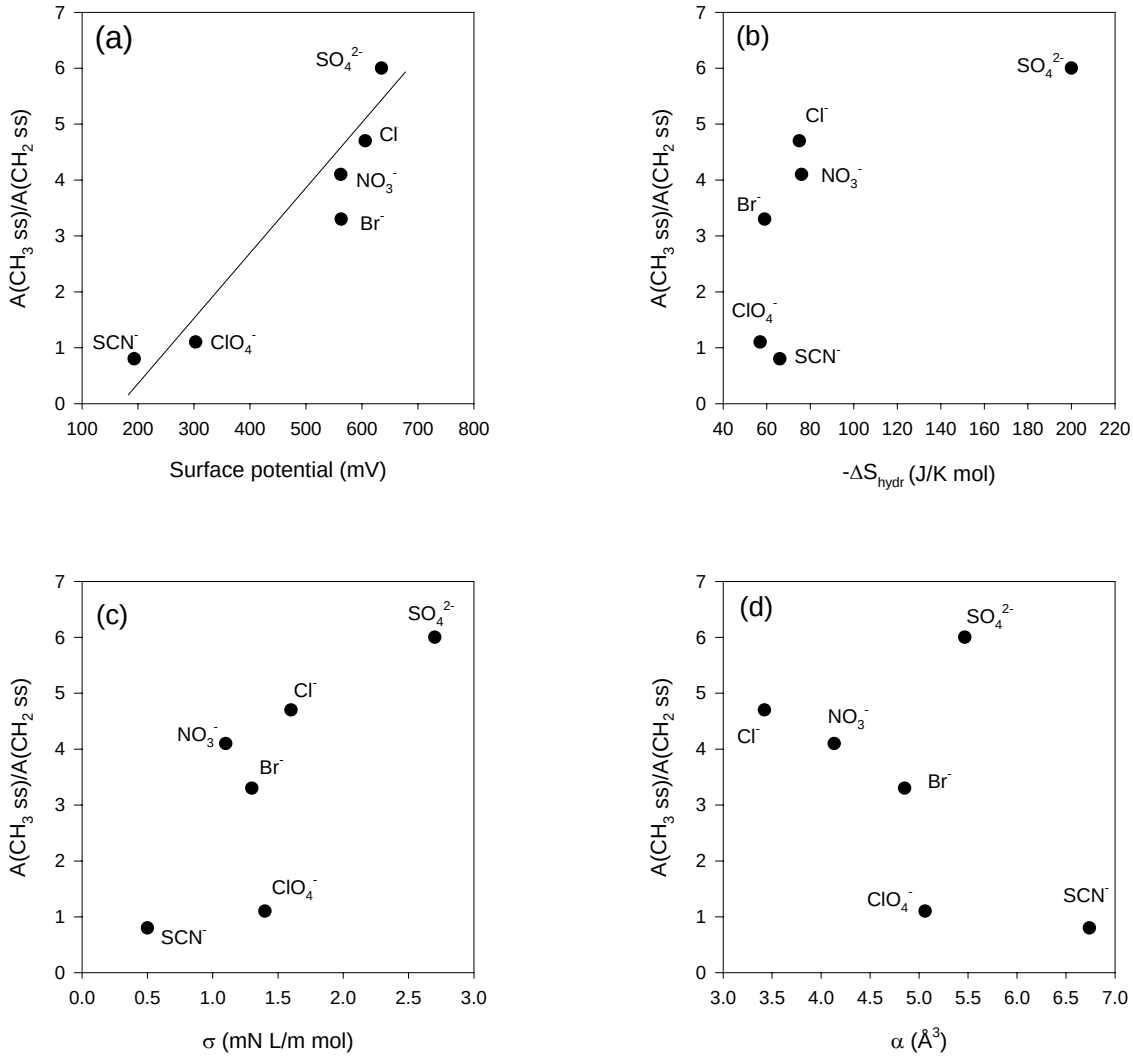

Figure 20. CH symmetric stretch ratios of ODA to various ion properties; (a) surface potential, (b) hydration entropy, (c) surface pressure increment, (d) polarizability.

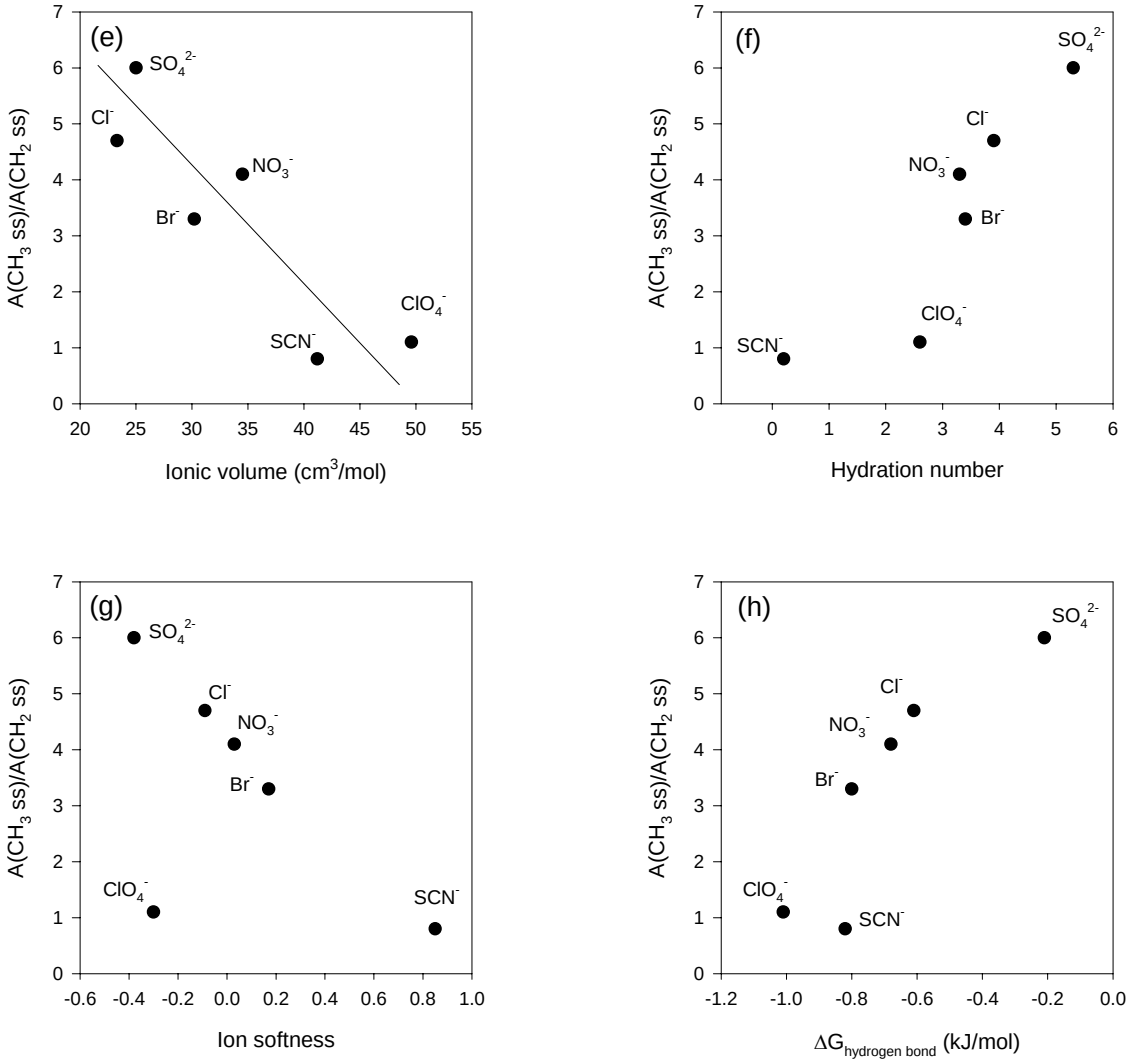

Figure 20 continued. (e) ionic volume, (f) hydration number, (g) ion softness and (h) free energy for hydration.

Next, surface potential data were collected at the air/ODA/subphase interface for each respective anion using the vibrating capacitor method (Table 2).

Table 2. Surface potentials for ODA, DDAB, and DLPC monolayers on subphases containing 10 mM salt (ODA and DDAB) and 100 mM salt (DLPC).

Salts	ODA	DDAB	DLPC
No salt	854	650	318
Na_2SO_4	635	500	308
NaCl	606	512	321
$NaNO_3$	562	337	293
NaBr	563	457	313
$NaClO_4$	303	273	300
NaSCN	193	298	280

As expected, the surface potential was greatest for ODA on pure water. This positive potential was generated by the protonation of some of the surface amines under these conditions. The addition of the various salts caused an attenuation of the potential in the same order as that seen above for alkyl chain ordering. In other words, the anions that could most efficiently partition into the monolayer caused the greatest attenuation of the surface potential, while those that were excluded showed the least effect. This finding is

in line with the notion that those anions which partition to the greatest extent into the monolayer had the highest interfacial concentration.

Interfacial Water Structure

Figure 21 shows the water spectra of ODA monolayers on 10mM salt solutions and 1M salt solutions. The spectra from the ODA monolayers on various salt solutions presented C-H peaks in 2800-3000 cm^{-1} region and OH stretch peaks from interfacial water molecules around 3200 cm^{-1} and 3400 cm^{-1}. Interfacial water showed its typical feature of two OH stretch peaks, one is around 3200 cm^{-1} and the other is around 3400 cm^{-1}. The 3200 cm^{-1} peak is OH symmetric stretch from highly hydrogen-bonded water molecules and due to intermolecular coupling.[20, 136] High intensity of 3200 cm^{-1} peak was observed from the interfaces with highly charged surfaces such as polyelectrolyte/silica and charged amphiphile/water, which suggest that the peak is related with the systems that have electrostatic contribution.[26, 99, 137] On the other hand, the peak near 3400 cm^{-1} is from less ordered water and similar to bulk liquid water, which lacks of some of hydrogen bonding connection.[18, 19, 30, 129, 138] In addition to OH peaks, ODA monolayer gives a feature around 3100 - 3150 cm^{-1}, which is from the positively charged amine group. The peak from NH_3^+ group, which is assigned to N^+-H symmetry stretch was also reported from the air/water interface of dodecylammonium chloride (DAC) solution.[99] As we reported earlier, perchlorate ion at 10mM concentration induces the highest water intensity and sulfate reduced the most, but differences among other ions are not quite distinguishable. Water intensities are related

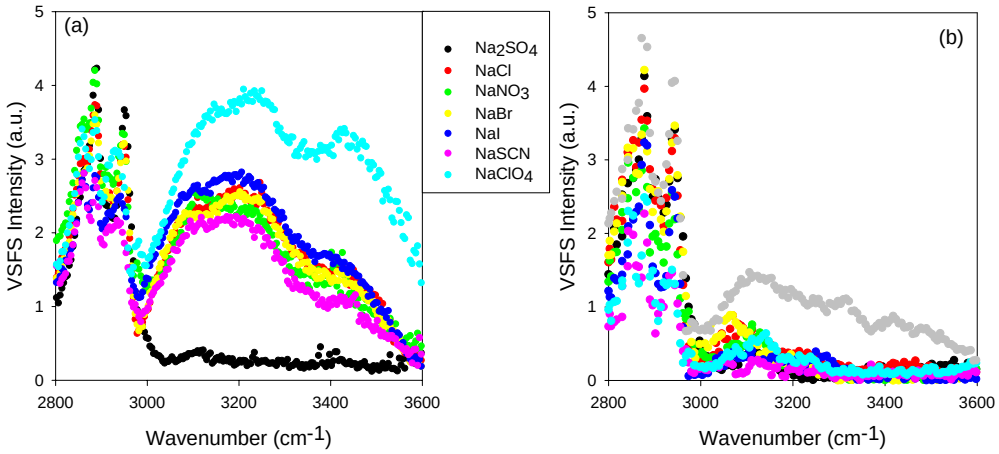

Figure 21. Sum frequency spectra of octadecylamine (ODA) monolayer on (a) 10mM (3.3mM for Na_2SO_4) and (b) 1M (0.33M for Na_2SO_4) sodium salt solutions.

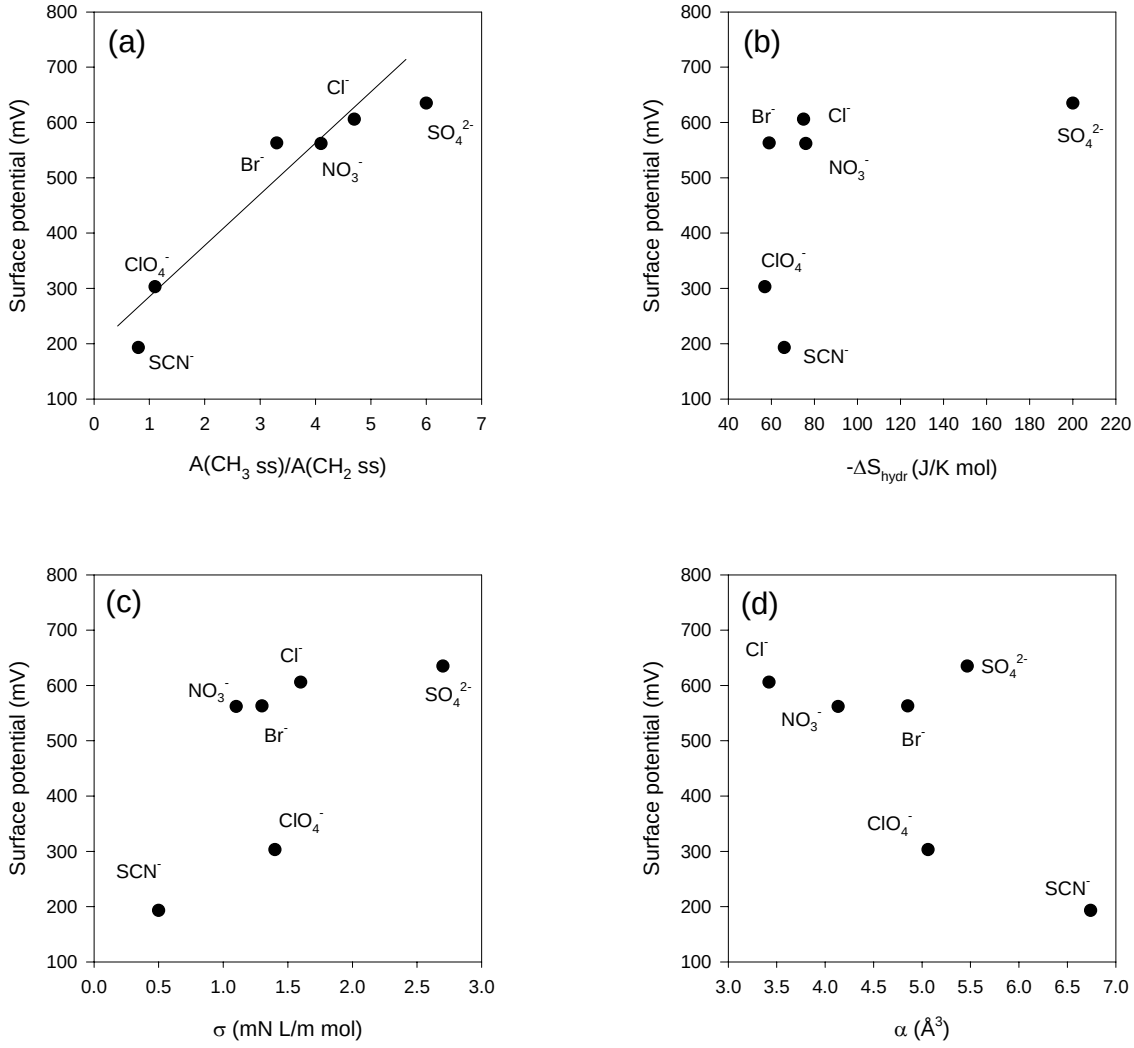

Figure 22. Surface potential of ODA to various ion properties; (a) surface potential, (b) hydration entropy, (c) surface pressure increment, (d) polarizability.

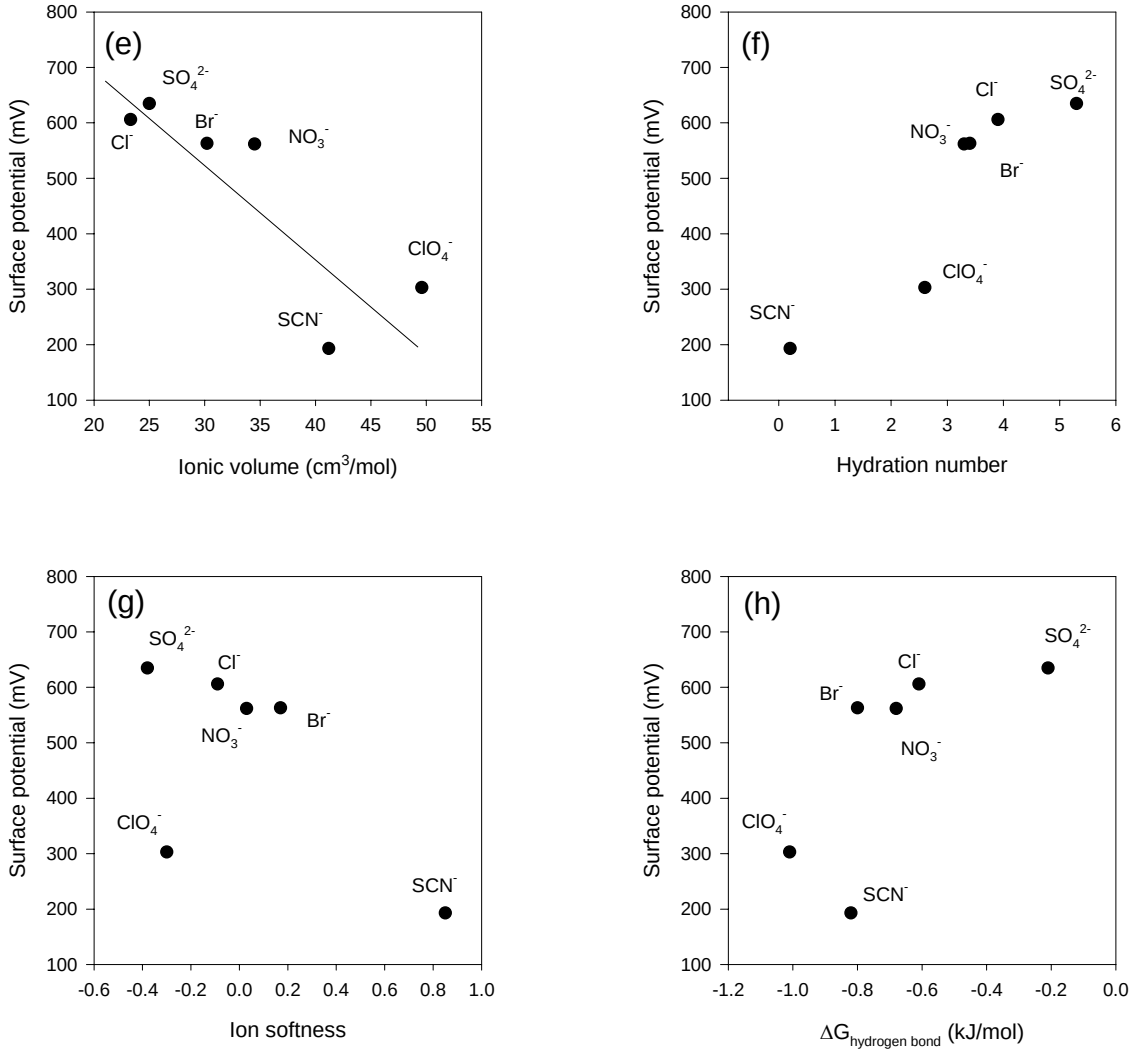

Figure 22 continued. (e) ionic volume, (f) hydration number, (g) ion softness and (h) free energy for hydration.

with surface potential, therefore differences in water intensities between ions could be understood from the surface potential plot against ion properties. (Figure 22)

The Hofmeister Effect on Dimethyldidodecylammonium Bromide (DDAB) Monolayer

Alkyl Chain Ordering

VSFS for DDAB monolayer on various salt solutions were shown in Figure 23. Each spectrum has four peaks at 2844 cm^{-1}, 2871 cm^{-1}, 2915 cm^{-1}, and 2933 cm^{-1}, which were assigned as CH_2 symmetric stretch (CH_2 SS) and CH_3 symmetric stretch (CH_3 SS), Fermi resonance of CH_2 SS, and Fermi resonance of CH_3 SS respectively. The spectra were fit to the Lorentzian function and the ratios of CH_3 SS to CH_2 SS were listed on Table 1 along with the ratio of ODA alkyl chains. Surprisingly the series of the ions for ordering DDAB alkyl chain was the opposite from that of ODA. For DDAB monolayers, sulfate ion shows the least effect on chain ordering, while thiocyanate ion shows the most effect. In the absence of ions, ODA monolayer is in gel phase at 20 °C and alkyl chains are well ordered. Therefore ion interaction to the monolayer is shown as disordering alkyl chains. Nevertheless DDAB monolayer is in free liquid phase at the same temperature and two alkyl chains have high degree of angle between them, which appeared as low CH_3/CH_2 ratio. Thus ion interaction to the monolayer happens to be ordering effect on the alkyl chains. Ions reduce repulsion among DDAB molecules via screening effect and binding event to the head group, which attenuate the surface charge (Table 2). Screening effect is only effective at low salt concentrations (<10mM),

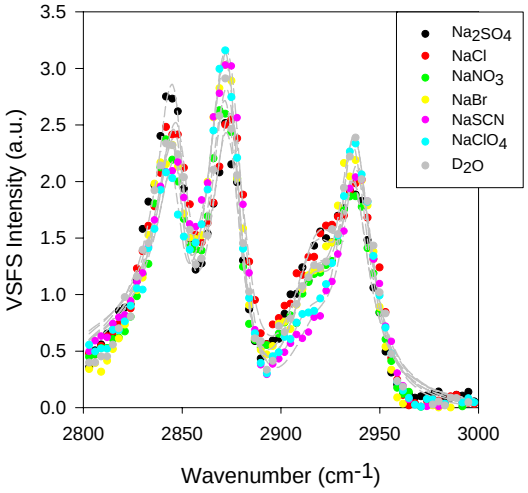

Figure 23. Sum frequency spectra of DDAB monolayer on 10mM sodium salt solution. The lines are the Lorentzian fit to the data.

where Gouy-Chapman theory is acceptable. Binding event is more plausible explanation at high concentrations. There are two possibilities in the way anions work. Ions could place under the monolayer and bridge the head groups and induce more densely packed monolayer, which will increase the CH_3/CH_2 ratio on the sum frequency spectrum. One could expect to see different molecular area for DDAB monolayer on different salt solutions if the monolayer is packed by ions. Such effect did not appear on our measurements (Figure 24). Only ODA monolayer showed a trend between molecular area and CH_3/CH_2 ratio, which means ions caused monolayer contracted and induced alkyl chains ordered by van der Waals interaction between the chains. Such trend was not observed for DDAB and further DLPC monolayers. The other possible explanation is as such; ions present at air/lipid/subphase interface and reduce the angle between alkyl chains, which induces high CH_3/CH_2 ratio on VSFS spectra. Fitting results from the VSFS spectra were plotted against various ion properties to explore which characteristics of ions cause the effect (Figure 25). The ratio between CH_3 symmetric stretch and CH_2 symmetric stretch showed a good correlation to the surface potential and ion volumes. Big and highly polarizable ions, such as perchlorate and thiocyanate, are more hydrophobic and possible to present at the interface than small and less polarizable ions resulting higher effect on alkyl chain ordering of DDAB.

Interfacial Water Structure

Interfacial water structure under DDAB monolayer was monitored at 10mM and 1M salt concentrations of subphases and VSFS spectra were presented in Figure 26.

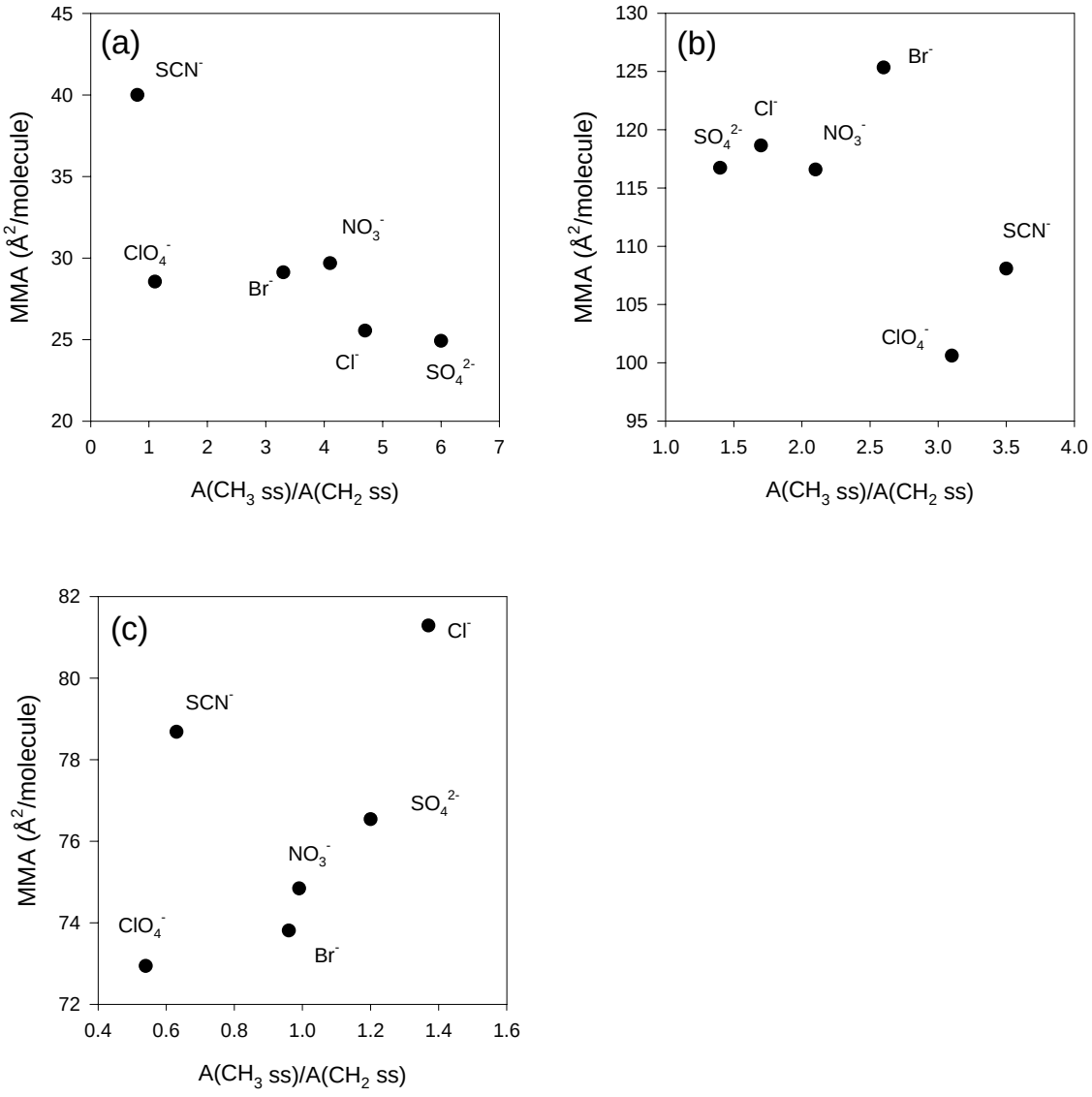

Figure 24. Mean molecular area of monolayers of (a) ODA, (b) DDAB, and (c) DLPC to CH symmetric stretch ratios.

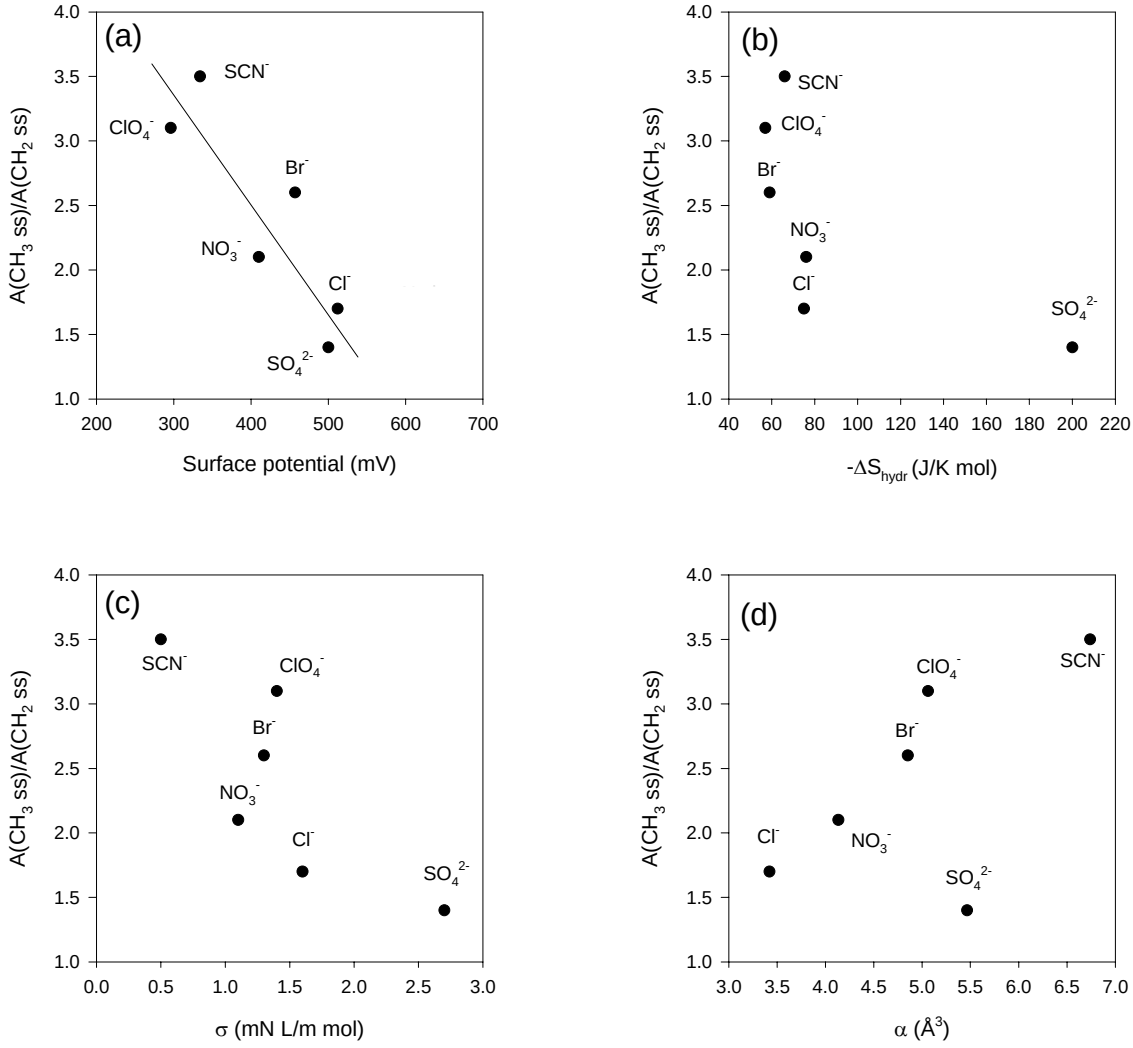

Figure 25. CH symmetric stretch ratios of DDAB to various ion properties; (a) surface potential, (b) hydration entropy, (c) surface pressure increment, (d) polarizability.

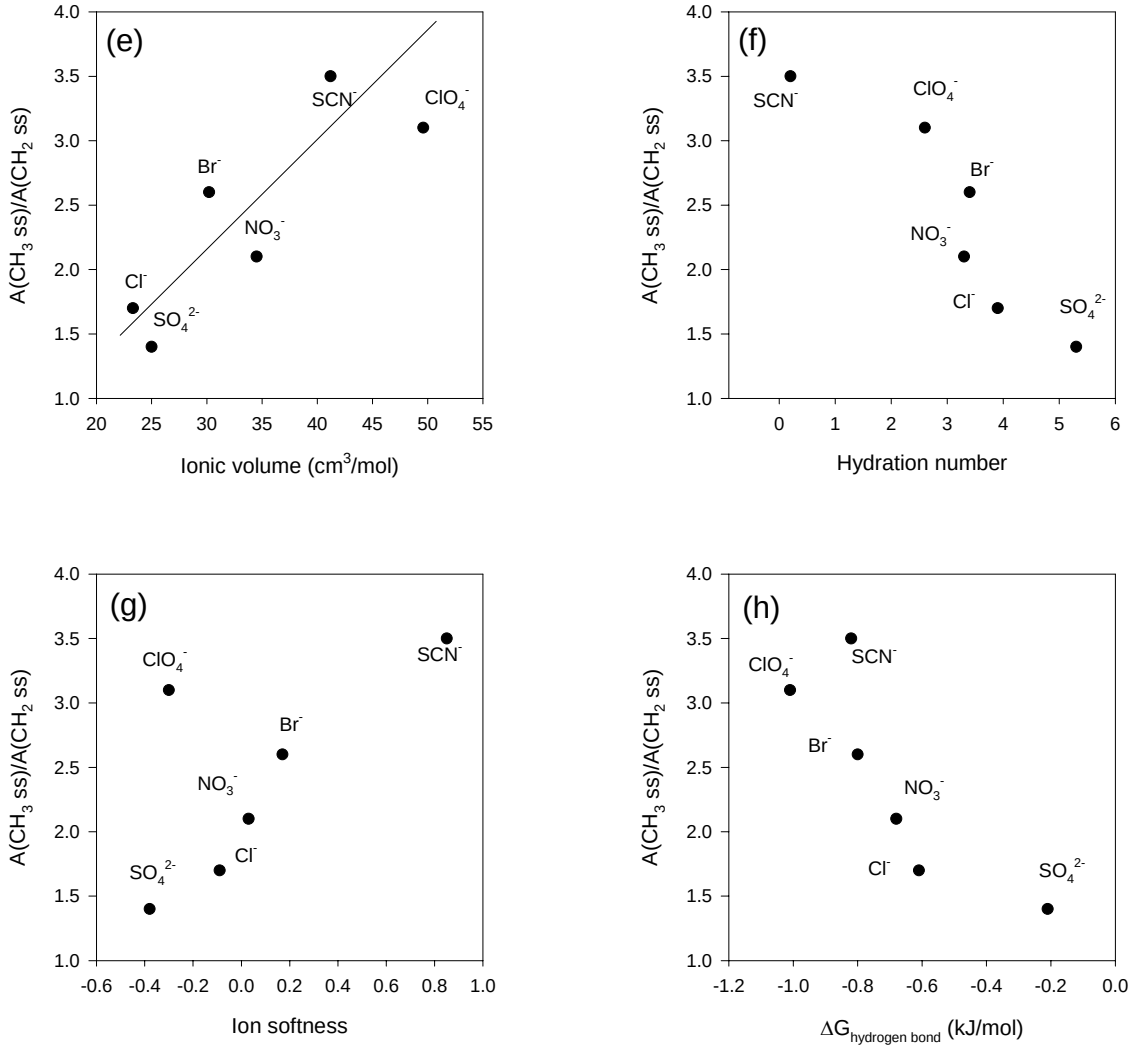

Figure 25 continued. (e) ionic volume, (f) hydration number, (g) ion softness and (h) free energy for hydration.

Chain deuterated DDAB was used for interfacial water study to avoid complication on the spectra from strong CH peaks from the alkyl chains. Two alkyl chains of DDAB were deuterated, but two methyl head groups were not, which give weak CH peaks in the region of 2800-3000 cm^{-1}. Two methyl head groups provide a hydrogen-bond-free environment, which gives us a good control for the hydrogen bonding effect of the head group.

Positive charge under the DDAB monolayer aligned water molecules through electrostatic interactions with the oxygen atom towards the monolayer and two hydrogen atoms to the bulk water. For 10mM salt solutions, salt solutions showed lower water intensities on both 3200 cm^{-1} and 3400 cm^{-1} peaks compared to the DI water spectrum. The ion effect on decreasing water intensity was ion-specific (Figure 26-a) and for 10mM concentration, which cannot be explained from Gouy-Chapman theory. The Debye length is the same for all 1:1 salts and should have the same effect on screening surface charge.[2] The order of water intensity at 10mM subphases was DI water > Cl^- > SO_4^{2-} > Br^- > NO_3^- > ClO_4^- > SCN^-. Ions followed the Hofmeister series except for sulfate ion. To understand this ion behavior, we plot the surface potential to various ion properties. The best relationship is found from ionic volume, which clearly showed that the screening effect is proportional to the size of the ions.

Interestingly, spectral shapes of ionic solutions at high concentrations (Figure 26-b) are different from those at lower concentrations (Figure 26-a). At 10 mM concentration, 3200 cm^{-1} peaks are higher than 3400 cm^{-1} peaks. Those spectral shapes

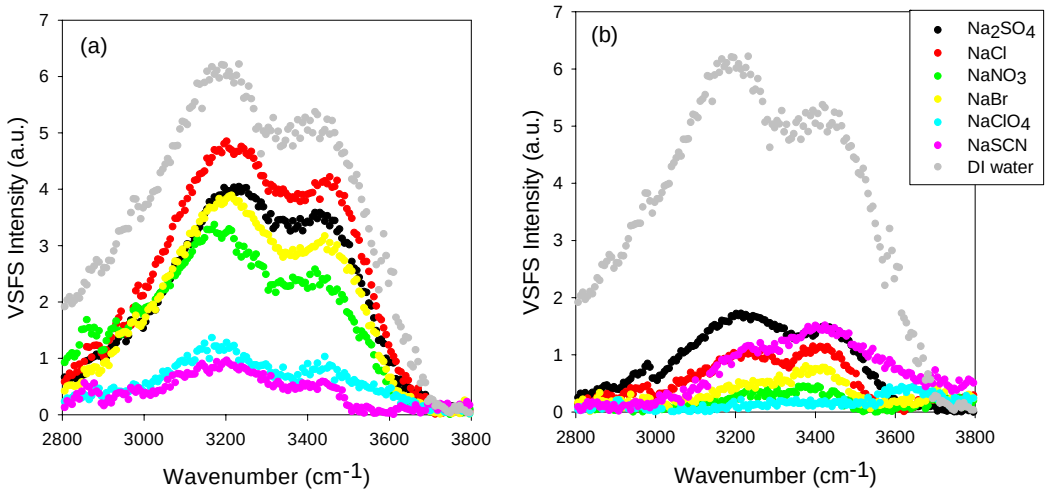

Figure 26. Sum frequency spectra of d_{50}-dimethyldidodecylammonium bromide (DDAB) monolayer on (a) 10mM (3.3mM for Na_2SO_4) and (b) 1M (0.33M for Na_2SO_4) sodium salt solutions.

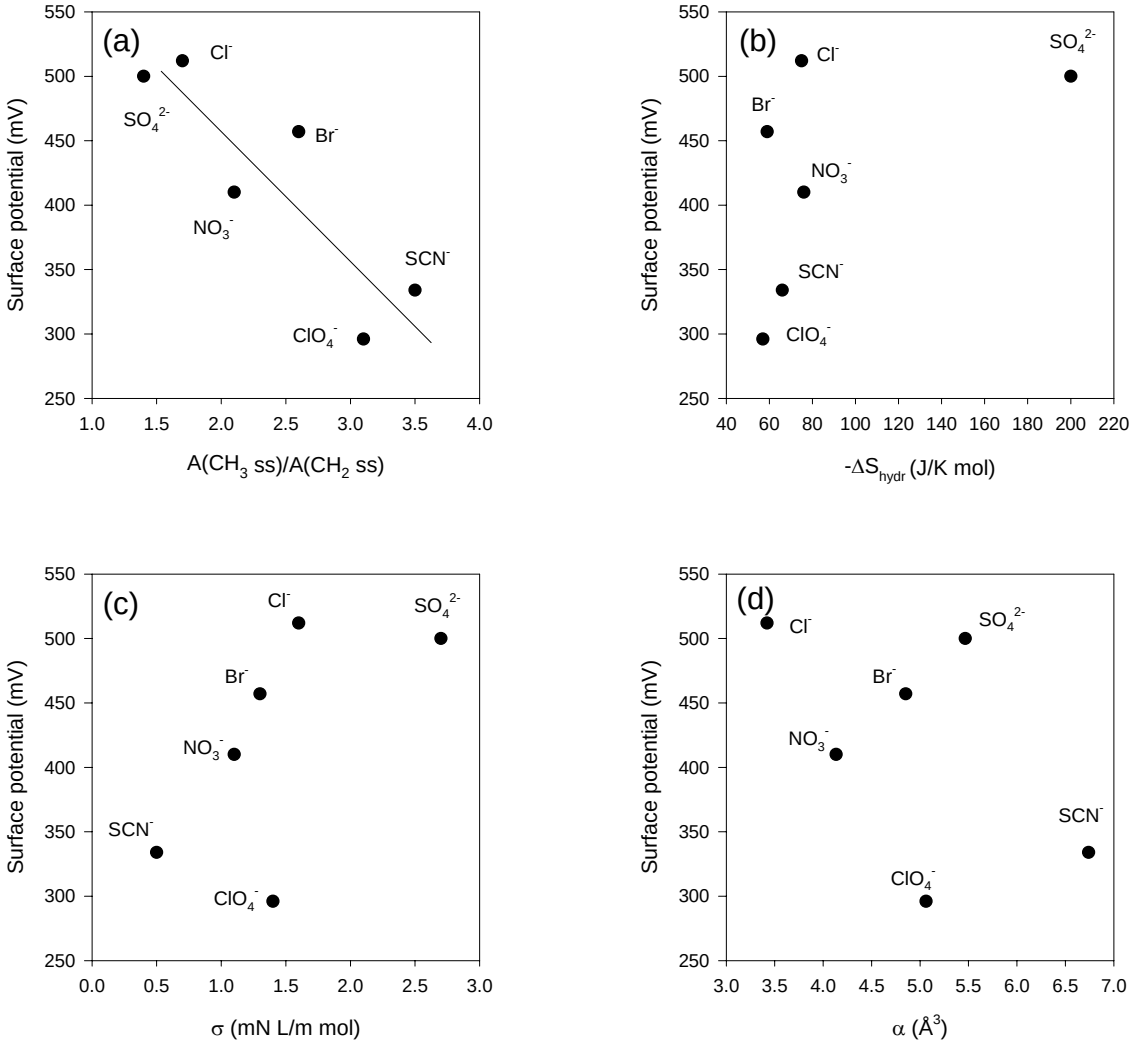

Figure 27. Surface potential of DDAB to various ion properties; (a) surface potential, (b) hydration entropy, (c) surface pressure increment, (d) polarizability.

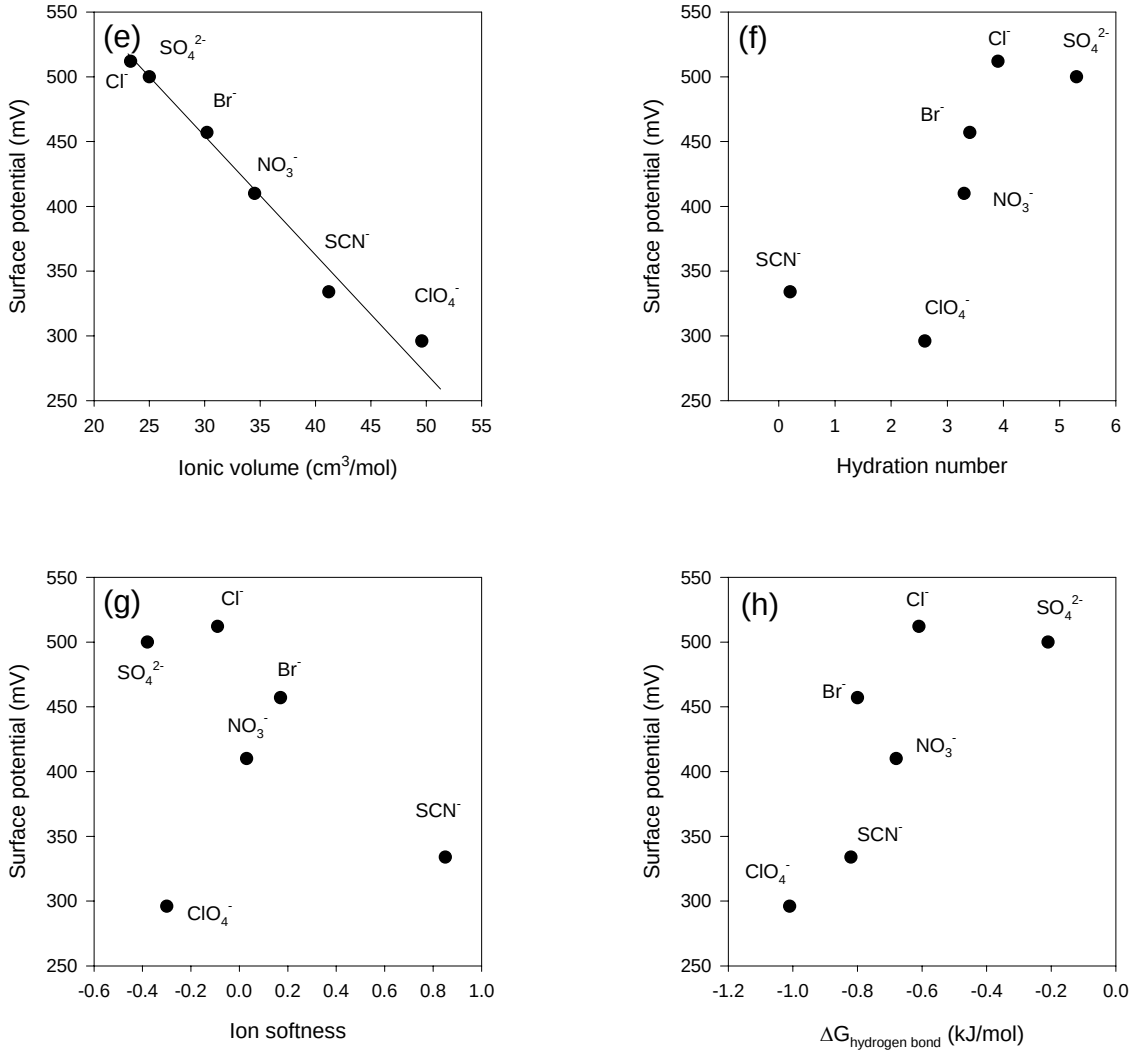

Figure 27 continued. (e) ionic volume, (f) hydration number, (g) ion softness and (h) free energy for hydration.

stay the same for fluoride and sulphate ions at 1M concentrations. Then the relative intensities are switched from 1M chloride solution. Now the 3400 cm^{-1} intensity is higher than 3200 cm^{-1}. Finally, both of the water structures totally disappeared at 1 M of perchlorate solution. At 1M solutions, both of the water peaks decreased, but change in 3200 cm^{-1} peak is relatively higher than that of 3400 cm^{-1} peak and ion specificity stays the same as 10mM concentration except for thiocyanate, which is different from the results with ODA monolayer. At high concentration, the surface charge is mostly screened by ions and interfacial water molecules lost the driving force that made them aligned. Thiocyanate shows high water intensity on the VSFS spectra because the ions align the water by polarizability. Different efficiencies of ions on screening effect are related with different surface potential. Surface potential of DDAB monolayer were plotted to ion properties on Figure 27.

Ionic Effect on 1,2-Dilauroyl-sn-Glycero-3-Phosphocholine (DLPC) Monolayer

Alkyl Chain Ordering

Glycerophospholipids are major components of biological membranes. Phosphotidylcholine (PC) is a zwitterionic lipid with a positively charged choline group bonded to a negatively charged phosphotidyl group. Dilauroylphosphotidyl choline (DLPC) has two saturated 12 carbon chains and phase transition temperature of -1°C, so that DLPC persists in liquid phase at room temperature. Binding of cations to the biological membranes are well studied and especially calcium binding to the membrane and membrane proteins are essential for their stabilities and activities.[139-142] Nonetheless, anion effect on lipid membranes are not well understood.[114, 143] Herein we applied VSFS

to investigate anion effect on DLPC alkyl chain ordering. Anion effect for DLPC was not observed at 10 mM salt solutions, where anions showed effect on ODA and DDAB monolayers. We suppose that anion population at the interface was not enough to show the effect on alkyl chain ordering. Since DLPC is zwitterionic, anionic affinity to the monolayer is significantly smaller than ODA and DDAB, which was also shown in minute change in surface potential measurements (Table 2). VSFS of DLPC monolayer on 100mM salt solutions in D_2O is shown in Figure 28. The order of anions' ability to order alkyl chains was similar to that of ODA, but much weaker. That might be because the interaction of anions to the alkyl chain is not strong enough to bring significant change on DLPC alkyl chains. The spectra were fit with the Lorentzian fitting, which is similar to the equation II-4, and the oscillator strength ratio for CH_3 symmetric stretch peak and CH_2 symmetric stretch peak were plotted against various ion properties (Figure 29). The higher the ratio, the higher the alkyl chain ordering is. The CH_3/CH_2 ratio of the DLPC monolayer showed the best correlation the ionic volume followed by to the hydration number, which is the Stokes radius and free energy of hydrogen bonding. In other words, big and hydrophobic ions such as thiocyanate showed best ability to disturb the alkyl chain ordering of DLPC monolayer. The order of ions' abilities to interact the DLPC monolayer is $Cl^- > SO_4^{2-} > NO_3^- > Br^- > SCN^- > ClO_4^-$. Thiocyanate ions order interfacial water more efficiently than sodium ions and sulfate ions. Those results are consistent to molecular dynamics results for head group tilting of phosphotidylcholine head group.[143] They also reported salt-induced water ordering is higher for big ions and

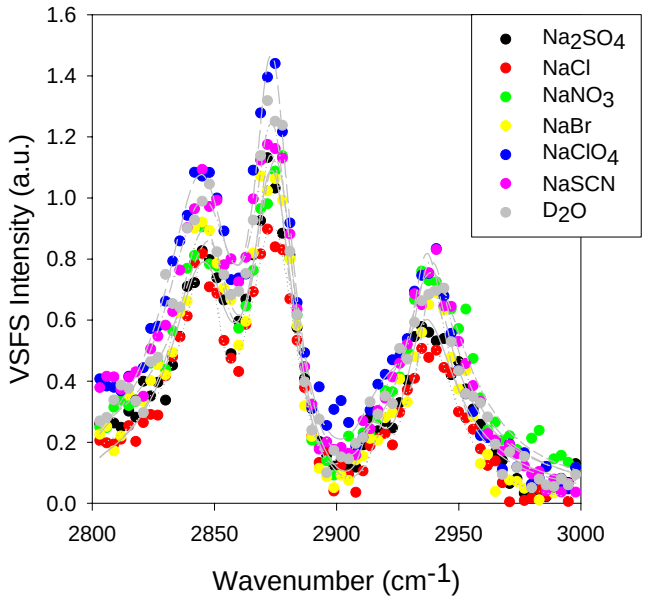

Figure 28. Sum frequency spectra of DLPC monolayer on 100mM sodium salt solution. The lines are the Lorentzian fit to the data.

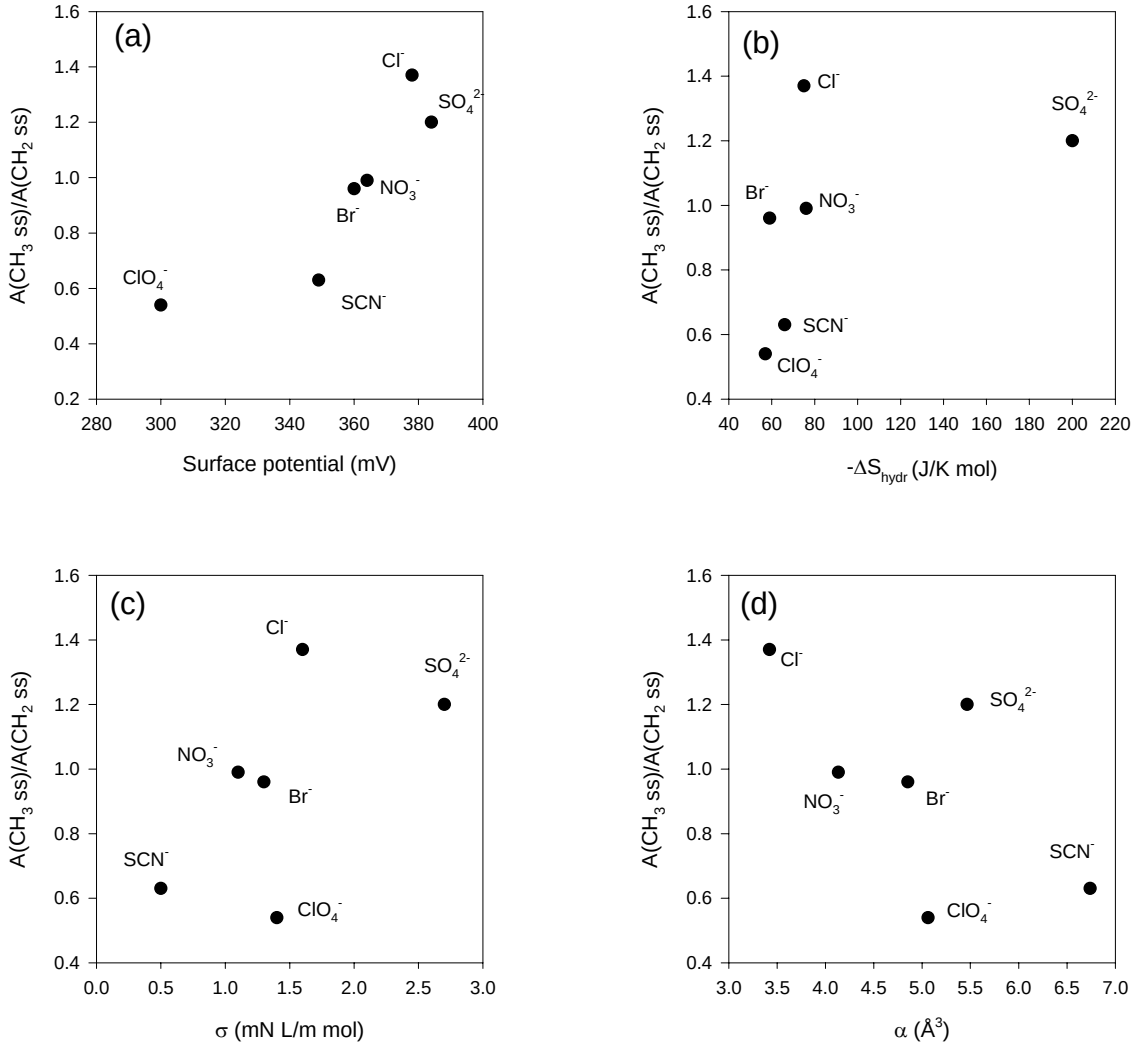

Figure 29. CH symmetric stretch ratios of DLPC to various ion properties; (a) surface potential, (b) hydration entropy, (c) surface pressure increment, (d) polarizability.

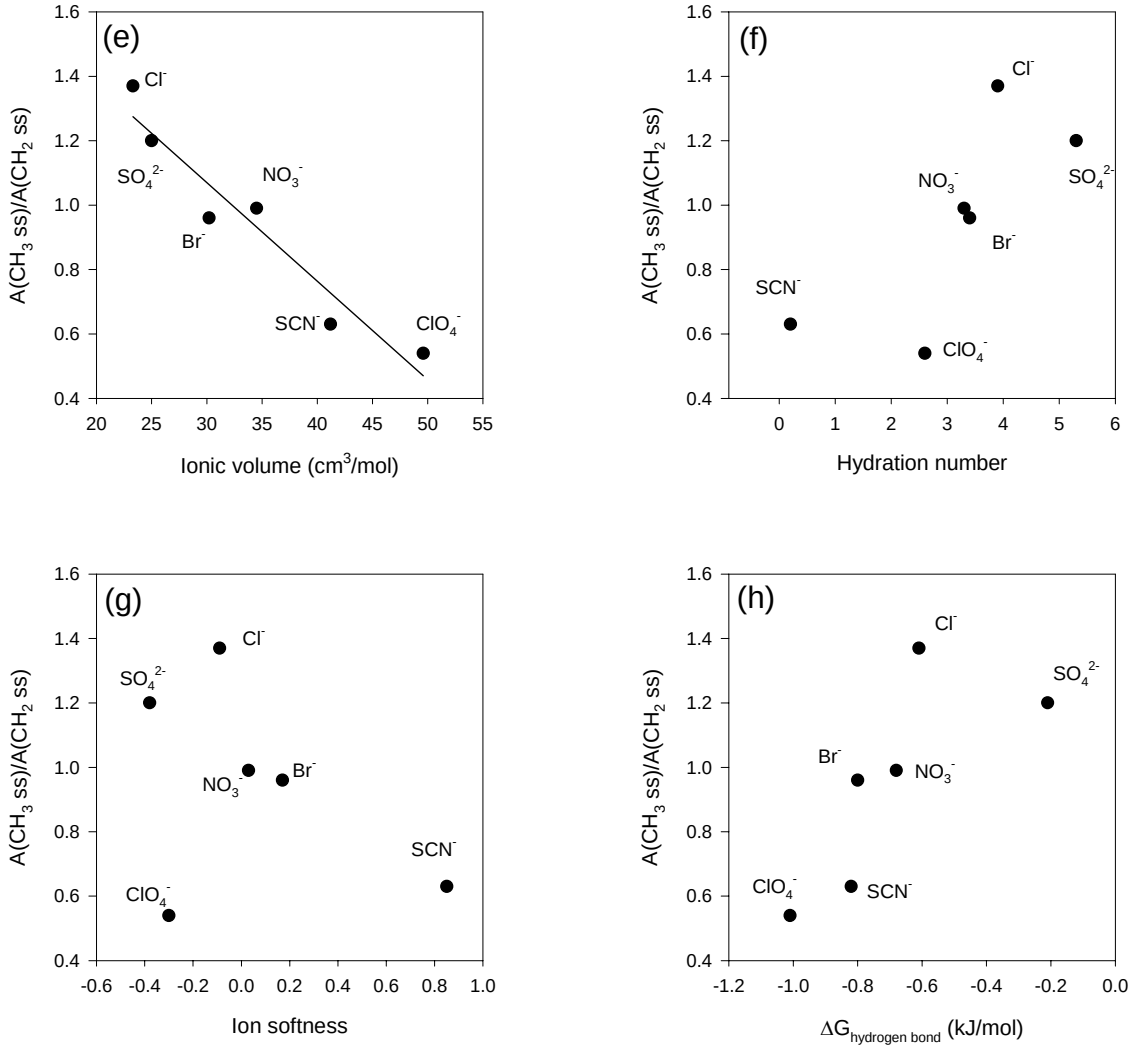

Figure 29 continued. (e) ionic volume, (f) hydration number, (g) ion softness and (h) free energy for hydration.

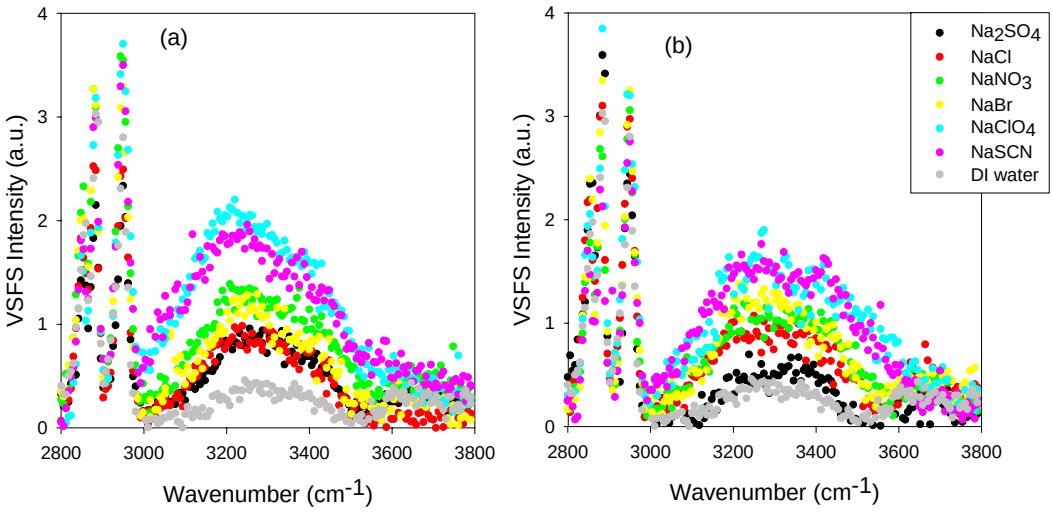

Figure 30. Sum frequency spectra of dilauroylphosphocholine (DLPC) monolayer on (a) 10 mM (3.3mM for Na_2SO_4) and (b) 1M (0.33M for Na_2SO_4) sodium salt solutions.

it is shown in the VSFS spectra of interfacial water, which is presented in this dissertation (Figure 30). It is already reported that sodium ions from NaCl salt binds to the carbonyl group or oxygen of phosphate on the PC bilayer.[144, 145] It is not clear which part the sodium binds, but it is sure sodium ions populated the upper most layer of the interface between DLPC monolayer and water. Anions in the solution are subject to interact with the positively charged choline group (Figure 31). Woolf and co-workers suggested that the big ions tilts the PC head group and prefers to be in hydrophobic environment of the alkyl chain are due to the repulsion between anions and the phosphate group. Nonetheless, it is still not clear whether the alkyl chain ordering was from the interaction of ions to the head group or to the alkyl chain directly because we did not observe any differences in effect of ions on the mean molecular are of DLPC monolayer (Figure 24). It is very interesting that anions did not change the molecular are, but did change the alkyl chain ordering, which is more likely from local tilting of head group by ions, but not from direct change in the alkyl chain area, for example causing gauche defects.

Interfacial Water Structure

The phosphotidylcholine (PC) head group of DLPC is zwiterionic and its ability to induce water alignment is much weaker than those of ODA and DDAB. PC head group is known to be neutral, but the dipoles in the choline and phosphotidyl groups induce surface potential as can be seen from Table 2. Oliveira and co-workers also reported the surface potential for DPPC and it was unexpectedly high as a neutral surface.[146] Even though there is a certain amount of surface potential on the DLPC

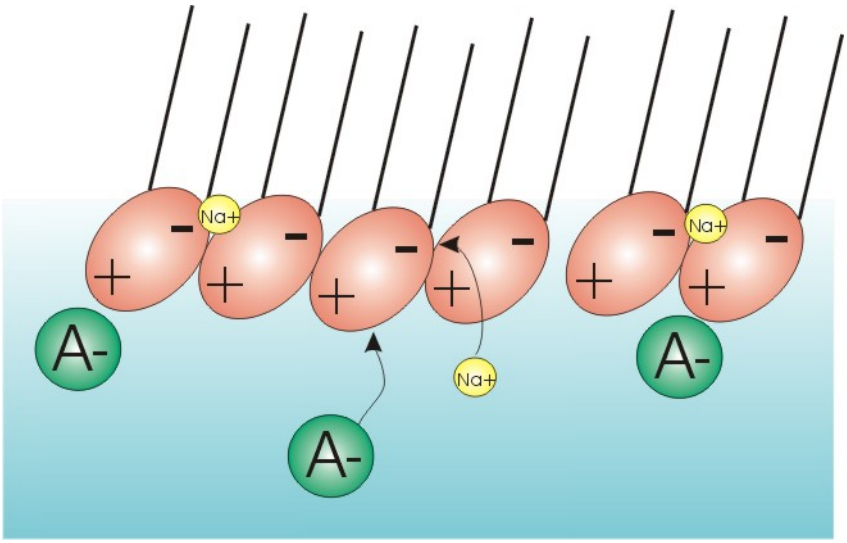

Figure 31. Schematic view of DLPC interaction with ions.

monolayer, our data (Figure 30) showed that electrostatic force from the surface could not be the main contribution for water alignment. If the surface potential were the main force, then the water peaks should be lower in the presence of ions compared to those of DI water, which is not the case in this work. We observed the opposite; water intensities increased in the presence of ions. Thiocyanate and perchlorate ordered water molecules the most and sulfate and chloride have the least effect. The effect of ions ordering water molecules is ClO_4^- > SCN^- > I^- > NO_3^- > Br^- > Cl^- > SO_4^{2-} > DI water. The order of ions is the same order of anion effect on alkyl chain disturbing as shown in this dissertation and the order stays very similar for higher concentration (1M). Theoretical study of PC head groups showed that there was no preferential orientation for water molecules in salt-free bilayer, but in the presence of salt water molecules were significantly ordered at the interface, which is well matched with our experimental results.[143] They explained that the double layer of ions induces this water ordering. In other words, water molecules were ordered between sodium ion and anions.

It is already shown in the alkyl chain study in this dissertation that big and hydrophobic ions have stronger interaction to the DLPC monolayer than smaller ions. Those big ions induce higher water density by inducing shedding solvation water from the head group and ions.[143] Therefore high water intensity was observed from big ions on the VSFS spectra. Differences in ion effects on water aligning under the DLPC monolayer also can be understood by ion population at air/water interface, which was calculated by Jungwirth and Tobias.[147] Their calculation revealed that big and

hydrophobic ions populated near the interface and small ions like chloride varied in the bulk phase and that the interfacial depth is bigger for big and polarizable ions.

DISCUSSION

Based on our VSFS results, we can describe the Hofmeister effect in the view of different factors governing in different environments.

Screening Effect

The head group of ODA is primary amine and forms strong hydrogen bonding with water molecules. Without ions, water molecules aligned under the monolayer by the electrostatic force of the positively charged head groups of the ODA. In ionic solutions, ions are also solvated and there should be competition between water molecules attracted by amine head group of ODA and water molecules in ion solvation shell to cause change in the interfacial water under monolayer as shown in Figure 32. Water molecules around the amine head groups are so strongly bound that it is unlikely to remove water molecules from the ODA head groups. Thus the mechanism of ion effect on the interfacial water change will be indirect, so to speak, by the screening effect. Sanchez-Ruiz and co-workers suggested the importance of the screening effect in protein interaction and pointed out the screening effect of ions are well correlated to the Hofmeister series.[117] Water intensity decreased a lot at 1M concentrations due to screening effect to the positive charge on the monolayer even though there is little ion specificity shown at 1M concentrations. Ion effect on interfacial water for ODA at 10mM concentration is not clear. One can expect a strong hydrogen-bonding maker

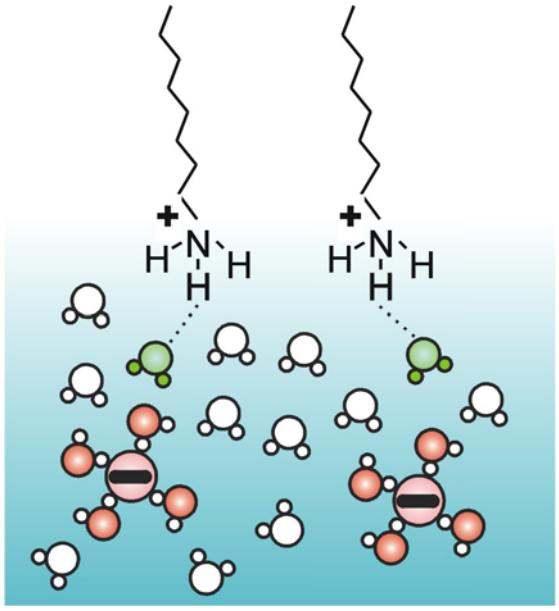

Figure 32. Schematic diagram of ODA monolayer on a salt solution.

such as fluoride and sulfate ions could win over the competition and removes water from the amine head group. On the other hand, thiocyanate and perchlorate ions will be weak competitors showing fewer disturbances on amine hydration shell, but VSFS data of water structure showed that the effect of ions for the water structure in the presence of strong hydrogen bonding is more complicated than one can expect. Screening effect was also monitored and easily interpreted for DDAB monolayer, which do not have hydrogen-bonding group. The order of water intensities for DDAB on 10mM sub=phases can be explained by different efficiencies of ions on screening effect, which depends on polarizability and ionic volume. It might look strange that sulfate and chloride switched the order, but it is reasonable once polarizability of sulfate is considered. Ion volume of sulfate is similar to that of chloride, but polarizability of sulfate is even greater than that of perchlorate (Table 3).[148] Most of all the Figure 20 and Figure 25 showed the surface potential, which was the main driving force to the anions for ODA and DDAB, has the best correlation to the ionic volume, which is related with the screening efficiency of ions.

Table 3. Ion properties in solution.

Anions	Ion volume (cm^3 mol^{-1})	Hydration number (Stokes radius, pm)	Water structure ΔG (HB)
SO_4^{2-}	25.0	5.3	-0.21
F^-	4.3	5.5	0.08
Cl^-	23.3	3.9	-0.61
NO_3^-	34.5	3.3	-0.68
Br^-	30.2	3.4	-0.80
ClO_4^-	49.6	2.6	-1.01
SCN^-	41.2	0.2	-0.82

Ion Binding

Results from the DDAB monolayer prevailed in another factor in the Hofmeister effect. It is notable that there is a significant difference in interfacial water alignment between nitrate and perchlorate at 10mM concentrations (Figure 26) even though their polarizabilities and ionic volumes were not quite different. That opens to another possible mechanism on the effect of perchlorate and thiocyanate ions from other ions. We propose that perchlorate and thiocyanate ions, which are large and poorly-solvated, have possibilities to shed their hydration shells partially or fully and bind to the hydrophobic head group of DDAB by adsorption or direct binding (Figure 33). The concepts of adsorption and binding were used for indirect binding to the monolayer with low degree of shedding ion solvation shells and direct binding with high degree of losing

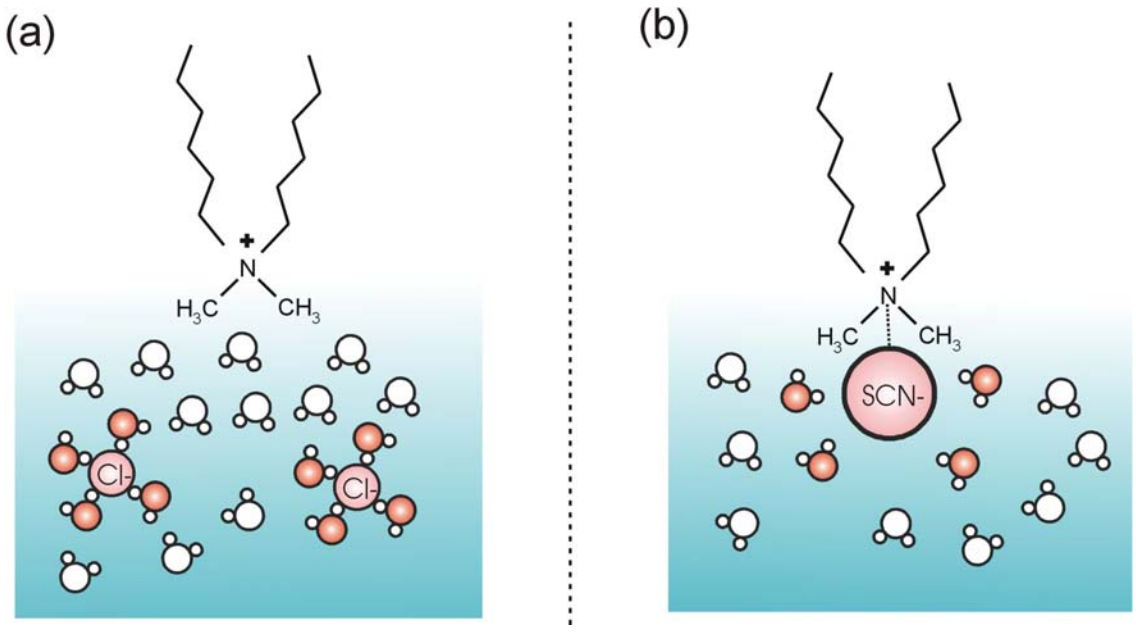

Figure 33. Schematic diagram of DDAB monolayer on (a) NaCl solution and (b) NaSCN solution. Sodium ion was not shown on the diagram.

solvating water respectively. Theoretical calculation showed that the solvating water around halides are tightly bound to fluoride and loosely to iodide.[12] Hydrogen-bond dynamics of solvating water in the presence of halide ions showed lifetime of O-H stretch vibration increased from fluoride to iodide, which explained hydrogen-bond interaction becomes weaker from fluoride to iodide and suggested higher possibility of direct binding for bigger and polarizable ions.[149] Adsorption and direct binding of these anions to the positive head group resulted neutralization of the charge on the surface and caused water alignments significantly disordered, which appeared as a big drop of water intensities in VSFS spectrum. Intensities of OH peaks depend on the abilities of ions to get closer to the DDAB head group. For a given ion, the solvation shell for the DDAB head group is very weak and ions could reach to the DDAB head group much closer than ODA head group. It is expected for bigger and highly polarizable ions like perchlorate to reach closer to the monolayer than small and less polarizable ions do.

At 1M concentration (Figure 26-b), most of the ions except for thiocyanate disturbed water alignment through adsorption mechanism, which was also shown as decrease in 3200 cm^{-1} peak intensity. Since ions bound to the head group neutralized the surface charge, the water molecules are no longer aligned by electrostatic interactions, which was the main contributor for 3200 cm^{-1} peak. Sulfate is always hydrated, thus disordering effect of sulfate was minor even at high concentration.

The driving force for the unexpected behavior of 1M thiocyanate solution is suspected to be different from that at 10mM concentration, where 3200 cm^{-1} peak was higher than 3400 cm^{-1} peak. Since the thiocyanate ion has the weakest hydration shell

(Table 3) and relatively smaller size compared to perchlorate ion, there is high possibility for thiocyanate ion to shed large portion of hydration water and binds directly to DDAB head group. SFG study of tetradecyltrimethylammonium ($C_{14}TA^+$) with thiocyanate ion showed that SCN^- ion presented in the Stern layer binding to the head group with sulfur atoms directing toward the monolayer. [150] It is possible for perchlorate to have the same effect as thiocyanate, but steric hindrance from bulky perchlorate ion made its binding to the head group less preferred. Similar steric hindrance was already reported to be a significant factor in ion binding.[120]

Hydrophobic Interaction and Dispersion Force

It is noteworthy that the ratio between CH_3 and CH_2 peaks for ODA, DDAB, and DLPC showed a good correlation to the ionic volume (Figures 20, 25, and 29 respectively), which explains that the hydrophobicity of ions is a key factor for the Hofmeister effect. Hydrophilic ions have strong interaction to a hydrophilic head group such as amine of ODA and big and hydrophobic ions have strong interaction to a hydrophobic head group such as choline group of DLPC (Figure 34). Hydrophobicity of ions is also related to the dispersion force, which was suggested by Ninham and co-workers to be an important factor for the Hofmeister effect in biological systems whenthe ionic strength is high enough (> 10mM) to saturate the screening effect.[121, 151-155] For a neutral system like DLPC, the dispersion force could be a significant contribution for the Hofmeister effect. There is possibility of dispersion force to align water molecules under DLPC monolayers on high concentration of salt solutions, which was shown in this paper.

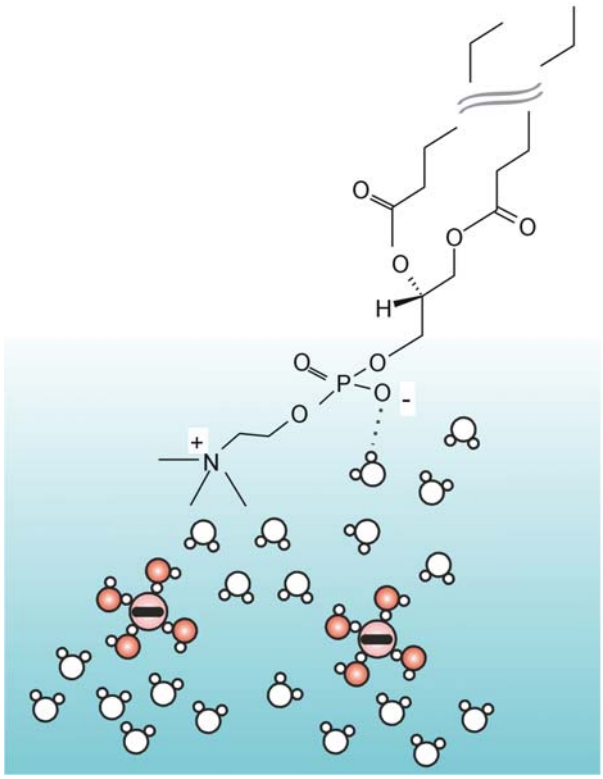

Figure 34. Schematic diagram of DPLC monolayer on a salt solution.

SUMMARY

In 1888 Hofmeister found that different amounts of salts are required to salt-out hen egg white protein out of the solution and listed ions according to their abilities to stabilize proteins; $SO_4^{2-} > H_2PO_4^- > CH_3COO^- > Cl^- > Br^- > I^- > ClO_4^- > SCN^-$. Since Hofmeister effect is phenomenon at the interface, interface specificity of sum frequency study can give valuable information on Hofmeister effect. There was not a technique to study the Hofmeister effect on water structure as well as on hydrophobic residues at the same time, but sum frequency spectroscopy is applicable to those studies. In this chapter we applied vibrational sum frequency spectroscopy to investigate the Hofmeister effect on hydrophobic residues of amphiphiles and on interfacial water structure for octadecylamine (ODA), dimethyldidodecylammonium bromide (DDAB), and 1,2-dilauroyl-sn-Glycero-3-Phosphocholine (DLPC) monolayers at air/water interface. Water structure making and breaking have been considered as a proper explanation for the Hofmeister effect, but recently many other factors are proposed, among them is screening effect, ion binding, and dispersion force. Our results showed that the Hofmeister effect is a combination of screening, ion binding, dispersion force as well as water structuring effects of ions and there is a different degree of importance on each factor for a given system. Various combinations of charge and hydrogen bonding character of the monolayers made us possible to resolve different contribution of each factor on the Hofmeister series.

CHAPTER VI

SUMMARY

Vibrational sum frequency spectroscopy (VSFS) is a nonlinear optical process that gives vibrational information of molecules at interfaces.[156] Intensity of the sum frequency signal is proportional to square of nonlinear polarizability, which depends on nonlinear susceptibility that is a sum of non-resonant and resonant part. Resonant susceptibility is proportional to the average number of molecules and the orientation average of them.[18, 19] Therefore SFG signal from the bulk, which has inversion symmetry, will be canceled and only molecules at interface give sum frequency signals. VSFS can be taken over wide frequency range enough to cover CH stretch from hydrophobic residues such as alkyl chains of amphiphile molecules and OH stretch from water, so that it is one of the best techniques to study biological interfaces.

In this dissertation VSFS was applied to investigate protein/solid interfaces, which is important to understand biofouling related with development of medical implants and biological sensors. Fibrinogen adsorption on a silica surface introduced a sharp peak near 3280 cm^{-1} on the vibrational sum frequency spectrum. Adsorption mechanism of fibrinogen was prevailed up to amino acid level by combination of VSFS with other surface probing techniques. Fibrinogen was fragmentized by plasmin to separately observe the contribution of αC fragments on fibrinogen absorption. VSFS of fibrinogen fragments showed that the adsorption behavior of fibrinogen was mainly from the αC fragments of the protein.

Ion ability to stabilize a protein was ordered by Hofmeister in 1888 as followed;

$SO_4^{2-} \cong HPO_4^{2-} > F^- > Cl^- > Br^- > NO_3^- > I^- (\cong ClO_4^-) > SCN^-$.

The series have been found in various biological phenomena, such as DNA-protein binding, enzyme activity, polymer adsorption, and pH measurements. The origin of such an effect is still ambiguous. Mainly it was understood as ion ability to enforce or disturb water structure. Recently other factors, such as screening effects, ion binding, and dispersion forces were suggested as proper explanations. We studied anion effects on alkyl chain ordering/disordering of amphiphile monolayers and interfacial water structures with VSFS. The results suggested that the Hofmeister effect is the convoluted effect among the screening effect, ion binding, and dispersion forces as well as altering water structure.

REFERENCES

(1) Tiefenauer L; Ros R. *Colloids Surf. B* **2002**, *23*, 95-114.

(2) Israelachvili, J. N. *Intermolecular & Surface Forces*. 2 ed.; Academic Press: London, 1992.

(3) Baszkin, A.; Norde, W. *Physical Chemistry of Biological Interfaces*. Marcel Dekker, Inc.: New York, 2000.

(4) Jung, S.-Y.; Lim, S.-M.; Albertorio, F.; Kim, G.; Gurau, M. C.; Yang, R. D.; Holden, M. A.; Cremer, P. S. *J. Am. Chem. Soc.* **2003**, *125*, 12782-12786.

(5) Horbett, T. A.; Brash, J. L. *Proteins at Interfaces II: Fundamentals and Applications*. American Chemical Society: Washington, DC, 1995.

(6) Hofmeister, F. *Arch. Exp. Pathol. Pharmakol.* **1888**, *24*, 247-260; *translated in* W. Kunz, J. Henle and B. W. Ninham, ' Zur Lehre von der Wirkung der Salze' (about the science of the effect of salts: Franz Hofmeister's historical papers, *Curr. Opin. Coll. Interface Sci.* **2004**, *9*, 19-37.

(7) Cacace, M. G.; Landau, E. M.; Ramsden, J. J. *Q. Rev. Biophys.* **1997**, *30*, 241-277.

(8) Lopez-Leon, T.; Jodar-Reyes, A. B.; Bastos-Gonzalez, D.; Ortega-Vinuesa, J. L. *J. Phys. Chem. B* **2003**, *107*, 5696-5708.

(9) Bostrom, M.; Craig, V.S.J.; Albion, R.; Williams, D.R.M.; Ninham, B.W. *J. Phys. Chem. B* **2003**, *107*, 2875-2878.

(10) Bostrom, M.; Tavares, F. W.; Bratko, D.; Ninham, B. W. *J. Phys. Chem. B* **2005**, *109*, 24489-24494.

(11) Collins, K. D.; Washabaugh, M. W. *Q. Rev. Biophys.* **1985**, *18*, 323-422.

(12) Hribar, B.; Southall, N. T.; Vlachy, V.; Dill, K. A. *J. Am. Chem. Soc.* **2002**, *124*, 12302-12311.

(13) Kabalnov A.; Olsson, U.; Wennerstrom, H. *J. Phys. Chem.* **1995**, *99*, 6220-6230.

(14) Bowron, D. T.; Finney, J. L. *J. Chem. Phys.* **2003**, *118*, 8357-8372.

(15) Altekar, W. *Biopolymers* **1977**, *16*, 341-368.

(16) Omta, A. W.; Kropman, M. F.; Woutersen, S.; Bakker, H. J. *Science* **2003**, *301*, 347-349.

(17) Shen, Y. R. *Nature* **1989**, *337*, 519-525.

(18) Shultz M.J.; Badelli, S.; Schnitzer, C.; Simonelli, D. *J. Phys. Chem. B* **2002**, *106*, 5313-5324.

(19) Miranda, P. B.; Shen, Y. R. *J. Phys. Chem. B* **1999**, *103*, 3292-3307.

(20) Richmond, G. L. *Chem. Rev.* **2002**, *102*, 2693-2724.

(21) Gragson, D. E.; Richmond, G. L. *J. Phys. Chem. B* **1998**, *102*, 3847-3861.

(22) Watry, M.R.; Richmond, G. L., *J. Phys. Chem. B* **2002**, *106*, 12517-12523.

(23) Scatena, L. F.; Richmond, G. L. *J. Phys. Chem. B* **2001**, *105*, 11240-11250.

(24) Scatena, L. F.; Brown, M. G.; Richmond, G. L. *Science* **2001**, *292*, 908-912.

(25) Kim, J.; Cremer, P. S. *Chem.Phys.Chem.* **2001**, *2*, 543-546.

(26) Kim, J.; Kim, G.; Cremer, P. S. *J. Am. Chem. Soc.* **2002**, *124*, 8751-8756.

(27) Kim, J.; Kim, G.; Cremer, P. S. *Langmuir* **2001**, *17*, 7255-7260.

(28) Kim, G.; Gurau, M.; Kim, J.; Cremer, P. S. *Langmuir* **2002**, *18*, 2807-2811.

(29) Kim, G.; Gurau, M.; Lim, S.; Cremer, P. *J. Phys. Chem. B* **2003**, *107*, 1403-1409.

(30) Wang, J; Chen, X; Clarke, M. L.; Chen, Z. *J. Phys. Chem. B* **2006**, *110*, 5017 - 5024.

(31) Gurau, M. C.; Castellana, E. T.; Albertorio, F.; Kataoka, S.; Lim, S.-M.; Yang, R. D.; Cremer, P. S. *J. Am. Chem. Soc.* **2003**, *125*, 11166-11167.

(32) Binnig, G.; Quate, C. F.; Gerber, C. *Phys. Rev. Lett.* **1986**, *56*, 930-933.

(33) Hansma, P. K.; Elings, V. B.; Marti, O.; Bracker, C. E. *Science* **1988**, *242*, 209-216.

(34) Hansma, H. G.; Hoh, J. H. *Annu. Rev. Biophys. Biomol. Struct.* **1994**, *23*, 115-139.

(35) Niemeyer, C. M. *Angew. Chem. Int. Ed.* **2001**, *40*, 4128-4158.

(36) Radmacher, M.; Tillmann, R. W.; Fritz, M.; Gaub, H. E. *Science* **1992**, *257*, 1900-1905.

(37) Axelrod, D.; Burghardt, T. P.; Thompson, N. L. *Annu. Rev. Biophys. Bio.* **1984**, *13*, 247-268.

(38) Nikon Inc. http://www.microscopyu.com/articles/fluorescence/tirf/tirfintro.html (accessed on March 20, 2006).

(39) Yang, T. L.; Jung, S. Y.; Mao, H. B.; Cremer, P. S. *Anal. Chem.* **2001**, *73*, 165-169.

(40) Yang, T. L.; Baryshnikova, O. K.; Mao, H. B.; Holden, M. A.; Cremer, P. S. *J. Am. Chem. Soc.* **2003**, *125*, 4779-4784.

(41) Sauerbrey, G. Z. *Zeitschrift Fur Physik* **1959**, *155*, 206-222.

(42) Hook, F.; Larsson, C.; Fant, C. *Encyclopedia of Surface and Colloid Science*, Hubbard, A. T., Ed. Marcel Dekker, Inc.: New York, 2002.

(43) Rodahl, M.; Hook, F.; Fredriksson, C.; Keller, C. A.; Krozer, A.; Brzezinski, P.; Voinova, M.; Kasemo, B. *Faraday Discuss.* **1997**, *107*, 229-246.

(44) Kronik, L.; Shapira, Y. *Surf. Sci. Rep.* **1999**, *37*, 1-206.

(45) Baikie, I. D. http://www.kelvinprobe.info (accessed on March 20, 2006).

(46) Davies, D. *Nat. Rev. Drug Discov.* **2003**, *2*, 114-122.

(47) Hanker, J. S.; Giammara, B. L. *Science* **1988**, *242*, 885-892.

(48) Holland, N. B.; Qiu, Y. X.; Ruegsegger, M.; Marchant, R. E. *Nature* **1998**, *392*, 799-801.

(49) Vroman, L.; Adams, A. L. *Surf. Sci.* **1969**, *16*, 438-446.

(50) Wojciechowski, P.; ten Hove, P.; Brash, J. L. *J. Colloid Interf. Sci.* **1986**, *111*, 455-465.

(51) Slack, S. M.; Horbett, T. A. *J. Biomat. Sci-Polym. E.* **1991**, *2*, 227-237.

(52) Santerre, J.P.; Tenhove, P.; Vanderkamp, N. H., Brash, J. L. *J. Biomed. Mater. Res.* **1992**, *26*, 39-57.

(53) Doolittle, R. F. *Annu. Rev. Biochem.* **1984**, *53*, 195-229.

(54) Holden M. A.; Cremer P.S. *Ann. Rev. Phys. Chem*. **2005**, *56*, 369-387.

(55) Cacciafesta, P.; Humphris, A. D. L.; Jandt, K. D.; Miles, M. J. *Langmuir* **2000**, *16*, 8167-8175.

(56) Ta, T. C.; Sykes, M. T.; McDermott, M. T. *Langmuir* **1998**, *14*, 2435-2443.

(57) Huang, N. P.; Michel, R.; Voros, J.; Textor, M.; Hofer, R.; Rossi, A.; Elbert, D. L.; Hubbell, J. A.; Spencer, N. D. *Langmuir* **2001**, *17*, 489-498.

(58) Slack, S. M.; Horbett, T. A. *J. Colloid Interf. Sci.* **1989**, *133*, 148-165.

(59) Zembala, M.; Déjardin, P. *Colloids Surf. B* **1994**, *3*, 119-129.

(60) Veklich, Y. I.; Gorkun, O. V.; Medved, L. V.; Nieuwenhuizen, W.; Weisel, J. W. *J. Biol. Chem.* **1993**, *268*, 13577-13585.

(61) Control experiments with just fibrinogen in the buffer solution demonstrated that exchange of adsorbed fibrinogen by species from the bulk was far slower and much less extensive than displacement by other proteins in human plasma.

(62) Weisel, J. W.; Stauffacher, C. V.; Bullitt, E.; Cohen, C. *Science* **1985**, *230*, 1388-1391.

(63) Sit, P. S.; Marchant, R. E. *Thromb. Haemostasis* **1999**, *82*, 1053-1060.

(64) Quantitative fluorescence measurements were performed and showed that ~75 antibodies nonspecifically adsorbed per square micron. It is, however, difficult to obtain an exact count of fibrinogen molecules containing a bound IgG from fluorescence. This is because each fibrinogen contains two binding sites.

(65) Shen, Y. R. *Nature* **1989**, *337*, 519-525.

(66) Wang, J.; Buck, S. M.; Even, M. A.; Chen, Z. *J. Am. Chem. Soc.* **2002**, *124*, 13302-13305.

(67) Wang, J.; Buck, S. M.; Chen, Z. *J. Phys. Chem. B* **2002**, *106*, 11666-11672.

(68) Kim, J.; Somorjai, G. A. *J. Am. Chem. Soc.* **2003**, *125*, 3150-3158.

(69) Du, Q.; Freysz, E.; Shen, Y. R. *Phys. Rev. Lett.* **1994**, *72*, 238-241.

(70) The NH stretch frequency from the lysine and arginine strongly overlap in the IR and Raman spectra.

(71) Nawrocki, J. *J. Chromatogr. A* **1997**, *779*, 29-71.

(72) Wirth, M. J.; Swinton, D. J. *J. Phys. Chem. B* **2001**, *105*, 1472-1477.

(73) Wirth, M. J.; Swinton, D. J.; Ludes, M. D. *J. Phys. Chem. B* **2003**, *107*, 6258-6268.

(74) Voet, D.; Voet, J. G. *Biochemistry*. 2nd ed.; John Wiley and Sons, Inc.: New York, 1995.

(75) Weisel, J. W.; Medved, L. *Fibrinogen*, New York Academy of Sciences: New York, 2001; Vol. 936.

(76) Vroman, L. *Interfacial Phenomena in Biological Systems*, Bender, M., Ed. Marcel Dekker, Inc.: New York, 1991; Vol. 39.

(77) Malmsten, M. *Colloids Surf. A* **1999**, *159*, 77-87.

(78) Kenausis, G. L.; Voros, J.; Elbert, D. L.; Huang, N.; Hofer, R.; Ruiz-Taylor, L.; Textor, M.; Hubbell, J. A.; Spencer, N. D. *J. Phys. Chem. B* **2000**, *104*, 3298-3309.

(79) Jones, V. W.; Kenseth, J. R.; Porter, M. D.; Mosher, C. L.; Henderson, E. *Anal. Chem.* **1998**, *70*, 1233-1241.

(80) Seigel, R. R.; Harder, P.; Dahint, R.; Grunze, M. *Anal. Chem.* **1997**, *69*, 3321-3328.

(81) Nygren, H.; Stenberg, M.; Karlsson, C. *J. Biomed. Mater. Res.* **1992**, *26*, 77-91.

(82) Yang, Z.; Mochalkin, I.; Veerapandian, L.; Riley, M.; Doolittle, R. F. *Proc. Natl. Acad. Sci. U.S.A.* **2000**, *97*, 3907-3912.

(83) Horbett, T. A.; Brash, J. L. *Proteins at Iinterfaces II : Fundamentals and Applications*. American Chemical Society: Washington, DC, 1995.

(84) Shen, M. C.; Wagner, M. S.; Castner, D. G.; Ratner, B. D.; Horbett, T. A. *Langmuir* **2003**, *19*, 1692-1699.

(85) Johnson, W. C.; Wang, J.; Chen, Z. *J. Phys. Chem. B* **2005**, *109*, 6280-6286.

(86) Holmlin, R. E.; Chen, X. X.; Chapman, R. G.; Takayama, S.; Whitesides, G. M. *Langmuir* **2001**, *17*, 2841-2850.

(87) Wertz, C. F.; Santore, M. M. *Langmuir* **2002**, *18*, 706-715.

(88) Ostuni, E.; Chen, C. S.; Ingber, D. E.; Whitesides, G. M. *Langmuir* **2001**, *17*, 2828-2834.

(89) Huang, N.-P.; Michel, R.; Voros, J.; Textor, M.; Hofer, R.; Rossi, A.; Elbert, D. L.; Hubbell, J. A.; Spencer, N. D. *Langmuir* **2001**, *17*, 489-498.

(90) Yongli, C.; Xiufang, Z.; Nanning, Z.; Tingying, Z.; Xingi, S. *J. Colloid Interf. Sci.* **1999**, *214*, 38-45.

(91) Ostuni, E.; Chapmen, R. G.; Liang, M. N.; Melueni, G.; Pier, G.; Ingber, D. E.; Whitesides, G. M. *Langmuir* **2001**, *17*, 5605-5620.

(92) Morrissey, B. W.; Stromberg, R. R. *J. Colloid Interf. Sci.* **1974**, *46*, 152-164.

(93) Malmsten, M. *J. Colloid Interf. Sci.* **1994**, *166*, 333-342.

(94) Ball, A.; Jones, R. A. L. *Langmuir* **1995**, 11, 3542-3548.

(95) Wang, J.; Chen, X. Y.; Clarke, M. L.; Chen, Z. *Proc. Natl. Acad. Sci. U. S. A.* **2005**, *102*, 4978-4983.

(96) Hook, F.; Rodahl, M.; Kasemo, B.; Brzezinski, P. *Proc. Natl. Acad. Sci. U. S. A.* **1998**, *95*, 12271-12276.

(97) Hook, F.; Kasemo, B.; Nylander, T.; Fant, C.; Sott, K.; Elwing, H. *Anal. Chem.* **2001**, *73*, 5796-5804.

(98) Hook, F.; Voros, J.; Rodahl, M.; Kurrat, R.; Boni, P.; Ramsden, J. J.; Textor, M.; Spencer, N. D.; Tengvall, P.; Gold, J.; Kasemo, B. *Colloids Surf., B* **2002**, *24*, 155-170.

(99) Gragson, D. E.; McCarty, B. M.; Richmond, G. L. *J. Am. Chem. Society* **1997**, *119*, 6144-6152.

(100) Gurau, M.; Kim, G.; Lim, S.; Albertorio, F.; Fleisher, H. C.; Cremer, P. S. *Chem.Phys.Chem.* **2003**, *4*, 1231-1233.

(101) Brooker, M. H.; Hancock, G.; Rice, B. C.; Shapter, J. *J. Raman Spectrosc.* **1989**, *20*, 683-694.

(102) Fraley, P. E.; Rao, K. N. *J. Mol. Spectrosc.* **1969**, *29*, 312-347.

(103) Pinchas, S.; Laulicht, I. *Infrared Spectra of Labeled Compounds*. Academic Press: London, 1971.

(104) Person, W. B.; Editor, *Studies in Physical and Theoretical Chemistry, Vol. 20: Vibrational Intensities in Infrared and Raman Spectroscopy*. Elsevier Scientific Pub. Co.: New York, 1982.

(105) Simons, W. W.; Editor, *The Sadtler Handbook of Infrared Spectra*. Sadtler Research Laboratories: Philadelphia, 1978.

(106) Popp, J.; Rosch, P.; Vogel, E.; Kiefer, W. *Progress in Surface Raman Spectroscopy - Theory, Techniques and Application*, Tian, Z. Q.; Ren, B.;Editor, Xiamen University Press: Xiamen, China, 2000.

(107) Liu, Y. L.; Cho, R. K.; Sakurai, K.; Miura, T.; Ozaki, Y. *Appl. Spectrosc.* **1994**, *48*, 1249-1254.

(108) Smith, D. L.; Zhang, Z. Q.; Liu, Y. Q. *Pure Appl. Chem.* **1994**, *66*, 89-94.

(109) Thevenonemeric, G.; Kozlowski, J.; Zhang, Z. Q.; Smith, D. L. *Anal. Chem.* **1992**, *64*, 2456-2458.

(110) Roach, P.; Farrar, D.; Perry, C. C. *J. Am. Chem. Soc.* **2005**, *127*, 8168-8173.

(111) Chen, X. Y.; Wang, J.; Sniadecki, J. J.; Even, M. A.; Chen, Z. *Langmuir* **2005**, *21*, 2662-2664.

(112) Watt, K. W. K.; Cottrell, B. A.; Strong, D. D.; Doolittle, R. F. *Biochemistry* **1979**, *18*, 5410-5416.

(113) Kohler, J.; Kirkland, J. J. *J. Chromatogr. A* **1987**, *385*, 125-150.

(114) Clarke, R. J.; Lupfert, C. *Biophys. J.* **1999**, *76*, 2614-2624.

(115) Kropman, M. F.; Bakker, H. J. *J. Am. Chem. Soc.* **2004**, *126*, 9135-9141.

(116) Gurau, M. C.; Lim, S.; Castellana, E. T.; Albertorio, F.; Kataoka, T.; Cremer, P. S. *J. Am. Chem. Soc.* **2004**, *126*, 10522-10523.

(117) Perez-Jimenez, R.; Godoy-Ruiz, R.; Ibarra-Molero, B.; Sanchez-Ruiz, J. M. *Biophys. J.* **2004**, *86*, 2414-2429.

(118) Kuehner, D. E.; Engmann, J.; Fergg, F.; Wernick, M.; Blanch, H. W.; Prausnitz, J. M. *J. Phys. Chem. B* **1999**, *103*, 1368-1374.

(119) Ramos, C. H. I.; Baldwin, R. L. *Protein Science* **2002**, *11*, 1771-1778.

(120) Jakubowska, A. *Chem.Phys.Chem.* **2005**, *6*, 1600-1605.

(121) Bostrom, M.; Williams, D. R. M.; Ninham, B. W. *Biophys. J.* **2003**, *85*, 686-694.

(122) Bostrom, M.; Williams, D. R. M.; Stewart, P. R.; Ninham, B. W. *Phys. Rev. E* **2003**, *68*, 041902-1-041092-6.

(123) Bostrom, M.; Williams, D. R. M.; Ninham, B. W. *Phys. Rev. Lett.* **2001**, *87,* 168103-1-168103-4.

(124) Mahanty, J.; Ninham, B. W. *Dispersion Forces*. Academic Press: New York 1976.

(125) Knock, M. M.; Bain, C. D. *Langmuir* **2000**, *16*, 2857-2865.

(126) Liu, D. F.; Ma, G.; Levering, L. M.; Allen, H. C. *J. Phys. Chem. B* **2004**, *108*, 2252-2260.

(127) Shen, Y. *The Principles of Nonlinear Optics*. John Wiley & Sons, Inc.: New York, 1984.

(128) Guyot-Sionnest, P.; Hunt, J. H.; Shen, Y. R. *Phys. Rev. Lett.* **1987**, *59*, 1597-1600.

(129) Miranda, P. B.; Du, Q.; Shen, Y. R. *Chem. Phys. Lett.* **1998**, *286*, 1-8.

(130) Conboy, J. C.; Messmer, M. C.; Richmond, G. L. *J. Phys. Chem. B* **1997**, *101*, 6724-6733.

(131) Guyotsionnest, P.; Superfine, R.; Hunt, J. H.; Shen, Y. R. *Phys. Rev. Lett.* **1988**, *144*, 1-5.

(132) Braun, R.; Casson, B. D.; Bain, C. D. *Chem. Phys. Lett.* **1995**, *245*, 326-334.

(133) Sachs, J. N.; Woolf, T. B. *J. Am. Chem. Soc.* **2003**, *125*, 8742-8743.

(134) Schnell, B.; Schurhammer, R.; Wipff, G. *J. Phys. Chem. B* **2004**, *108*, 2285-2294.

(135) Shapovalov, V.; Tronin, A. *Langmuir*, **1997**, *13*, 4870-4876.

(136) Buch, V. *J. Phys. Chem. B* **2005**, *109*, 17771-17774.

(137) Kim, J.; Cremer, P. S. *J. Am. Chem. Soc.* **2000**, *122*, 12371-12372.

(138) Richmond, G. L. *Annu. Rev. Phys. Chem.*, **2001**, *52*, 357-389.

(139) Cunningham, B. A.; Lis, L. J. *J. Colloid Interf. Sci.* **1989**, *128*, 15-25.

(140) Leckband, D. E.; Helm, C. A.; Israelachvili, J. *Biochemistry* **1993**, *32*, 1127-1140.

(141) Lis, L. J.; Lis, W. T.; Parsegian, V. A.; Rand, R. P. *Biochemistry* **1981**, *20*, 1771-1777.

(142) Starling, A. P.; East, J. M.; Lee, A. G. *Biochemistry* **1993**, *32*, 1593-1600.

(143) Sachs, J. N.; Nanda, H.; Petrache, H. I.; Woolf, T. B. *Biophys. J.* **2004**, *86*, 3772-3782.

(144) Bockmann, R. A.; Hac, A.; Heimburg, T.; Grubmuller, H. *Biophys. J.* **2003**, *85*, 1647-1655.

(145) Garcia-Manyes, S.; Oncins, G.; Sanz, F. *Biophys. J.* **2005**, *89*, 1812-1826.

(146) Shapovalov, V. L.; Shub, B. R.; Oliveira, O. N. *Colloid. Surface. A* **2002**, *198*, 195-206.

(147) Jungwirth, P.; Tobias, D. J. *J. Phys. Chem. B* **2002**, *106*, 6361-6373.

(148) Marcus, Y. *Ion Properties*. Marcel Dekker, Inc.: New York, 1997.

(149) Kropman, M. F.; Bakker, H. J. *Science* **2001**, *291*, 2118-2120.

(150) Duffy, D. C.; Ward, R. N.; Davies, P. B.; Bain, C. D. *J. Am. Chem. Soc.* **1994**, *116*, 1125-1126.

(151) Bostrom, M.; Williams, D. R. M.; Ninham, B. W. *Langmuir* **2001**, *17*, 4475-4478.

(152) Bostrom, M.; Tavares, F. W.; Finet, S.; Skouri-Panet, F.; Tardieu, A.; Ninham, B. W. *Biophys. Chem.* **2005**, *117*, 217-224.

(153) Bostrom, M.; Ninham, B. W. *Biophys. Chem.* **2005,** *114*, 95-101.

(154) Bostrom, V.; Kunz, W.; Ninham, B. W. *Langmuir* **2005**, *21*, 2619-2623.

(155) Bostrom, M.; Ninham, B. W. *J. Phys. Chem. B* **2004**, *108*, 12593-12595.

(156) Shen, Y. R. *Surf. Sci.* **1994**, *299/300*, 551-562.

VITA

Name Soon Mi Lim

Address Department of Chemistry, 3255 TAMU
College Station, TX77843-3255

E-mail Address slim@mail.chem.tamu.edu

Education

Ph.D., Chemistry, *May 06*
Texas A&M University
M.S., Chemistry, *February 98*
Inha University, South Korea, Advisor: Dr. Young S. Choi
Thesis title: Fluorescence Excitation Spectroscopy of OClO cooled in Supersonic Jet Expansions
B.S., Chemistry, *February 96*
Inha University, South Korea

Recent Papers

1. Is Water Structure Related to the Hofmeister Effect?: A Vibrational Sum Frequency Spectroscopy Study.
   Soon-Mi Lim, Marc C Gurau, Sho Kataoka, and Paul S. Cremer
   In preparation

2. Deeper Look at the Vroman Effect: Vibrational Sum Frequency Study on Fibrinogen Fragment Adsorptions.
   Soon-Mi Lim, Seung-Yong Jung, Fernando Albertorio, and Paul S. Cremer
   In preparation

3. On the Mechanism of the Hofmeister Effect.
   Marc C. Gurau, **Soon-Mi Lim,** Edward T. Castellana, Fernando Albertorio, Sho Kataoka and Paul S. Cremer
   J. Am. Chem. Soc. **2004**, *126*, 10522-10523

4. The Vroman Effect: A Molecular Level Description of Fibrinogen Displacement.
   Seung-Yong Jung, **Soon-Mi Lim**, Fernando Albertorio, Gibum Kim, Marc C. Gurau, Richard D. Yang, Matthew A. Holden, and Paul S. Cremer
   J. Am. Chem. Soc. **2003**, *125*, 12782-12786